SPH High Velocity Impact Analysis

A Birdstrike Windshield Application

Arcangelo Grimaldi

Department of Aerospace Engineering

University of Naples Federico II

A thesis submitted for the degree of

Doctor of Philosophy in Aerospace Engineering

13^{th} January 2011

... to my loving Ale.

Acknowledgements

First of all I would like to express my sincere gratitude to Prof. Francesco Marulo, Full Professor of the Department of Aerospace Engineering, University of Naples "Federico II", who has been my supervisor since the beginning of my study. He provided me with many helpful suggestions, important advice and constant encouragement. During the course of this work he was an essential guide for me, and I will remember forever that to work with him was a privilege for me.

I also wish to express my appreciation to Professors De Rosa and Franco for the valuable suggestions and constructive advices they gave me.

Special thanks are due to my two friends and collegues Dr. Tiziano Polito and Dr. Michele Guida for their friendship and support. It was an honour and a pleasure to work with them during these years.

Special gratitude goes to Prof. David J. Benson for giving me valuable academic instructions and suggestions that improved the quality of this study, during my permanence as visiting scholar at Department of Structural Engineering, University of California San Diego, CA, USA.

Sincere thanks to mrs Colino for helping and supporting me during these years and for donating its friendships gratuitously.

My special appreciation goes to my dear parents, my sister Tonia, my "brothers" Domenico and Fabio, and my friends Francesco and Milena, who always encouraged and supported me on my study.

Finally, I would like to express very special thanks to my loving Alessandra. She helped me to concentrate on completing this dissertation and supported mentally during the course of this work. Without her help and encouragement, this study and all my life would not have been the same.

Abstract

This dissertation is the result of a research focused on the study, with the help of finite element analysis , of an aircraft windshield-surround structure with an innovative configuration, that satisfies the bird-strike requirement according to the EASA Certification Specifications 25.631 on the "Bird-strike Damage" [CS25.631 (2003)].

The first step was the numerical analysis of a simplified, but realistic, square flat windshield model subjected to impact by a 1.8 kg bird model at 155m/s with an impact angle of 90°. The FE-SPH coupled approach was used to simulate the birdstrike by using the explicit finite element solver code LS-Dyna.

The second step was the execution of a parametric analysis on the square model to estimate the influence of the target geometry, the impact angle, and the plate curvature on the impact response of the windshield structure. The goal of these numerical simulations was the evaluation of the windshield capability to absorb the impact energy, involving during a birdstrike event, in a safe and efficient way without any damage.

Finally it was developed a numerical simulation of birdstrike event on a full-scale aircraft windshield-surround model. This FE numerical analysis showed the capability of the real innovative windshield to withstand to the impact force transferred by the bird during the impact and permitted the definition of some guidelines to execute a certification test simulation and to give an impact test article proposal, needed for a design of an airplane windshield structure able to resist to a birdstrike event in according with the conditions stated in the CS 25 standard requirements.

Contents

List of Figures

List of Tables

Chapter 1

Introduction

1.1 Overview

During its life cycle an aircraft flies on the risk of impacting foreign objects. According to the aeronautical specifications, with the term "birdstrike" we mean the collision between a bird and an aircraft front facing component, which includes windshield, nacelles, wing leading edge and compressor blade.

The probability of an accident is higher in the airport area during the take-off and landing phases, and especially in the early morning and late afternoon. In recent years the severity and importance of the birdstrike has grown because of the remarkable increase of the air traffic and airplane performances in term of velocity, followed by an increment of energy density and impulsive loads during the impact.

The birdstrike is not only relative to the flight safety, but also to not negligible maintenance costs, which the companies must meet to repair possible damages in case of an accident. In order to better understand the nature of birdstrike and also prevent the hazard of an accident, they have been formed international committees, such as the Birdstrike Committee USA. Only in the United States more than 60000 wildlife strikes to civil aircraft have been reported between 1990 and 2005 (Figure 1.1). The annual cost of the wildlife strikes to the USA civil aviation industry is estimated to be in excess of 530000 hours of aircraft downtime and $614 million in monetary losses ($470 million per year in direct costs and $144 million per year in associated costs) [Cleary *et al.* (2003)].

Therefore more and more companies and government authorities have initiated advanced research and development programs to ensure that every structural part of an aircraft is able to withstand the loads due to a high velocity impact and at least guarantee the safe landing of the airplane, in according to the International Certification Standards.

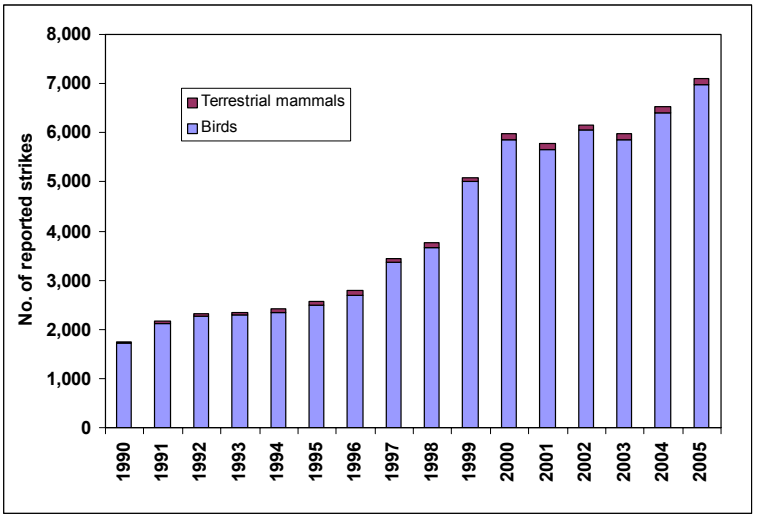

Figure 1.1: Number of reported strikes to civil aircraft, USA, 1990-2005

Both Federal Aviation Administration (FAA) and European Aviation Safety Agency (EASA) list regulations for the aircraft certification process to ensure that the front facing aircraft components should be capable of withstanding birdstrikes at critical flight speed to a certain degree (Table 1.1).

Aircraft Component	Bird Weight	FAR Section
Windshields and Frames	4 lb	25.775 (b), 25.775 (c)
Wing Leading Edges	4 lb	25.571(e)(l)
Empennage Leading Edges	8 lb	25.631, 25.571(e)(l)
Engine - Inlet Lip	4 lb	25.571(e)(I)
Engine - Fan Integrity	4 lb	33.77, 25.571(e)(l)
Engine - Continued Operation	Up to 8 of 1.5 lb birds	33.77,25.571(e)(I)

Table 1.1: FAR - Birdstrike Test Requirements

For instance, the EASA birdstrike airworthiness requirements relevant to the large airplane windshield are specified under the Certification Specifications (CS) 25 Section 775, which states that:

- *Internal panes must be made of non splintering material.*
- *Windshield panes directly in front of the pilots in the normal conduct of their duties, and the supporting structures for these panes, must withstand, without penetration, the bird impact conditions specified in CS 25.631.*
- *Unless it can be shown by analysis or tests that the probability of occurrence of a critical windshield fragmentation condition is of a low order, the aeroplane*

must have a means to minimise the danger to the pilots from flying windshield fragments due to bird impact. This must be shown for each transparent pane in the cockpit.

- *The windshield panes in front of the pilots must be arranged so that, assuming the loss of vision through any one panel, one or more panels remain available for use by a pilot seated at a pilot station to permit continued safe flight and landing.*

Where the bird strike conditions are specified under the Section CS 25.631 (Bird-strike damage): *"The aeroplane must be designed to assure capability of continued safe flight and landing of the aeroplane after impact with a 4 lb bird when the velocity of the aeroplane (relative to the bird along the aeroplane's flight path) is equal to VC at sea-level or 0.85 VC at 2438 m (8000 ft), whichever is the more critical. Compliance may be shown by analysis only when based on tests carried out on sufficiently representative structures of similar design."*

For the final certification both FAA and EASA require full-scale tests to demonstrate the efficiency of every bird-proof structures, like a windshield. Because of the excessive costs necessary to the execution of the test, the manufacturers perform many numerical analysis of the birdstrike event with explicit nonlinear finite element (FE) codes in order to decrease the number of destructive tests required and to avoid any delay during the certification.

Explicit FE analysis is a numerical technique used in case of highly non linear behaviour of materials with inelastic strains, high strain rates and large deformations, such as it occurs during a birdstrike. For a birdstrike phenomenon, to obtain a good prediction of the impact loads and damage of an aircraft structure under impact loading, it is essential to adopt a realistic material model for a bird and its associated material and geometrical parameters. To achieve an accurate bird model an explicit code, like LSTC/LS-Dyna [Hallquist (2006)], offers different approaches to modeling:

1. the Lagrangian approach.
2. the Arbitrary Lagrangian Eulerian (ALE) approach.
3. the Smoothed Particle Hydrodynamics (SPH) approach.

The first and the third methods are based on the Lagrangian finite element formulation, with the difference that in case of SPH approach the bird is modeled with

a meshless technique, in which the elements are a set of discrete and mutually interacting nodes. Instead in the ALE method the bird material flows relative to an Eulerian mesh and the impacting loads are transferred to the Lagrangian mesh (the impacted structure) through an ALE coupling algorithm. Each method presents both advantages and disadvantages, so the choice of the more appropriate approach for the modeling is often connected to the experience of the user, as well as the nature of crash phenomenon.

1.2 Literature Review

The birdstrike is a well-know phenomenon, some impacts were recorded since the first decades of the 1900's [Thorpe (2003)].

In the past various scientists studied the birdstrike with several empirical design methods, in order to define the characteristics (thickness, material, etc...) of the aircraft components able to resist at birdstrike events.
In the 1970's, the validation of the bird-proof components was solely dependent on experiments, because of the absence of numerical tools.

A birdstrike event can be account as a collision between a structural element and a soft body (the bird). Barber *et al.* (1975) were the first to analyse this kind of problem with this approach by performing an experimental campaign of bird impacts against a rigid circular plate. They focused on the peaks pressure generated during the impact and found these are independent by the bird dimensions but proportional to the square of the impact velocity. Furthermore they found that a pressure time-history is composed by four different phases: a) an initial shock (Hugoniot pressure), b) an impact shock decay, c) a steady state phase and d) a final decay of the pressure, in the following chapter these will be treated deeply.

Barber & Peterson (1976) and later Barber *et al.* (1977) performed a series of birdstrike tests on rigid plate and turbo-machinery too. They concluded that the behaviour of the bird can be assimilated to a fluid one, and so showed that bird-loading model treats the bird model as a fluid dynamic process.

Shortly thereafter, Wilbeck (1977) showed that, in case of high velocity impact, the response of the bird is similar to that of the water for which the strength of the material is extremely small compared with the impact loads.

Later Cassenti (1979) studied analytically the experiment carried out by Barber *et al.* (1977) during the 1970's and developed the governing equations for a soft body

impact on a rigid plate. By relating the conservation equation with the constitutive equation of the material he achieved the analytical expression of the Hugoniot pressure generated in the beginning of the event.

Because of the difficult to conduct test with real bird, many scientists studied the possibility to use different dummy bird substitute. Allock & Collin (1969) were the first to determine prime constituents of substitute bird model by studying wax, foam, emulsions, and gelatin as substitute materials for birds. Wilbeck & Rand (1981) found that the gelatin, with the specific gravity of water, produces a loading profile similar to real birds and the response depends on material density and not on material strength.

Since 1980's the exponential growth in the speed of computers and the even greater decline in the cost of computational resources were the major contributions to obtaining of good results with crash analysis software. Explicit nonlinear finite element (FE) codes, which are available in several high-end commercial FE solvers, used for this kind of problem, can show a considerable amount of useful information to the designer with regard to the mechanisms involved in a birdstrike event, that could potentially improve the offered level of crashworthiness, prior to conducting expensive experimental tests.

Niering (1990) studied the birdstrike problem numerically and modeled the bird using a Lagrangian approach. His research provided different methods of computer simulation for the birdstrike event, but presented the need for an improvement due to large distortions experienced by the bird in the Lagrangian model. For this reason Airoldi & Cacchione (2006) evaluated and improved the accuracy of bird impact numerical analyses performed with the finite element explicit code PAM-CRASH (2008), focusing on the modeling of the spatial and temporal pressure distributions exerted on the target by the impacting body. A Lagrangian approach is adopted, interfacing the FE solver code with an automatic trial-and-error procedure for the elimination of the excessively distorted elements. One of the most recent study using a Lagrangian approach is the work of Guan *et al.* (2008), who modeled bird impact against fan rotor blades.

Some authors provided various recommendations for the modeling bird behaviour using alternative approaches, like Arbitrary Lagrangian Eulerian (ALE). Benson (1992) published a detailed review of the general methods for Lagrangian and Eulerian hydrocodes, that are currently used to solve transient large deformation problems in solid mechanics. He provided the first public light on the basis for the methods used in commercial codes for impact analyses. Another extensive description of the ALE method was presented by Stroker (1997), who studied applications of the

ALE method in the forming processes. To explain the ALE method, Stoker included a section with fundamentals of continuum mechanics, followed by a derivation of the ALE motion description, and a mathematical formulation used for calculations.

Later Langrand *et al.* (2001) modeled the bird impact against rigid targets using both the Lagrangian and ALE formulations in Radioss (2008), whereas Shultz & Peters (2002) presented ALE models for bird impacting the inlet fan blades of a jet engine using LS-DYNA [Hallquist (2006)] and Ansys (2006) software. Linder (2003) and Donea *et al.* (2004) produced a detailed description of the ALE formulation, that combines the advantages of the Lagrangian and Eulerian methods without the disadvantages associated to each method. Souli *et al.* (2004) studied the problem of the birdstrike by LS-Dyna [Hallquist (2006)] using a multi-material ALE formulation, they obtained an acceptable bird deformation and small energy loss.

Between the end of the 1990's and the beginning of the 2000's many authors analysed problems of fluid-structure interaction, like birdstrike, with the Smoothed Particle Hydrodynamics (SPH) approach. Hut *et al.* (1997) discussed various implementations of SPH method. The main findings of the work consisted of a clarification of the computational requirements for the SPH method and estimation of the cost/performance to boost the efficiency of the high-end general purpose computers. Birnbaum *et al.* (1997) analysed bird impact simulation problem by using all modeling techniques (Lagrangian, Eulerian, ALE and SPH) to simulate the fluid-structure interaction. Lacome (2000) gave an important contribution for the description of the conventions used for the selection of the smoothing length and provided important informations regarding the SPH process of the neighbour search in the interpolation and for the SPH approximations for the equations of energy and mass conservation.

Other authors used SPH approach to model the birdstrike phenomenon, in particular Ubels *et al.* (2003) and McCarthy *et al.* (2004) investigated the bird impact on an aircraft wing leading edge structure using PAM-CRASH software. They showed that the SPH methodology was able to capture the breakup of the bird into debris particle after the collision. Guida *et al.* (2011) found that the Lagrangian-SPH combination provided the best results in terms of impact visualization and a good prediction of the deceleration of the projectile, compared to the test results .

The birdstrike as well as involving several front facing components of the aircraft, can concern different kind of materials too. In the recent years many authors analysed and simulated the birdstrike event against a specific part of the airplane. Georgiadis *et al.* (2008) provided a validated simulation methodology to support the birdstrike certification of the carbon fibre epoxy composite moveable trailing edge

of the Boeing 787 Dreamliner. Anghileri *et al.* (2004) performed numerical simulation of the bird impact against the intake of turbofan engine and discussed the advantages and disadvantages about using of different bird modelling techniques. Hanssen *et al.* (2006) investigated bird impact against aluminium foam-based sandwich panel using the ALE approach. Guida (2008) developed a finite element model for simulating the birdstrike test on the tailplane leading edge structure. He studied the impact on a composite component made of aluminium skin and flexcore as interior sandwich structure, and found good correlation between the numerical and experimental results.

The windshield structure plays a key role relating to the birdstrike problem, because of its exposure in front of the airplane. So many authors developed study in order to design bird-proof windshield for protecting the safety of aircraft. Yang *et al.* (2003) elaborated an experimental and FEM of windshield subjected to high speed bird impact. Liu *et al.* (2008) focused on the analysis of an effective numerical method to simulate bird impact aircraft windshield events, using the SPH approach and the explicit finite element program PAM-CRASH. Recently Salehi *et al.* (2010) investigated the effect of the birdstrike on different aircraft windows both numerically and experimentally. He studied structures made up of different geometries and materials by using various modeling approach (ALE and SPH).

1.3 Aim of Present Work

The aim of this research work was to define a scientific and methodological approach to the study of the birdstrike problem. It was developed a particular application focused on the verification and design of a bird-proof windshield of a business jet airplane in according with international aeronautical specifications and requirements. It was studied an innovative concept of aircraft windshield, composed by just two windshield panels, unlike most part of the commercial airplane windshield configurations made up of four or more panels.

Firstly it was studied a simplified square panel model subject to the birdstrike event, and generated a FE model performed adopting SPH modeling approach using LSTC/LS-Dyna explicit solver code. A parametric analysis was executed to evaluate the effects on the structural response of a windshield of: 1) the target geometry, 2) the impact angle and 3) the plate curvature. The target is to evaluate the capability of windshield to absorb the impact energy, involving during a birdstrike event, in a safe and efficient way without any damage. The second part of the work was focused on the development of an effective numerical method to simulate the birdstrike on

a real aircraft windshield model. The collection of results and experiences achieved by the previous simplified realistic model was applied to perform a certification test simulation and define possible guidelines for structural design of an airplane windshield including the bird impact requirements.

1.4 Outlines of the Thesis

Chapter 2 provides an extensive description of the theoretical aspect of the birdstrike phenomenon. Chapter 3 presents a description of the basic theory of nonlinear analysis and a brief review for the following finite element modeling approaches: a) pure Lagrangian, b) Arbitrary Lagrangian Eulerian (ALE), and c) Smoothed Particle Hydrodynamics (SPH). Chapter 4 presents an explanation of the projectile (bird) and target structure (square plate and real windshield) properties, focusing on the geometry, boundary conditions, and mechanical behaviour of the materials. Chapter 5 specifies the methodology of simulation of the windshield birdstrike event by the LS-Dyna explicit nonlinear FE solver, both for the simplified square model and real windshield, in terms of materials, boundary conditions and contact modeling. Furthermore it is presented a brief overview of the capabilities of the pre and post-processing software tools used for the simulation. Chapter 6 describes the numerical results of the simulation and the parametric study of the impact response of the structure as changing of the bird impact angle, curvature and lay-up thickness configurations of the plate. Finally Chapter 7 presents the conclusions of the research work and a guidelines assessment regard to the design of a bird-proof aircraft windshield structure.

Chapter 2

Birdstrike Theory

2.1 Physics Overview

There are three categories of impact events:

- Elastic impact,
- Plastic impact,
- Hydrodynamic impact.

The elastic impacts are typically low speed events, and the stresses generated because of the collision are lower then the material yield stress. So the nature and duration of the impact depend on the elastic modulus and the elastic wave velocities of the material.

In case of higher impact speeds the produced stresses cause a plastic deformation of the material target and this kind of collision constitute the plastic impact category. For those events, the material strength is still a dominating factor.

Finally, for higher impact velocities again the stresses generated by deceleration of the projectile greatly exceed the yield stress. This is a hydrodynamic regime, for which the projectile can be treated as fluids, and it is the material density which dominates the behaviour of the parts instead of material strength.

The birdstrike fall into this category of impact, where the bird do not bounce and impact response is determined by the length of the bird and by the initial impact velocity but not by the material strength.

A hydrodynamic event like this one is a non-steady fluid dynamic process that has four distinct phases:

1. Initial impact
2. Impact pressure decay
3. Steady flow
4. Flow termination

2.1.1 Initial impact

When the bird impacts the target plate, a fragmentation of the projectile particles appears and a shock propagates into the bird, the Figure 2.1 shows a sketch of this phase on the left and a frame of a real experimental test on the right. As the shock wave propagates into the bird it brings the bird material behind the shock to rest. The pressure in the shock compressed region is initially very high and uniform across the impact area.

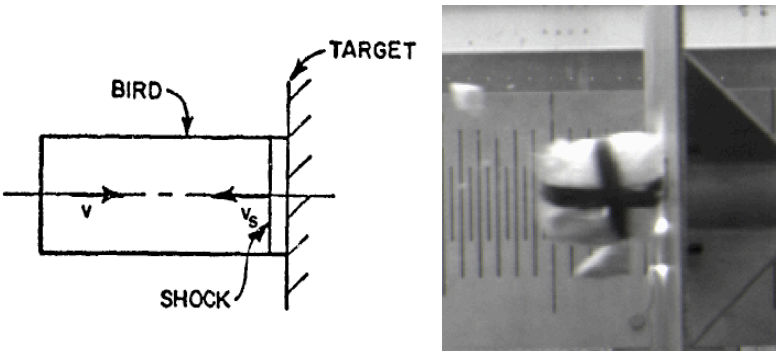

Figure 2.1: Initial impact phase

For the normal impact of a cylinder on a rigid plate, the flow across a shock can be considered one-dimensional, adiabatic, and irreversible. The pressure behind the shock (Hugoniot pressure) may then be derived from the shock relation as:

$$p = \rho v_s v \tag{2.1}$$

where

p is the pressure behind the shock,

ρ is the density of the bird,

v_s is the shock velocity,

v is the impact velocity.

Generally, the bird material hydrodynamic response can be characterised by a polynomial interpolation of the curve relating the pressure to the density, given by equation 2.2 [Wilbeck & Rand (1981)]:

$$p = \rho_p u_{sp} u_0 \left(\frac{\rho_t u_{st}}{\rho_p u_{sp} + \rho_t u_{st}} \right) \tag{2.2}$$

where

ρ_p is the density of the projectile,

ρ_t is the density of the target,

u_{sp} is the projectile shock wave velocity,

u_{st} is the target shock wave velocity,

u_0 is the projectile's initial velocity.

In equation 2.2 the initial peak pressure depends only on densities and velocities and not on the length or cross-sectional area of the projectile.

The edge of the projectile is a free surface and the material near the edge is subjected to a very high stress gradient. This stress gradient causes the material to accelerate radially outward and a release wave is formed. The arrival of this release wave at the center of the bird marks the end of the initial impact and the beginning of the decay process.

2.1.2 Impact pressure decay

At initial impact a shock begins to propagate into the projectile and radial release waves propagate in towards the center from the free surface edges of the projectile (Figure 2.2). The problem can no longer be considered to be one-dimensional in nature. For the normal impact of a cylinder, the problem is two-dimensional and axisymmetric.

The radial pressure distribution is given by equation 2.3:

$$p_r = p e^{-\frac{kr}{R(t)}} \tag{2.3}$$

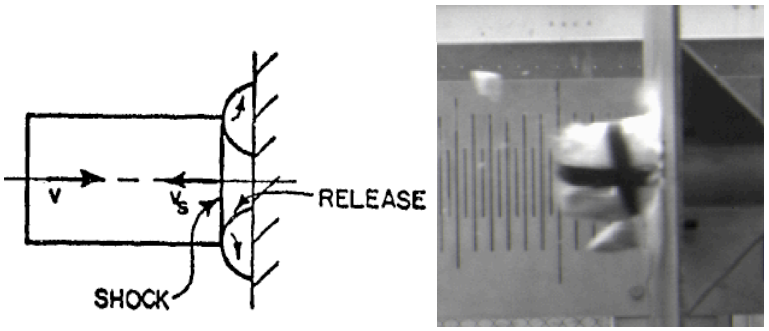

Figure 2.2: Initial impact

where

p_c is obtained from equation 2.2,

K is a constant,

r is the radial distance from the center of the impact region,

$R(t)$ is the maximum contact radius at time t.

The duration of this high pressure event is on the order of tens of milliseconds. Figure 2.3 shows when the release waves have converged at point B, the center of impact. The pressure on the target at the center of impact now begins to decay. After the release waves have converged at the center of the shock (point c) a region of fully shocked material no longer exists. The curvature of the shock is due to the release process, which has weakened the shock more at the edges than at the center.

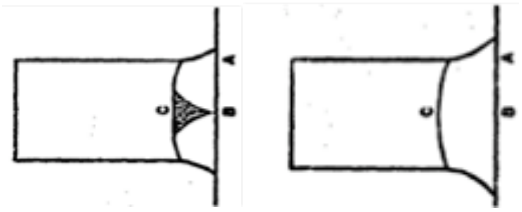

Figure 2.3: Impact pressure decay phase

For a projectile of sufficient length, steady flow should be set up after several reflections of the radial release waves. A projectile with a length somewhat greater than L_c (critical length) should undergo complete shock decay to steady flow. A longer steady flow regime is expected at low velocities than at high velocities.

The details of pressure variation with time during the decay process are extremely difficult to predict. In addition to the geometrical complexities, complete shock release material properties for the bird must be known. This is something we may be able to understand through simulation.

2.1.3 Steady flow

As the radial pressures decrease during the shock pressure decay, shear stresses develop in the projectile material. If the shear strength of the material is sufficient to withstand these shear stresses, the radial motion of the projectile will be restricted. If, however, the shear stresses in the projectile are greater than the shear strength of the material, the material will "flow"(Figure 2.4).

The shear strength of birds is low enough that the pressures generated are usually sufficient to cause flow. The bird can be considered to behave as a fluid. After several reflections of the release waves, a condition of steady flow is established and steady pressure and velocity fields are established.

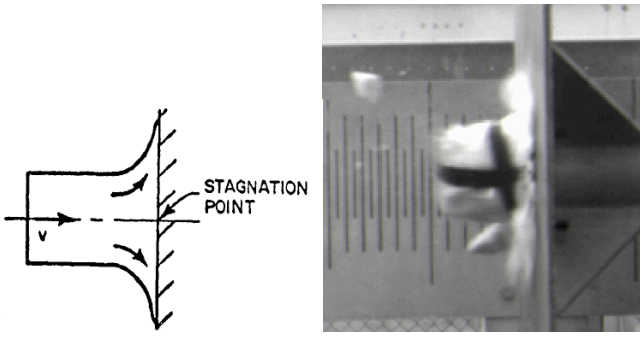

Figure 2.4: Steady flow phase

Using potential flow theory, [Wilbeck & Rand (1981)] calculated the steady flow pressure for a supersonic bird impact at normal incidence. He found that the pressure at the center of impact (the stagnation pressure) could be approximately given by the expression below:

$$p_s = \frac{1}{2}\rho_0 v^2 \tag{2.4}$$

where ρ_0 is the density of the material with zero porosity and v the impact velocity.

This implies that the steady flow pressure at the center of impact is almost independent of porosity. The decrease in density due to porosity is apparently offset by the increase in compressibility.

2.1.4 Flow termination

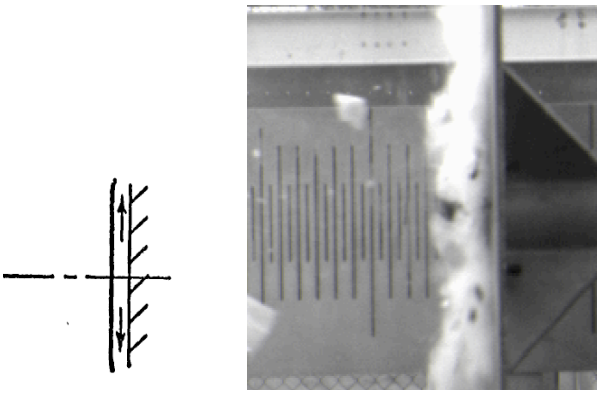

Figure 2.5: Flow termination phase

During impact, bird material is "turned" near the target surface. As the fluid nears the target surface the velocity decreases and the local pressure increases. In the time of the steady flow a pressure field is set up in the fluid. As the end of the projectile enters this pressure field, the field is disrupted due to the intrusion of a free surface (the end of the bird).

Steady flow no longer exists and the pressures at the impact surface decrease (Figure 2.5). The pressure decrease continues until the end of the projectile reaches the surface of the plate. At this time the impact event is ended.

2.2 Momentum Transfer

Figure 2.6 shows the behaviour of the bird before and after the impact.

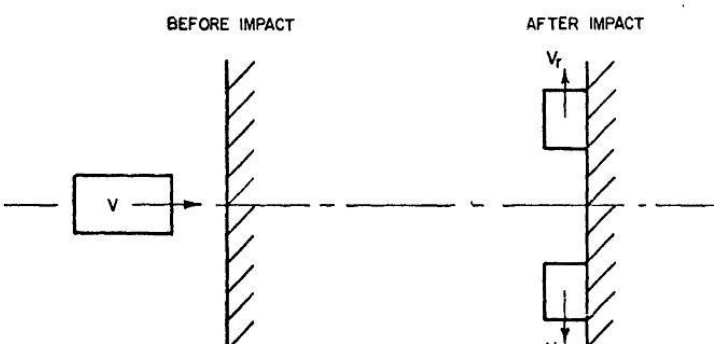

Figure 2.6: Momentum transfer

The initial momentum of the bird along trajectory is simply mv, where m is the mass of the bird and v is the initial impact velocity of the bird. Since the bird has only radial velocity then the momentum of the bird along trajectory after impact is zero. Therefore, the momentum transferred to the target during the impact is simply equal to mv. It is interesting to notice that, extending this concept to oblique impacts, only the component of momentum normal to the impact surface is transferred to the target and the momentum transfer is given by:

$$I = mv \sin\theta \tag{2.5}$$

where θ is the angle between trajectory and the surface of the target. The equation 2.5 describes the impulse imposed onto a rigid target during impact when the bird is assumed to be a fluid body.

2.3 Impact Duration

The *impact duration* is the time elapsed from the moment when the bird touches the target until there is no further bird material flowing onto the target. It is define as *squash-up time* T_s and is given by:

$$T_s = \frac{l}{v} \tag{2.6}$$

where

l is the length of the bird,

v is the initial impact velocity.

The situation is different in case of oblique impact (Figure 2.7), because the effective length of the bird, l_{eff}, is:

$$l_{eff} = l + d\tan\vartheta \tag{2.7}$$

where d is the diameter of the bird and ϑ is the angle of impact.

2.4 Average Impact Force

A main effect of a birdstrike is the energy transfer to the airplane structure impacted, it can be estimated by approximately simple calculations. After the impact the

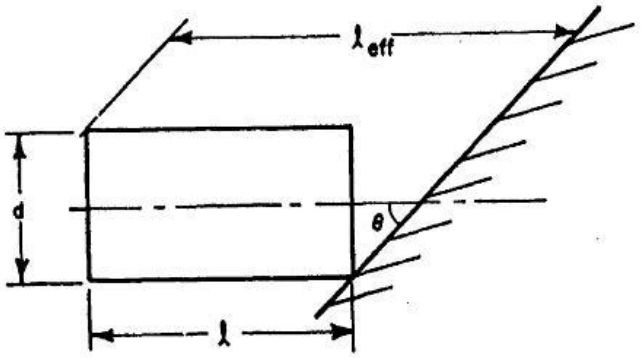

Figure 2.7: Oblique impact effective bird length

change in a bird's kinetic energy can be defined by the equation 2.8:

$$\Delta KE = W = Fd = \frac{1}{2}mv^2 \tag{2.8}$$

where

W is the work,

F is the impact force,

d is the distance over which the force is delivered,

m is the mass of the bird,

v is the velocity of the aircraft.

Whereas the force that the airplane felt is given by equation 2.9:

$$F = \frac{\Delta KE}{d} = \frac{mv^2}{2d} \tag{2.9}$$

If we further assume that the bird can be represented as a sphere then:

$$F = \frac{mv^2}{2r} \tag{2.10}$$

where r is the sphere radius, and then the bird's size depends on its mass m:

$$m = \rho V = \frac{4}{3}\pi r^3 \rho \tag{2.11}$$

where ρ is the bird density and V is the sphere's volume.

The combination of the equations 2.10 and 2.11 gives:

$$F = \frac{2\pi r^2 \rho v^2}{3} \tag{2.12}$$

that is to say the impact force is proportional to bird mass and the square of impact speed.

In case of deformable flat target, the force transferred from a bird is highly dependent upon the form and extent of the deformation. Concerning the fluid cylinder model the initial impact will create a concave deformation which will probably delay the formation of release waves. The shape also tends to turn the flow resulting in a greater momentum (and thus greater) force transfer.

$$F = \sum \frac{\Delta m \Delta v}{\Delta t} \tag{2.13}$$

where $\Delta v = v_0 - v_1$.
For a rigid flat target $v_1 = 0$
For a deformable flat target $v_1 < 0$

Although there is a potentially greater transferral of force, a considerable amount of the energy will be used in further deforming the target. Thus the force at the target ends (or reaction points) may be less than in the rigid case.

Chapter 3

Impact Modeling Methodology

3.1 Basics of Non-linear Analysis

This section reviews nonlinear structural problems by looking at the event and physical sources of nonlinear behavior.

The finite element method (FEM), or finite element analysis (FEA), is based on the idea of building a complicated object with simple blocks, or, dividing a complicated object into small and manageable pieces (elements and nodes). In the Figure 3.1 is shown a plate with hole subjected to a compression load and its FEM discretization.

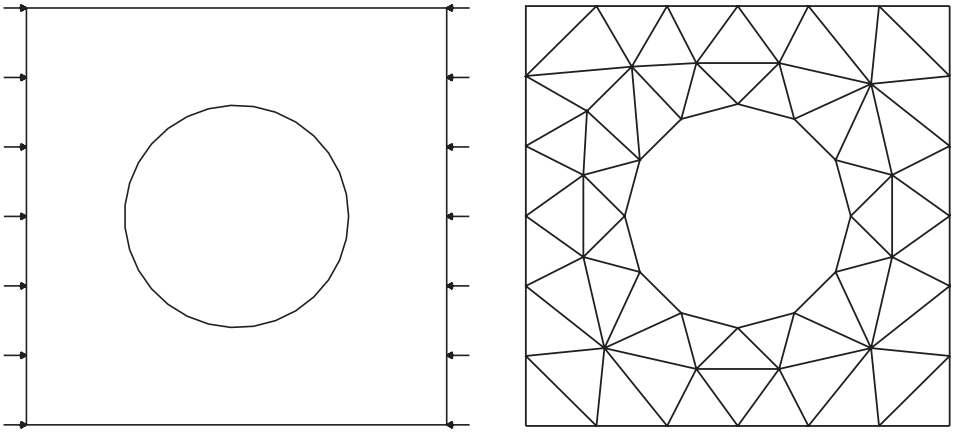

(a) Plate with hole (b) Finite Element Model

Figure 3.1: FEM discretization

The finite element method (FEM) consists of the following five steps:

1. **Preprocessing**: subdividing the problem domain into finite elements.

2. **Element formulation**: development of equations for elements.
3. **Assembly**: obtaining the equations of the entire system from the equations of individual elements.
4. **Solving the equations**.
5. **Postprocessing**: determining quantities of interest, such as stresses and strains, and obtaining visualizations of the response.

The fundamental FEA equation is:

$$Ku_e = F \tag{3.1}$$

where K is the stiffness matrix, u_e the element displacements and F the applied loads.

The solution of the equation is usually "straightforward" and can be reached in a single step by applying of F, inverting of K. Furthermore it is possible to go back and determine the stress σ and the strain ϵ.

Nonlinear structural analysis is the prediction of the response of nonlinear structures by model-based simulations, like Finite Element Analysis and the relative equations are usually solved by incremental methods, such as the implicit or explicit methods.

Nonlinearities can rise for many reasons. For structural analysis there are four sources of nonlinear behavior and the corresponding nonlinear effects are identified by the terms *material*, *geometric*, *force B.C.* and *displacement B.C.*, in which B.C. means "Boundary Conditions"

In the following subsections these sources of nonlinearities are correlated to the physics in more detail.

3.1.1 Geometric Nonlinearity

The physical source of the geometric nonlinearity is related to a not negligible change in geometry as the structure deforms, and it is taken into account in setting up the strain-displacement and equilibrium equations. In this case a structure shows large deformations and there is a nonlinear relationship between the strain ϵ and the displacement u:

$$\epsilon = \frac{1}{2}(\frac{\partial u}{\partial x} + \frac{\partial u^T}{\partial x} + \frac{\partial u}{\partial x}\frac{\partial u^T}{\partial x}) = B(u_e)u_e \tag{3.2}$$

Engineering applications of geometric nonlinear structural analysis can be:

- Slender structures in aerospace, civil and mechanical engineering.
- Tensile structures such as cables and inflatable membranes.
- Metal and plastic forming.
- Stability analysis of all types.

3.1.2 Material Nonlinearity

The material behavior depends on current deformation state and possibly past history of the deformation and other constitutive variables, like prestress, temperature and time, may be involved.

In case of material nonlinearity rises a nonlinear constitutive law of the material and a nonlinear relationship $\sigma - \epsilon$. An application of this type of nonlinearity can be found for structures that undergo nonlinear elasticity, plasticity, viscoelasticity, creep, or inelastic rate effects.

3.1.3 Force and Displacement BC Nonlinearity

If a structure is subjected to forces or displacements dependent on deformation, it can rise a BC (Boundary Condition) nonlinearity.

The most important engineering application for the force BC nonlinearity concerns pressure loads of fluids. These include aerodynamic and hydrodynamic loads caused by the motion of aeriform and hydroform fluids, like wind loads, wave loads and drag forces. Whereas the displacement BC nonlinearity may be involved in case of structural contact problem.

Non-structural applications of this problem pertain to the more general class of free boundary problems, for example: ice melting, phase changes and flow in porous media. The determination of the essential boundary conditions is a key part of the solution process.

3.2 Modeling Approaches

There is no a unique "best" numerical method to analyse the impact phenomenon, and in particular the fluid-structure interaction problems. During a single impact analysis it could be often useful to couple different numerical solvers in order to treat each domain of the problem more appropriately. For each methodology it can

be described both strengths and weaknesses, for that many times the right choice of more suitable modeling approach is function of the user expertise.

The four main modeling methods that are currently available are: the Lagrangian mesh, the Eulerian mesh, the Arbitrary Lagrangian-Eulerian (ALE) mesh, and the Smooth Particle Hydrodynamic (SPH) method.

3.2.1 Lagrangian Formulation

The Lagrangian modeling method divides a volume into a large number of small geometries called *elements*, and it is generally well suited for the description of solid materials impact problems, for which the numerical mesh moves and distorts as shown in Figure 3.2.

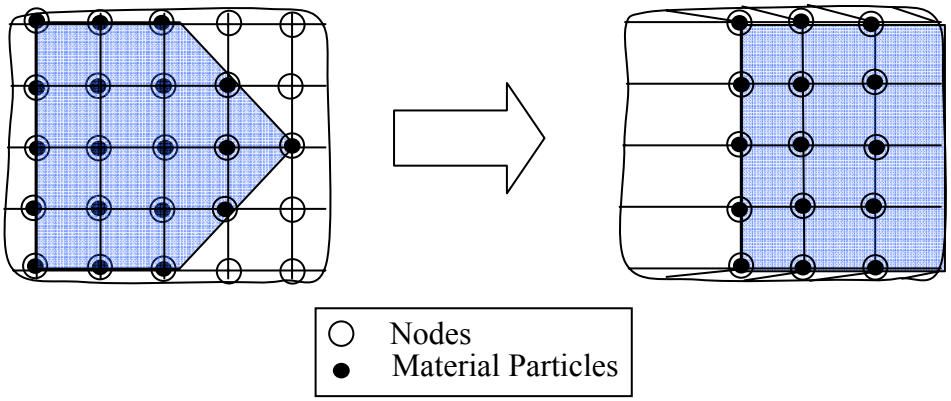

Figure 3.2: Description of motion for Lagrangian formulation

The main difference between the various formulations is the choice of the reference coordinates for the description of the motion. The Lagrangian method uses *material coordinates* as the reference. The nodes of the Lagrangian mesh are associated to particles in the material under examination; therefore each node of the mesh follows an individual particle in motion. The history dependent material properties are also well described in Lagrangian approach because of the ability to easily track history dependent materials.

Furthermore free surfaces and material interfaces are located at cell boundaries and as such are well maintained throughout the calculation, this implies that the imposition of boundary condition is simplified too.

While Lagrangian approach is particularly well suited for the description of solid behaviour, its main drawback is that, due the nature of the formulation for severe deformations, the numerical mesh may become overly distorted with a resulting

small time-step and possible loss of accuracy. In that case the numerical solution can only be carried out to a certain point before the Lagrangian mesh distortions cause the analysis to be stopped due to a very small time-step. Also, since in this method the material moves with the mesh, if the material suffers large deformations, the mesh will also suffer equal deformation and this leads to results inaccuracy and numerical instabilities (mesh tangling and/or negative volume).

However, programs may include additional features, like rezoning and erosion, that may be applied to a Lagrangian solution to extend the analysis. For element erosion, the distorted elements are deleted from the mesh by imposing a plastic strain limit. Deleting elements that exceed a pre-imposed plastic strain threshold value resolves both negative volumes and time step decrement issues. On the other hand deleting these elements also removes mass and strain energy from the structure, thus violating both conservation of mass and conservation of energy principles. Instead the rezoning procedure involves a step-by-step re-meshing of the distorted Lagrangian mesh, and it could carry out an increase of solution time and numerical errors associated with the approximations. For these reasons the technique works best for cases that need few re-meshing steps.

Advantages	**Disadvantages**	**Enhancements**
Efficiency, fewer computations per time-step relative to other solver	Element distortion ca lead to small timestep	Rezoninig and erosion
Clear definition of material interfaces and boundaries	Cell distortion can lead to grid tangling and inaccuracies	Rezoninig and erosion
Good time history information	Thin section need small time-steps	Use structural solvers
Good for strength modeling	Complex logic for sliding interfaces	
Simpler code		

Table 3.1: Attributes of the Lagrangian formulation

3.2.2 Eulerian Formulation

In the Eulerian technique the mesh is basically treated as a control volume, i.e. the mesh remains fixed and the material under study flows through the mesh, as shown in Figure 3.3.

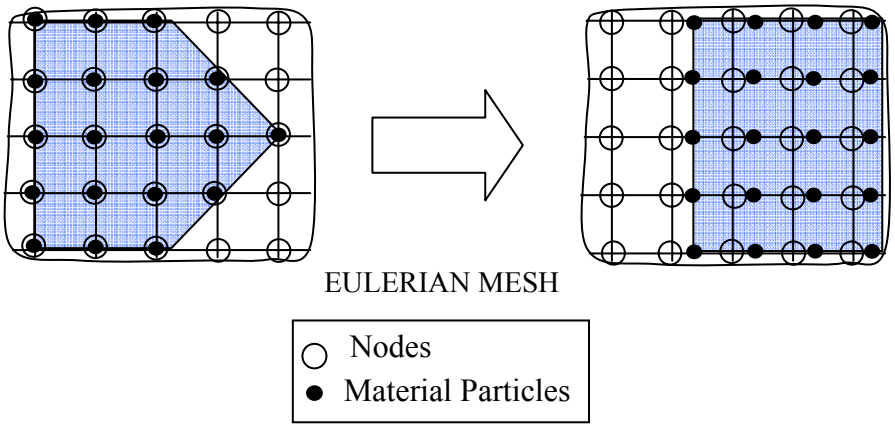

Figure 3.3: Description of motion for Eulerian formulation

Since the mesh does not move, there is no possibility of mesh deformation, which is a major disadvantage of the Lagrangian method. In addition, an Eulerian technique completely avoids the difficulties associated with the time step reduction required by the type of highly deformed domains encountered by the Lagrangian technique, when used in explicit time integration solutions.

This method is applied mostly to the simulation of fluid behaviour, such as water/fuel sloshing, although it has been applied to solid simulation too.

The major disadvantage of this method is the difficulty to keep track of the material behaviour history, for which it is necessary the use of more sophisticated techniques. This required more computations than in the Lagrangian methods, which leads to longer simulation time for the same level of accuracy when compared to the Lagrangian technique.

Advantages	**Disadvantages**	**Enhancements**
No grid distortion	More computations per cycle than Lagrangian	Simplified Euler formulation without strength
Large deformations handled	Diffusion of material boundaries	Sophisticated interface tracking implementations
Allow mixing of different materials within cells	Need finer zoning for similar accuracy compared to Lagrangian and iterative equation of state solvers for multiple material cell	Use of higher order techniques

Table 3.2: Attributes of the Eulerian formulation

3.2.3 ALE Formulation

The third modeling method is the Arbitrary Lagrangian-Eulerian (ALE) method. It can be considered like a combination of the Lagrangian and Eulerian formulation in which it is possible the advantages of both methods while also minimising the disadvantages. Unlike the Eulerian method, for which the material moves through a fixed mesh, in the ALE modeling, the material flows in the mesh, but this last can move and stretch if needed, in order to follow the boundary motion and prevent the mesh tangling, as shown in the Figure 3.4.

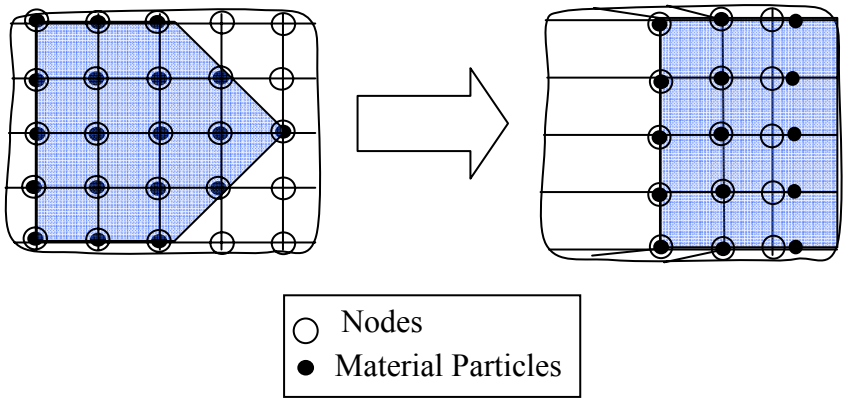

Figure 3.4: Description of motion for ALE formulation

Due to a good set of the background mesh motion from the user, it is possible to minimize the mesh distortions and obtain the best results. In this way a large number of elements can be eliminated and calculating time reduced, thereby providing a computational time saving. In particular at each time step, it can evaluate the position of the material with respect to the nodes figure, and the coupling with the solid structure is done by tracking the relative displacements between the coupled Lagrangian nodes and the fluid.

To better understand the ALE mechanism it can consider a 2D example, shown in the Figure 3.5.

By the Lagrangian modeling (case 1) the nodes of the mesh (red) are attached to the imaginary material "points". These nodes move and deform with the material.

By the Eulerian modeling (case 2) it can consider two overlapping meshes, one is a background mesh which is fixed in space (cyan), and the other is attached to the material (red) which flows through the former fixed mesh. This may be visualized in two steps: first the material is deformed in a Lagrangian step, just like the Lagrangian formulation, and then the element state variables in the Lagrangian

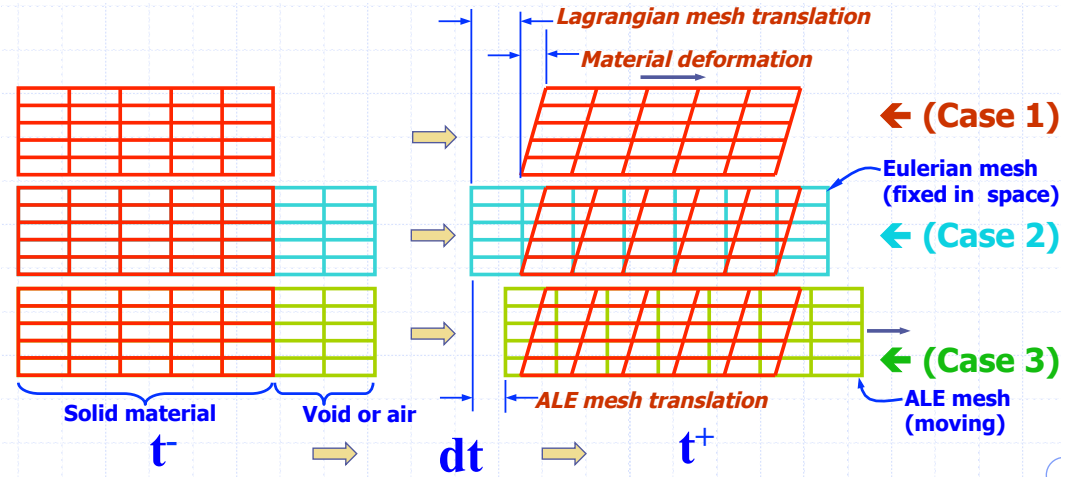

Figure 3.5: Formulations comparison

elements (red) are mapped onto the fixed (background) reference Eulerian mesh (cyan).

Finally by the ALE modeling (case 3) it can consider two overlapping meshes, one is a background mesh which can moves arbitrarily in space (green), and the other is attached to the material (red) which flows through the former moving mesh. This may be visualized in two steps again: first, the material is deformed in a Lagrangian step, just like the Lagrangian formulation, and then the Lagrangian elements (red) are remapped onto the moving (background) reference ALE mesh (green).

Advantages	Disadvantages	Enhancements
Wide range of applicability with arbitrary mesh motions (automatic rezoning)	Need to specify mesh motion constrains	
Clear definition of material interfaces and boundaries	Cell distortions can lead to grid tangling and inaccuracies	Rezoning and erosion
Good time history information	Thin sections need small time-steps	

Table 3.3: Attributes of the ALE Formulation

3.2.4 SPH Formulation

The Smooth Particle Hydrodynamics is a Lagrangian meshless technique and was developed by Monaghan (1992) in the late 1970's for astrophysics problems with application to hypervelocity impacts (~10 km/s) where the material shatters upon

impact. It is both effective and accurate at modeling material deformation as well as adaptable in terms of specific material models and besides to solve computational fluid dynamic problems, it can be also applied for continuum mechanics problems with large deformations, as crash simulations.

The main difference between the classical FE method and SPH is the methodology of discretization of the model, as shown in the Figure 3.6.

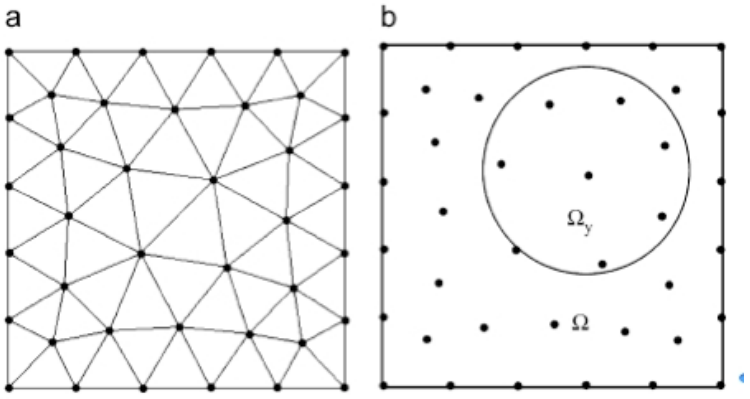

Figure 3.6: Discretization of volume: a) FEM b) SPH

In the SPH formulation the fluid is represented as a set of moving particles, each one representing an interpolation point, where all the fluid properties are known. The estimation of the field variables at any point is allowed by an interpolation formula, called kernel function.

In the definition of the methodology a very important role is played from the neighbour search procedure, i.e. the evaluation step-by-step of which particle will interact with the others. This influence of each particle is established inside of a sphere of radius of 2h, called support domain Ω_h, where h is the smoothing length, as shown in the Figure 3.7. The smoothing length of every particle changes with the time. When particles separate the smoothing length increases, while when they come close to each other, the smoothing length decreases accordingly. It is necessary to keep enough particles in the neighbourhood to validate the approximation of continuum variables.

Because of the gridless nature of the methodology, the SPH does not suffer from the usual disadvantage relative to mesh tangling in large deformation problems, like a pure Lagrangian formulation, and uses fewer elements than the ALE method, avoids the material interface problems associated with it. Again it allows the modeling of fragmentation and fracture phenomena, and, as well as the Lagrangian formulation, the SPH method allows a good tracking of the material deformation and history

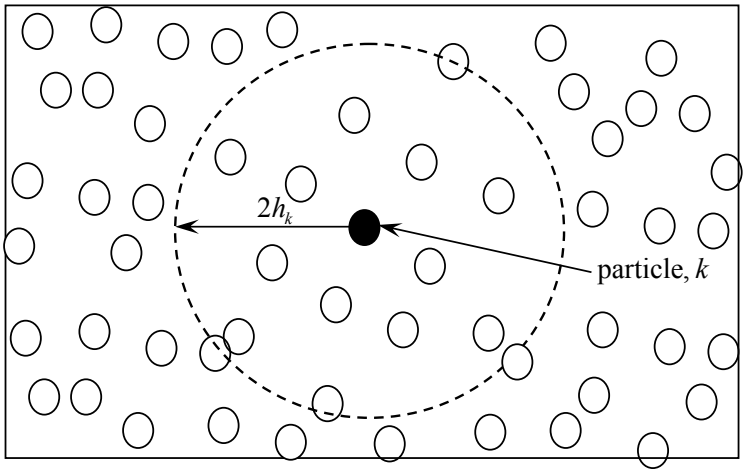

Figure 3.7: Domain of the sphere in the SPH method

Nevertheless it remains some disadvantages about the stability and consistency of the methodology. One disadvantage is the computationally demanding of the method, both in memory and in CPU time. This can be overcome using a parallel analysis with more than one CPU. Furthermore another disadvantage can be the difficulty of establishing the boundary conditions with a loss of smoothness and accuracy.

Chapter 4

Bird and Target Description

4.1 Geometry

In this section a geometry description of the target structure onto which the projectile (bird) impacts is reported. The application studied in this work is relative to a birdstrike event against a windshield structure of a business jet airplane.

Generally a windshield-surround structure of a general aviation airplane, and in particular of a business jet, is made up of at least four panels, as shown in the Figure 4.1.

(a) Hawker 400XP

(b) Learjet 60

(c) Citation Sovereign

(d) Gulfstream G150

Figure 4.1: Typical windshield-surround structures of business jet airplanes

In this work, instead, it has been studied an *innovative* configuration of a windshield structure composed of just two panels, as shown in the sketch of Figure 4.2.

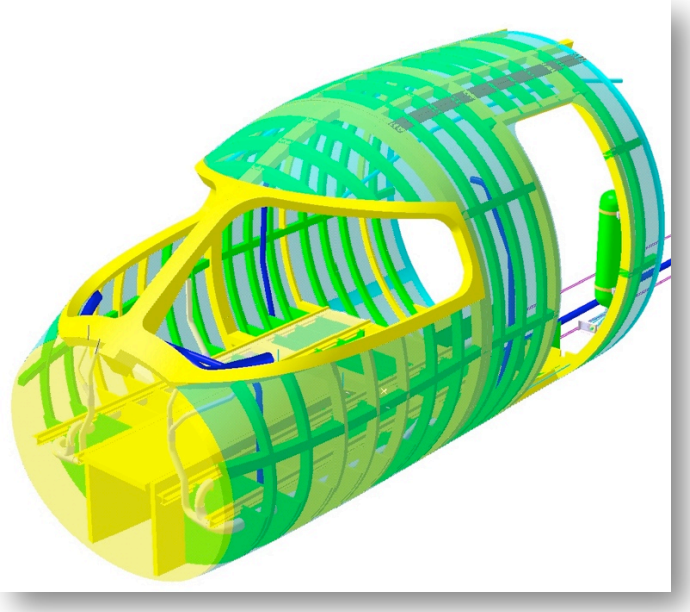

Figure 4.2: Innovative configuration of windshield structure

The International Certification Standards prescribe a windshield structure must, not only, withstand to the birdstrike event without penetration, but also avoid a complete fragmentation of all transparencies, so that to ensure a sufficient vision through at least one panel to permit continued safe flight and landing. This specification could be critical in the case of the windshield studied in this work because an impact on a transparent could cause a damage on the other panel too, or again an impact on the center beam, which divides the two panels, could create a fragmentation of both transparencies at the same time with following loss of visibility.

In the Table 4.1 are shown the main characteristics of each windshield panel:

Configuration	**Surface**	**Thickness**	**Weight**
Double curvature	$A = 1.3m^2$	$th = 20mm$	$W = 60Kg$

Table 4.1: Windshield properties

Whereas a schematic plot of the left windshield transparent model is shown in Figure 4.3.

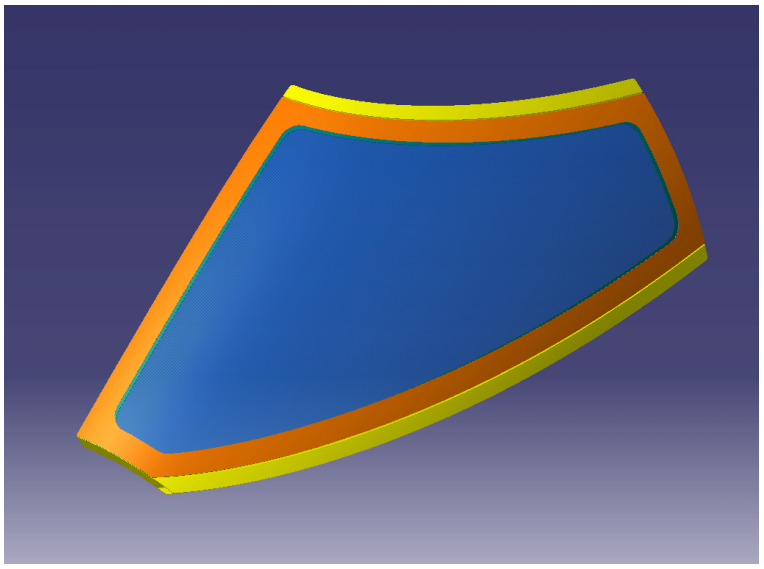

Figure 4.3: Configuration of left windshield-surround structure

Before studying a full-scale model of the real windshield structure, it has been carried out a preliminary parametric analysis of the birdstrike phenomenon through a series of numerical simulations on a simplified but representative structure, shown in Figure 4.4. This simplified model is a square flat plate made up of the same materials and lay-up configuration of the full-scale structure.

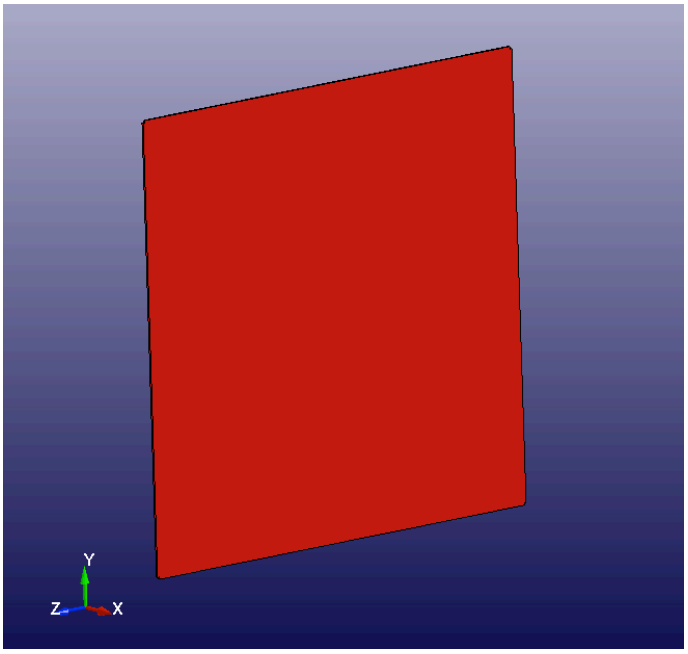

Figure 4.4: Simplified windshield model

This parametric analysis was useful to identify the most important parameters that affect the impact response of the target structure in case of bird impact and to give the chance for the definition of some best guidelines for the design and optimization process of bird-proof windshield structure.

About the projectile configuration, in according with the Certification Requirements, the weight of the bird is $W = 1.8kg$, the density is $\rho = 950kg/m^3$, and the geometric model is approximated as a right circular cylinder, as shown in the Figure 4.5:

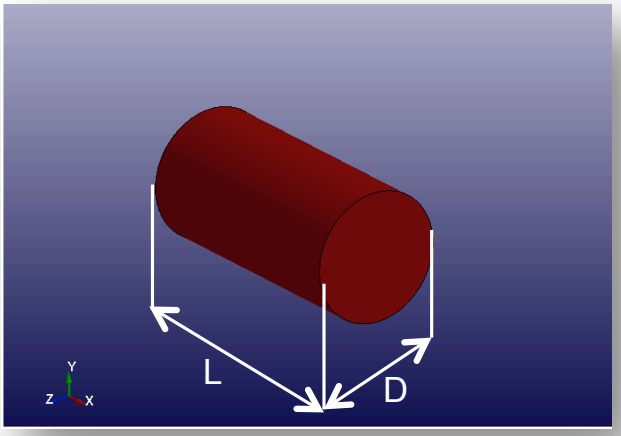

Figure 4.5: Simplified windshield model

where

$$D = \sqrt[3]{\frac{2W}{\pi\rho}} = 0.106m \tag{4.1}$$

and

$$L = 2D = 0.212m \tag{4.2}$$

4.2 Mechanical Behaviour of Materials

4.2.1 Windshield

In order to comply with fail-safe requirements an aircraft windshield is built by laminated glass.

Laminated glass is a type of safety glass used in different fields of the industrial applications, e.g. in automotive structures [Timmel *et al.* (2007)], as well as aerospace, and permits to avoid serious injuries of the passengers in case of an impact event

The basic construction of a laminated glass involves two panels of glass joined to a polyvinyl butyral (PVB) interlayer, as shown in the Figure 4.6. In the case of an impact, such as the birdstrike, the splinters, caused by the glass failure, remain connected to the PVB-interlayer.

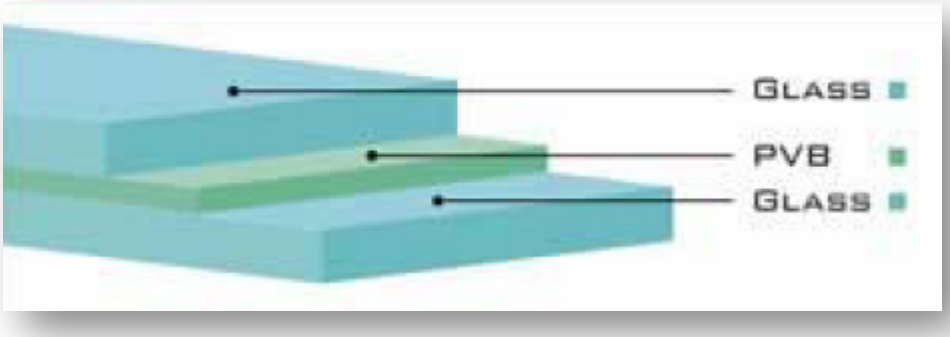

Figure 4.6: Glass laminated

In a short-time dynamics event the glass and PVB layers work in a different way. For small deformations the glass determines the elastic behaviour of the composite, while for large deformations it is not able to withstand load any more; in this case the PVB-interlayer plays a key role, because still has a load-carrying capacity left

The glass laminate studied in this work consists of three plies of tempered glass and two plies of a polyvinyl butyral (PVB) interlayer.

In this research they have been investigated different thickness lay-up configuration, in order to obtain some design guidelines for the optimization of the thickness structure lay-up. For instance in the Figure 4.7 it is shown a configuration for which the thickness of each glass layer is equal to PVB-interlayer one.

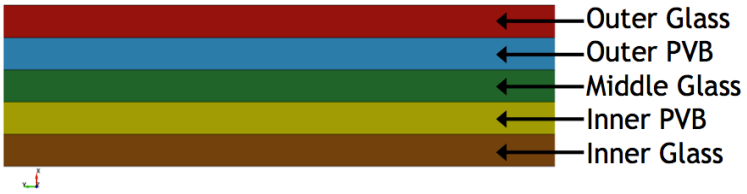

Figure 4.7: Windshield lay-up configuration

4.2.1.1 Glass

The glass is an amorphous, transparent and isotropic material, with characteristics of high brittleness if subjected to both dynamic and static loads. The most prevalent type of glass is soda-lime glass, mainly made up of silica and several minor components. The Table 4.3 shows the glass mechanical properties.

Density	Poisson ratio	Young modulus	Failure strain
$\rho = 2500kg/m^3$	$\nu = 0.22$	$E = 6.895 \cdot 10^{10} N/m^2$	$\epsilon_f = 0.35\%$

Table 4.2: Glass properties

In order to model the glass we considered it to be an elastic-plastic material with an infinitely small plastic part of the $\sigma - \epsilon$ curve so that we could treat it like brittle material. Figure 4.8 shows the stress strain curve, the ultimate tensile stress is equal to rupture stress and yield stress at the same time because of the brittleness of the material.

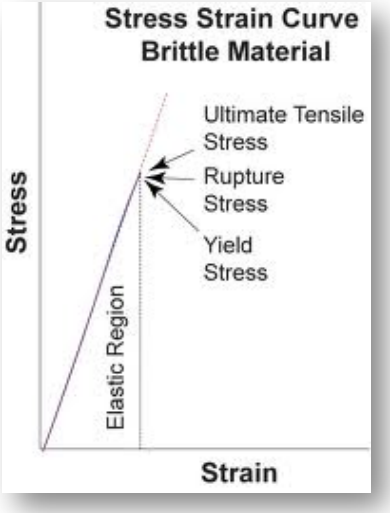

Figure 4.8: Glass $\sigma - \epsilon$ curve

4.2.1.2 Plastic Interlayer

The plastic material is the PVB (Polyvinil butyral) and it is interposed between two layers of glass. It has typical characteristics of a viscoelastic interlayer. This type of material shows good characteristics of strength and transparency, besides allowing a high deformation before the failure and a good tearing strength. The Table 4.3 shows standard literature characteristics of the PVB material.

Density	$\rho = 1076 kg/m^3$
Short-time shear modulus	$G_0 = 0.33 \cdot 10^9 N/m^2$
Long-time shear modulus	$G_\infty = 0.69 \cdot 10^6 N/m^2$
Bulk modulus	$K = 2.0 \cdot 10^6 N/m^2$
Decay coefficient	$\beta = 12.6 s^{-1}$
Failure strain	175%

Table 4.3: PVB-interlayer properties

The interlayer gives a special impact strength to the glass, which can absorb a part of the impact energy thanks to its deformation. Furthermore it avoids the fragmentation of glass by its adhesive property, which could be very dangerous for the occupants of the aircraft. The interlayer is modelled as a linear viscoelastic material, and we can write the shear relaxation behavior (Equation 4.3) [Hermann & Peterson (1968)]:

$$G(t) = G_\infty + (G_0 + G_\infty)e^{-\beta t} \tag{4.3}$$

The plot of this function is shown in Figure 4.9:

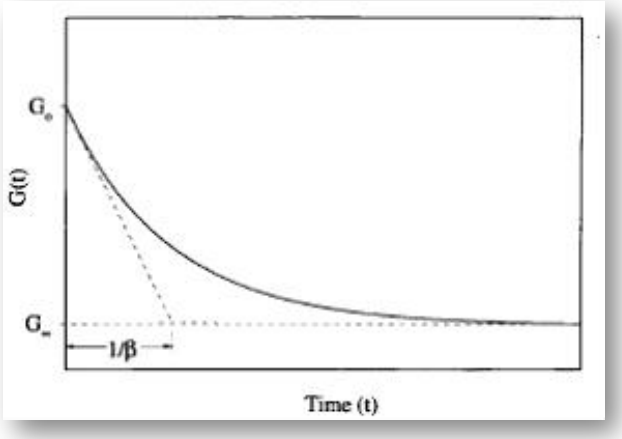

Figure 4.9: PVB shear modulus function

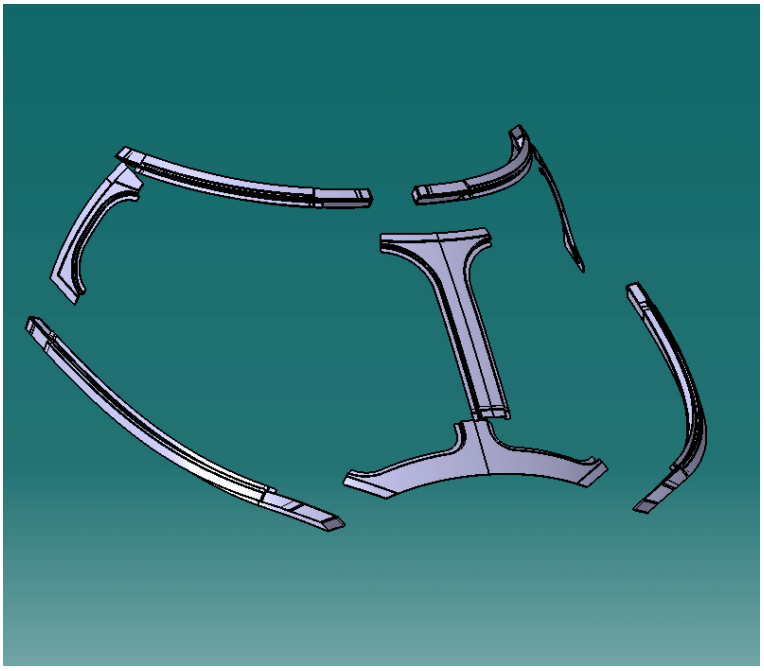

Figure 4.10: Windshield-surround structure

The Young modulus of the interlayer $[E_p]$ and the Poisson coefficient $[\nu_p]$ are defined by equations 4.4 and 4.5:

$$E_p = \frac{9KG_0}{3K + G_0} \tag{4.4}$$

$$\nu_p = \frac{3K - 2G_0}{6K + 2G_0} \tag{4.5}$$

Known K and G_0 it is possible to obtain the properties of the material. About the PVB used for the windshield installation, since the impact duration is in the range of milliseconds, the stress relaxation modulus $G(t)$ of PVB changes very little during impact, so in this short time, PVB behaves like a solid glassy material with $G(t) = G_0$.

4.3 Boundary Conditions

In the Figure 4.10 is shown an exploded view drawing of the windshield surround structure.

The left and right windshield surrounds are composed of aluminum center and lateral beams surrounding the windshield transparencies and are connected to the

surrounding cockpit structure of the aircraft. The Figures 4.11 show the left windshield-surround installation and the sections of the center and lateral beams.

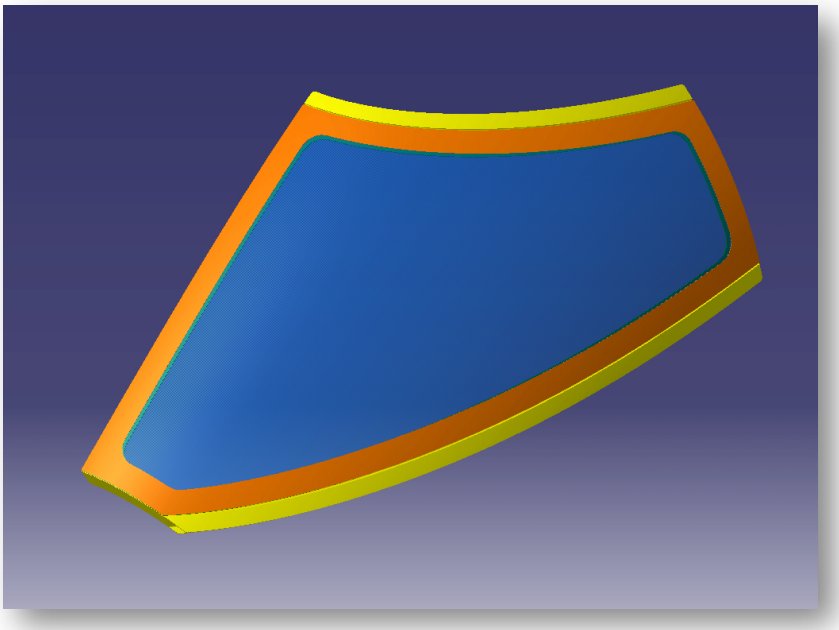

(a) Left Windshield-Surround Structure

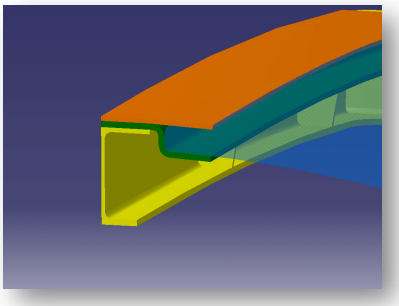

(b) Center Beam

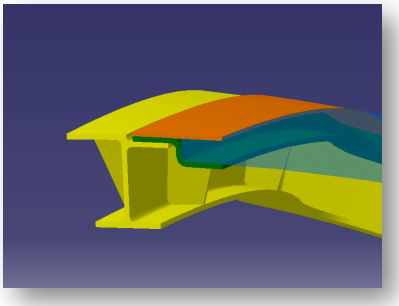

(c) Lateral Beam

Figure 4.11: Windshield-surround installation

It is clear that a key role is played by the joint technique used to stick together the layers of the glass laminate. In fact the choice of a method, like the glue, rather than the bolts, can appreciably affect the performances of the structure in case of both static and dynamic load application. In the figure 4.12 is shown the section of a typical windshield-surround installation by a bolted solution. For instance in this case the presence of bolts could produce a considerable concentration of stress in the holes, with following initial failure and crack propagation of the glass layers subjected to the dynamic load, as well as the birdstrike.

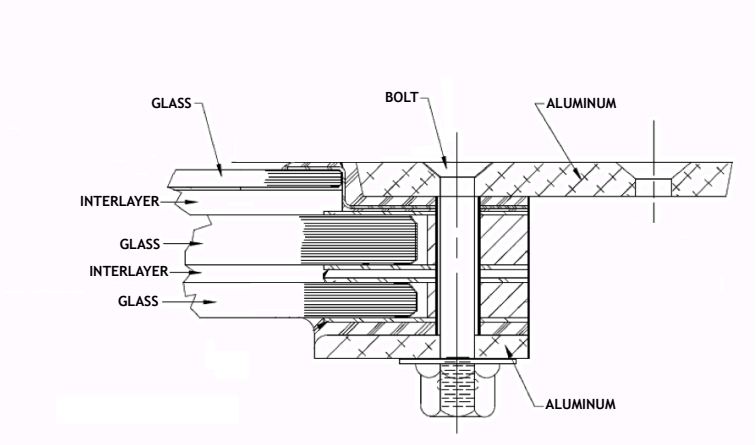

Figure 4.12: Section of windshield-surround installation

Chapter 5

Explicit Non-linear FE Analysis

5.1 Simulation of Birdstrike Event

The explicit Finite Element analysis is a numerical method used to analyse structure made up of materials with behaviour highly non-linear. This is the case that occurs during a crash or impact situations, for which the materials show large deformations, inelastic strains and high strain rates. The method is specifically well suited to the birdstrike phenomenon for which there is an interaction between materials, and generally the geometry changes significantly during the event. In this work the commercial explicit FE software LS-Dyna [Hallquist (2006)] was used for all numerical simulations.

The solver algorithm is based on the choice of the appropriate time-step used in the solution. It is necessary that it is smaller than the time taken for the propagation of a shock wave through the smallest element in the model. The time-step in LS-Dyna is generally limited by stability. Usually, the time step falls during an analysis as elements become deformed, but it is also possible for the time-step to rise. LS-Dyna automatically calculates the largest time-step which can be used without triggering numerical instability; it is not possible to force the code to use a time-step larger than this. It is, however, possible to force the code to use a time-step smaller than the calculated value, either by defining a multiplying factor.

Instability (shown by rapidly rising energy and "floating overflow" error) will occur if the period of any mode of deformation in the model is less than π times the time step.

LS-Dyna checks all elements when calculating the required time-step. For solid, shell and beam the time-step can be estimated roughly using the formula 5.1:

$$\Delta t = 0.9\frac{l}{c} \tag{5.1}$$

where l is the smallest element dimension and c the speed of sound in the material (Equation 5.2). Shell thickness and beam section dimensions are ignored when finding l. Rigid elements are not included.

$$c = \sqrt{\frac{E}{\rho}} \tag{5.2}$$

Typically a resulting time step is of the order of a microsecond or less and it means that to complete a simulation they are required thousands of structural analysis. For example, for the birdstrike phenomenon presented herein spanned approximately 10ms, requiring up to 12 hours of CPU analysis.

5.2 Pre-processing Software Tools

All input and output to the LS-Dyna solver is in the form of text files. There are many pre- and postprocessors software designed to build a finite element model and analyse the results. In this work it has been used the LS-PrePost program [Hallquist (2005)], shown in the Figure 5.1. It is an advanced pre and postprocessor that is delivered free with LS-DYNA. The user interface is designed to be both efficient and intuitive and it runs on different operative systems.

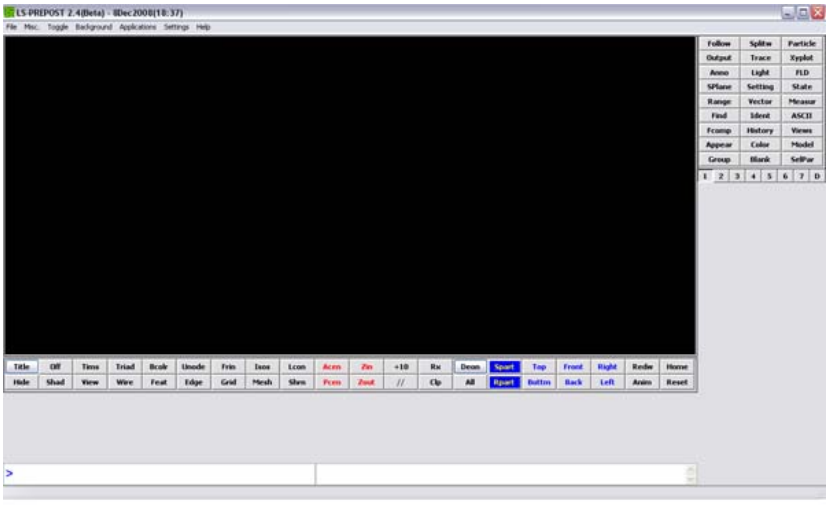

Figure 5.1: LS-PrePost software

This software tool includes functionality to import and simplify CAD geometry, mesh with finite elements, and apply loads and constraints. The tool allows the user to submit an analysis to LS-Dyna, to import the results and show them graphically (animation, fringe plotting and curve plotting).

5.3 Windshield FE Analysis

In the present work before to perform the numerical simulation of the full-scale windshield model, it was carried out a preliminary parametric numerical analysis of a simplified, but realistic, structure subjected to the birdstrike phenomenon. This simplified model is a $1m \times 1m$ square flat plate made up of the same materials and lay-up configuration of the full-scale structure.

Both the square plate and the full-scale windshield are glass laminate, composed of 3 layers of glass and 2 layers of PVB-interlayer. In the Figure 5.2 is shown an exploded view of the FE target square model. The numerical model consists of 5 plies and each of these was modeled by default 3D eight-nodes brick elements. The element size was approximately $5mm$ and the mesh is uniform throughout the thickness.

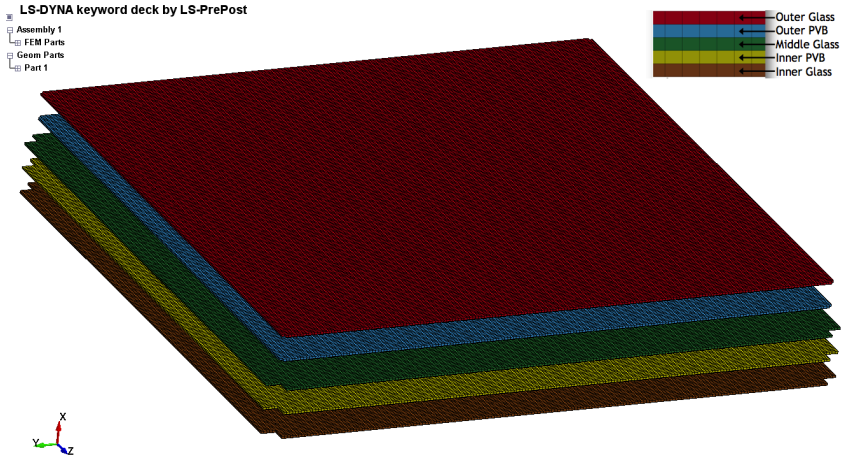

Figure 5.2: Square plate FE model

As well as the simplified square plate model, it was applied the same procedure for the FE discretization process of the full-scale windshield structure. Numerically each layer of the laminate was modeled by solid elements, but because of the curvature of the windshield it was modeled by both eight-nodes and six-nodes elements. In the Figure 5.3 is shown the FE model of the left windshield panel.

In the Table 5.1 is reported the thickness of each layer of the real glass laminate. It must take into account that the averaged thickness of a glass ply is twice as much as the interlayer one.

About the material modeling the glass ply was modeled by a bilinear elastic-plastic material law with negligible plastic region using the LS-Dyna MAT-PLASTIC-

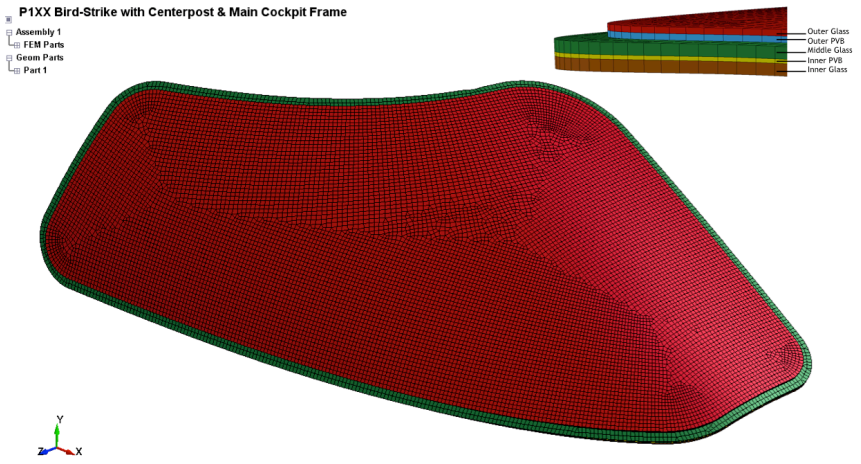

Figure 5.3: Full-scale left windshield FE model

Outer Glass	Outer PVB	Middle Glass	Inner PVB	Inner Glass
$3.0mm$	$3.0mm$	$6.5mm$	$2.5mm$	$5.0mm$

Table 5.1: Thickness distribution of the full-scale model

KINEMATIC Card, this model is suited to model isotropic and kinematic hardening plasticity with the option of including rate effects.

Whereas the PVB-interlayer ply was modeled by a viscoelastic material law using the LS-Dyna MAT-VISCOELASTIC Card.

5.4 Bird Model

The SPH approach, implemented in the explicit finite element code LS-Dyna, was used for the modeling of the bird. The numerical model consists of 28620 SPH nodes with an average distance between two nodes of $5mm$, as shown in the Figure 5.4.

In this work in according to the International Certification Standards every simulation is performed with a bird impact velocity equal to $155m/s$.

The appropriate substitute bird has a density of $950kg/m^3$ and a porosity of 10%, i.e. it is composed of 90% of water and 10% of air.

Regardless of the modeling method chosen, a fluid dynamic material model was used for the bird modeling. In particular it was defined a material constitutive model to relate $\Delta\sigma$ to $\Delta\epsilon$ and an equation of state to relate Δp to ΔV, where

$\Delta\sigma$ is the variation of the stress

$\Delta\epsilon$ is the variation of the strain

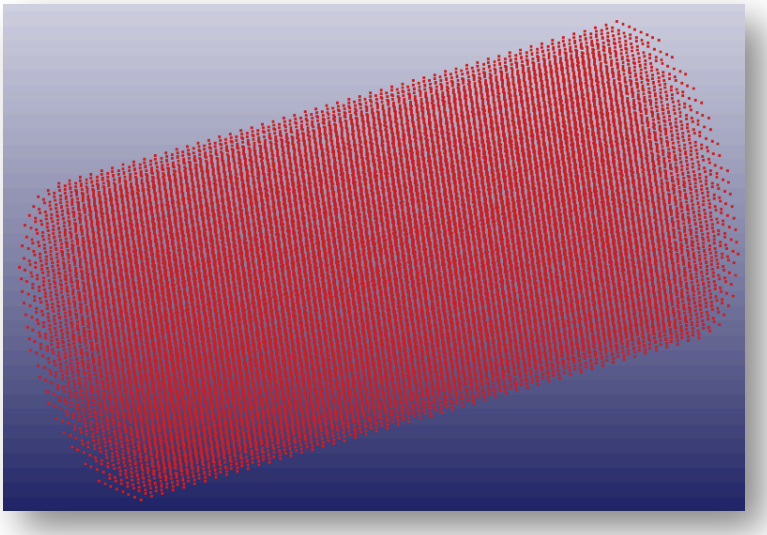

Figure 5.4: Bird SPH Model

Δp is the variation of the pressure

ΔV is the variation of the pressure

The MAT-NULL Card calculates the pressure p from a specified tabulated equation of state 5.3, defined by the LS-Dyna EOS-TABULATED Card.

$$p = C(\epsilon_v) \tag{5.3}$$

where ϵ_v is the volumetric strain given by the natural logarithm of the relative volume V.

The values of the equation of state parameters are shown in the Table 5.2.

	1	**2**	**3**	**4**	**5**	**6**	**7**	**8**	**9**	**10**
ϵ_V	0.000	−0.105	−0.118	−0.128	−0.137	−0.154	−0.169	−0.183	−0.195	−0.217
$C[Pa]$	0.000	$2.37 \cdot 10^8$	$4.25 \cdot 10^8$	$5.86 \cdot 10^8$	$7.27 \cdot 10^8$	$9.72 \cdot 10^8$	$1.18 \cdot 10^9$	$1.37 \cdot 10^9$	$1.54 \cdot 10^9$	$1.84 \cdot 10^9$

Table 5.2: Tabulated equation of state

5.5 Boundary Conditions

An important part of this analysis is the modeling of the surround structures and the definition of its interaction with the windshield.

The Figures 5.5(a) and 5.5(b) show the FE model of the C-beam that surrounding the square flat plate model and its section, whereas the Figure 5.5(c) shows the section of a typical windshield-surround installation.

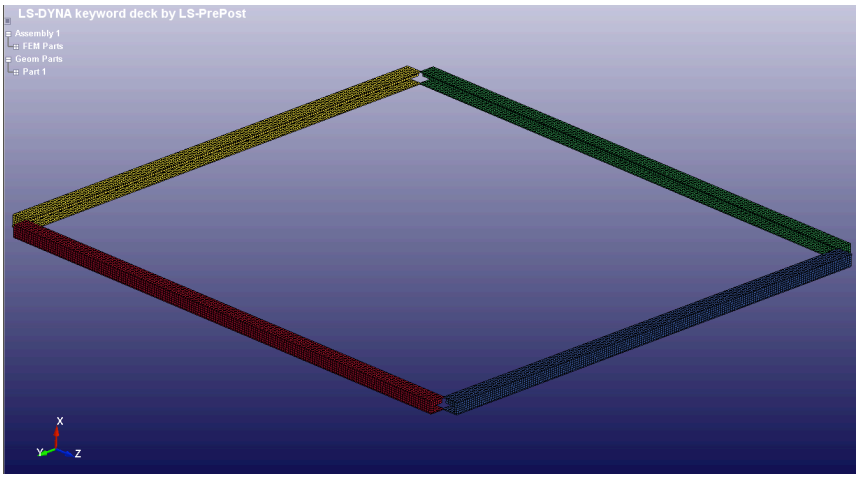

(a) Surround Structure

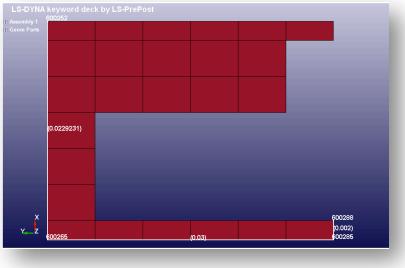

(b) C-Beam Section

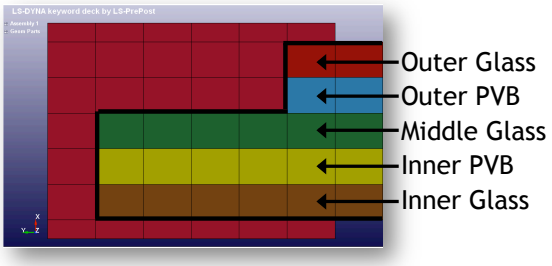

(c) Windshield-Surround Interaction

Figure 5.5: Windshield-surround installation for the simplified model

As well as for the laminate layers the surround structure was modeled by eight-nodes brick elements. In this phase about the interaction between surround and laminate it has not been considered the presence of the bolts, but a simple plug approach. In the next section it will be a deeper description of the contacts definition between the windshield and the surround. On the first approximations the boundary conditions are defined fixing every translational and rotational degree of freedom of the surround contour.

It was used the same FE procedure for the modeling of full-scale surround structure, taking into account the curvature of the beams again. The Figure 5.6(a) shows the FE model of the surround structure, whereas in the Figure 5.6(b) is shown its exploded view, from which is possible to see the groove of the lower part of the surround where the laminate is plugged.

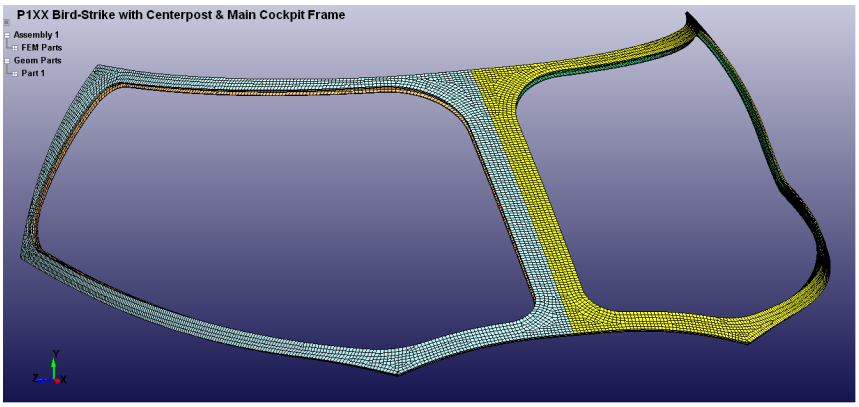

(a) FE Model

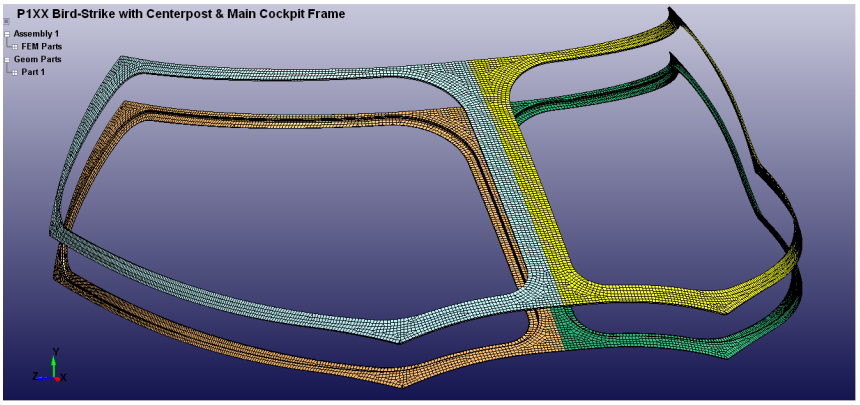

(b) Exploded View

Figure 5.6: Full-scale surround structure

The Figure 5.7 shows the main structural components about which the cockpit structure is composed, in detail there is a main frame, 20 surround frames, a center beam and a bulk head. It was used a different modeling approach for each component, taking into account its particular structural function and the expectable impact response. As shown in the Figure 5.8, the main frame was modeled by 1D beam element fixing only the two bottom nodes. The center beam was modeled by 1D beam element too, and it is connected to the main frame, the surround frames and the surround structure. Both the surround frames and the bulk head are modeled by avoiding the translational degree of freedom along the y- and z-directions, perpendicular to the bird impact direction x, by the BOUNDARY-SPC-SET Card.

Furthermore the connection between the main frame and the rear part of the surround structure was simulated by the CONSTRAINED-INTERPOLATION Card. With this constrain type, the motion of a single dependent node is interpolated from the motion of a set of independent nodes. It is useful for the load redistribution of a load, which can be either a translational force or moment, applied to the dependent node to the surrounding independent nodes.

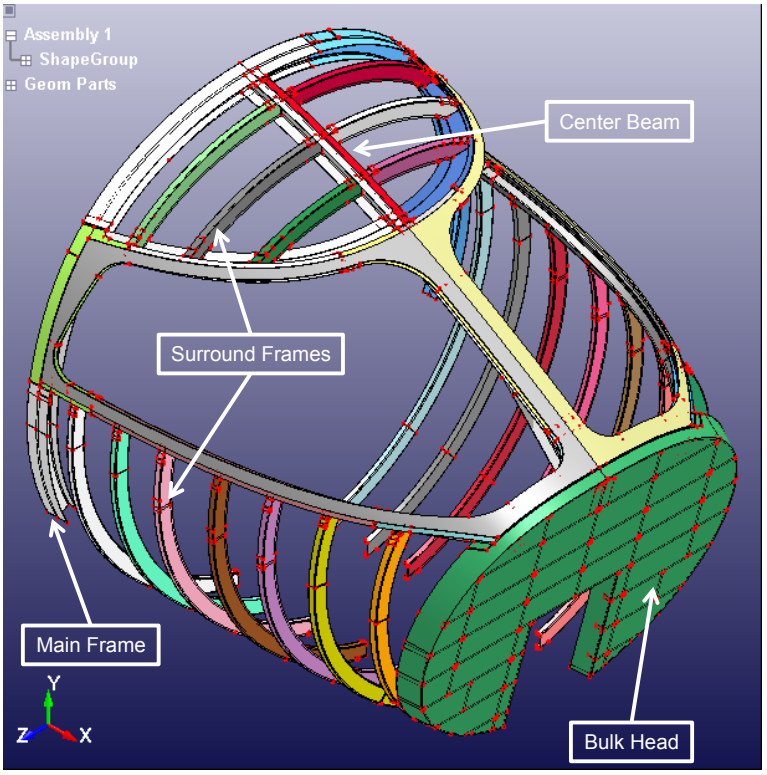

Figure 5.7: Geometry of the cockpit structures

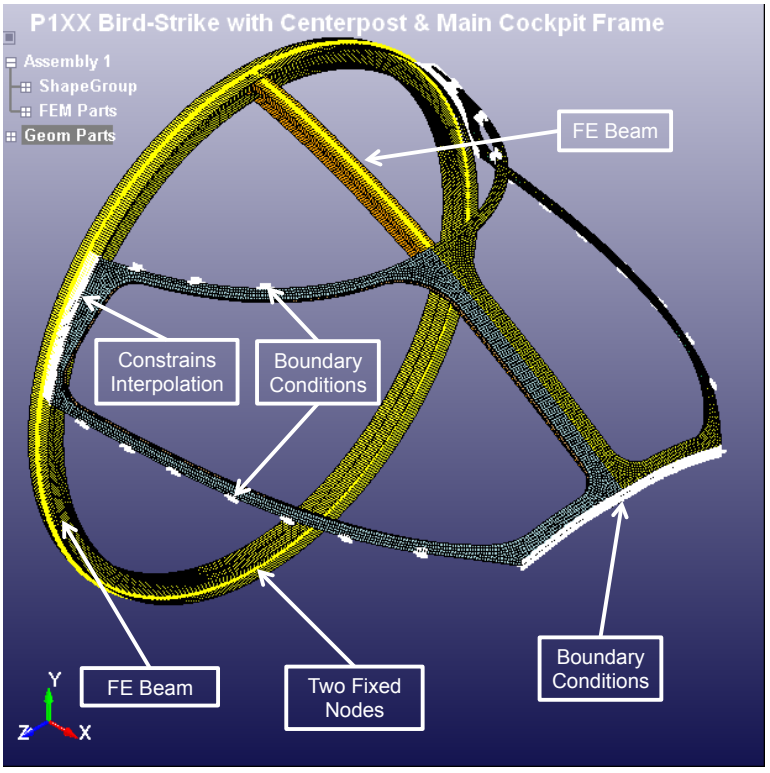

Figure 5.8: FE model of the cockpit structures

5.6 Contact Modelling

The Figures 5.9 and 5.10 show the whole FE models for both birdstrike cases analysed, the simplified square plate model and the full-scale windshield structures. In order to obtain an adequate simulation of the transfer load, the interaction between the bird SPH nodes and the structure finite elements was modeling by a contact algorithm. Furthermore it was also defined a contact for each couple of side layers of the laminate, and a contact between the whole laminate and the surround structure.

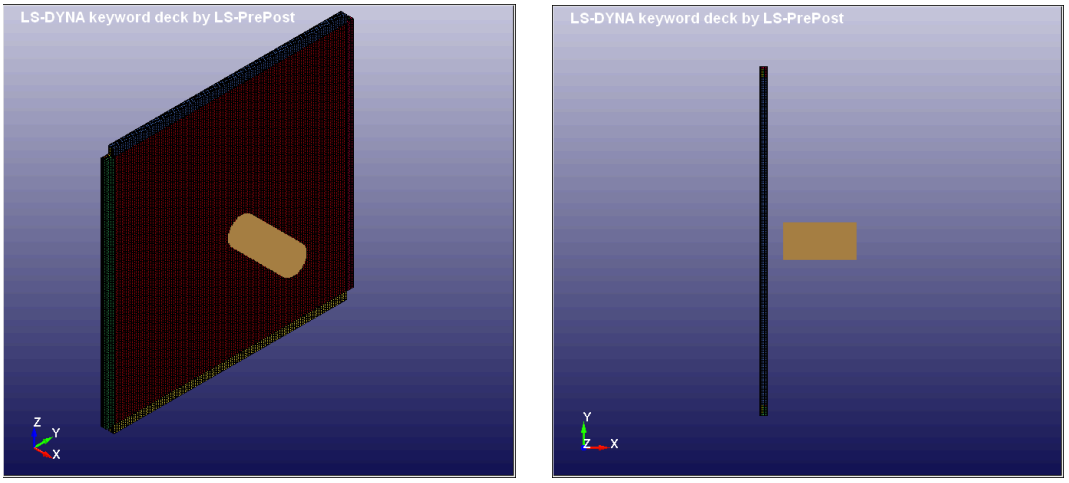

(a) Iso view (b) Lateral View

Figure 5.9: Simplified square plate vs Bird - FE model

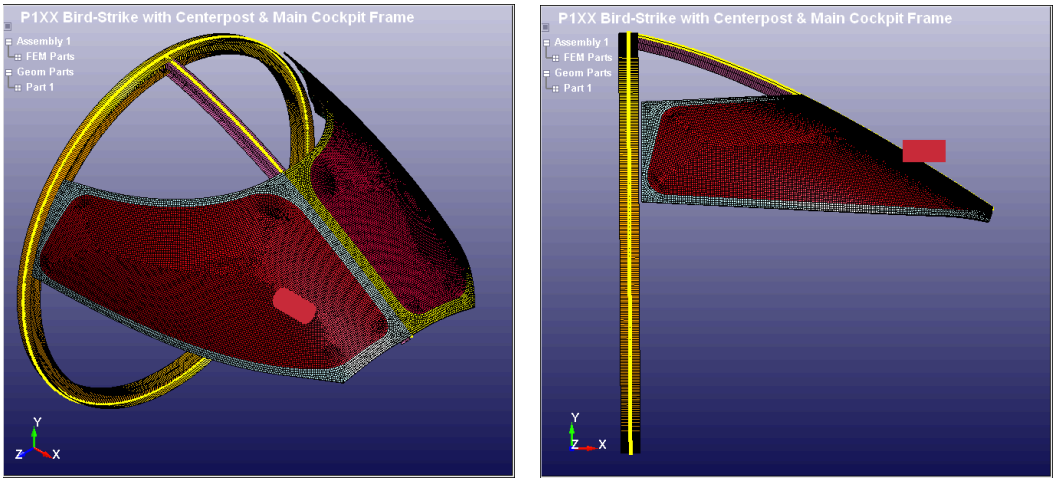

(a) Iso view (b) Lateral View

Figure 5.10: Full-scale windshield vs Bird - FE model

Contact treatment forms an integral part of many large deformation problems. Accurate modeling of contact interfaces between bodies is crucial to the prediction

capability of the finite element simulations. LS-DYNA offers a large number of contact types.

A contact is defined by identifying (via parts, part sets, segment sets, and/or node sets) what locations are to be checked for potential penetration of a "slave" node through a "master" segment, as shown in the Figure 5.11. A search for penetrations is made every time-step.

In this work it was used the penalty-based contact, for which when a penetration is found a force proportional to the penetration depth is applied to resist, and ultimately eliminate the penetration. All contacts defined are based on the one-way treatment. The "one-way" term in one way contact is used to indicate that only the user-specified slave nodes are checked for penetration of the master segments.

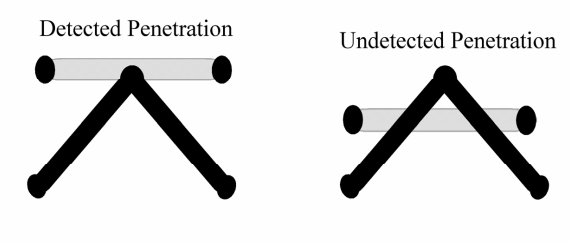

Figure 5.11: Contact penetration search

Contact surfaces are defined using sets, which can contain "segments" (3- or 4-node element faces), nodes, shell elements, or parts. If the set contains parts, all the elements made of those parts are included in the contact. Generally, two sets are defined, the slave and the master. Any entity in the slave set can contact any entity in the master set and vice versa.

In order to model the transfer load between the bird and the target structure, it was used a CONTACT-AUTOMATIC-NODES-TO-SURFACE Card (Figure 5.12), for which each slave node is checked for penetration through a master segment.

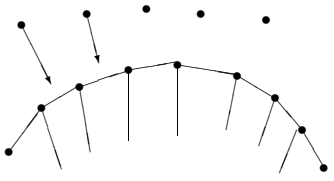

Figure 5.12: Contact automatic nodes to surface

Instead a CONTACT-TIED-SURFACE-TO-SURFACE Card (Figure 5.13) was used to model the interaction between two side laminate plies. In tied contact types, the slave nodes are constrained to move with the master surface, i.e. the tied contact surfaces "glue" the slaves to the masters. The slave and master segments should initially be coplanar.

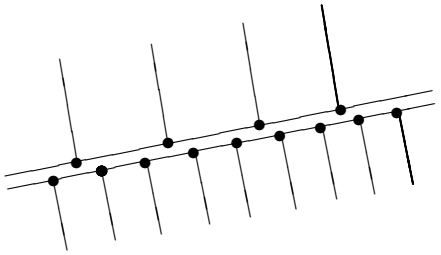

Figure 5.13: Contact tied surface to surface

At the beginning of the simulation, the nearest master segment for each slave node is located based on an orthogonal projection of the slave node to the master segment. If the slave node is deemed "close" to the master segment based on established criteria, the slave node is moved to the master surface. Of the two surfaces in contact, the coarser one should be defined as the master. Only translational degrees of freedom are affected from this type of contact and the slave nodes are effectively "pinned" to the master surface.

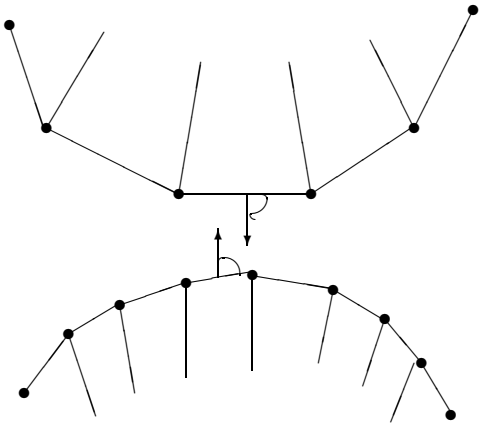

Figure 5.14: Contact automatic surface to surface

Finally the contact between the whole laminate and the surround structure it was modeled by the CONTACT-AUTOMATIC-SURFACE-TO-SURFACE Card (Figure 5.14), defining the entire glass laminate as the slave entity and the surround as the master one.

About the contact output, there are numerous output files pertaining to contact which can be written by LS-Dyna, and the LS-PrePost can read these output files and plot the results. The most common contact-related output file, RCFORC, is produced by including a DATABASE-RCFORC Card in the input deck file. RCFORC is an ASCII file containing resultant contact forces for the slave and master sides of each contact interface. The forces are written in the global coordinate system. By including a DATABASE-SLEOUT Card, contact interface energies are written to the ASCII output file SLEOUT.

Chapter 6

Results and Discussion

6.1 Birdstrike vs the Square Windshield Model

This section presents the numerical results of the bird impact on the simplified square plate windshield, as shown in the Figure 6.1. As mentioned in the previous sections, a cylinder with length-to-diameter ratio of 2 was predefined for the current $1.8kg$ ($4lb$) bird model, with a diameter of $0.106m$. This soft projectile traveling with an incident velocity of $155m/s$ striking the $1m \times 1m$ flat target with and impact angle of 90° respect to the horizontal x-axis. In the Figure 6.2 it is shown the lay-up configuration of the windshield. The thickness of each ply is equal to $4mm$ for a total thickness of $20mm$

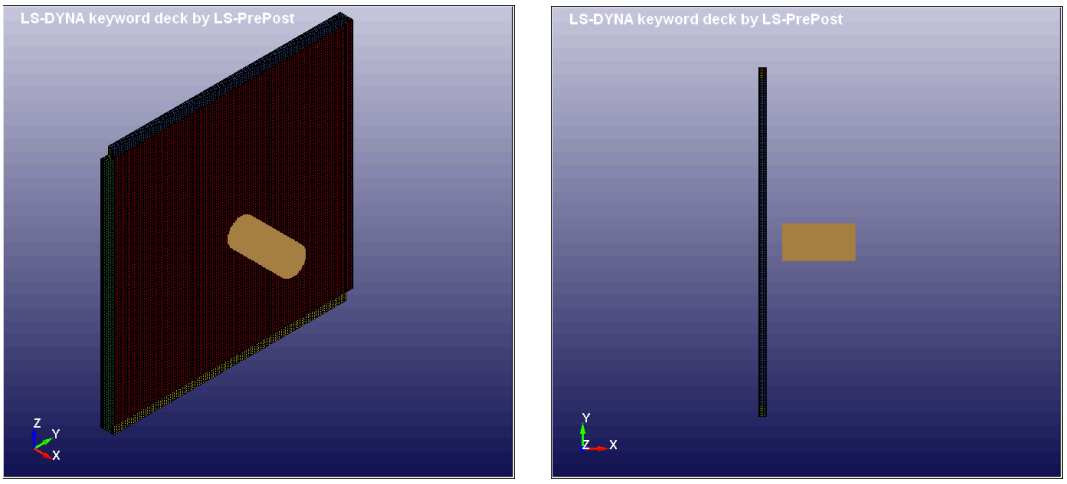

(a) Iso view (b) Lateral view

Figure 6.1: Birdstrike vs Simplified square windshield

Every analysis was performed on a 8-processor HP Workstation machine with a WIN64 version of LS-Dyna3D (V971), taking approximately 12 h of wall clock time

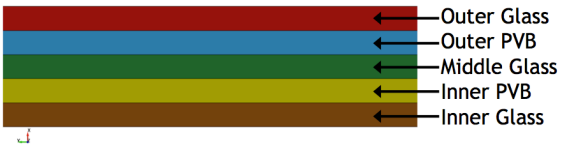

Figure 6.2: Thickness lay-up configuration

to complete the numerical analysis. It was set the output interval at $50\mu s$ for a total event time of 0.005 s, with producing of an output database of more than $4GB$ size.

To better understand the behavior of the plate during the impact, in the following pages is presented a series of plots about the evolution of the phenomenon and its main physical characteristics.

The Figures 6.3 and 6.4 show a sequence plots about the deformation behaviour of the impacted panels, from the moment of the impact until the bird is completely squashed into the panel. During the first 2 milliseconds it is happens the transfer of the almost 90% of the bird load to the plate, with a consistent deformation of the center of the model, correspondent to the bird impacted zone. Instead during the following 3 milliseconds it can see an expansion of the plate deformation from the center zone to the plate edges, because of the presence of the PVB-interlayer. Furthermore it is clearly visible the deformation of the bird during the impact, and its squashing into the windshield is adequately simulated by the SPH modeling approach.

In the Figures 6.5 and 6.6 are reported the failure propagations of the each layer of the glass laminate. About the glass plies it can already see a crack initiation after just 1 millisecond, and a propagation of this from the center to the angles of the plate. As it was expected, the failure of the glass layers is more noticeable for the inner glass layer, because of its more intensive bending. It must take into account that in this work it was not investigated the influence of the mesh on the failure propagation. As shown, the outer PVB-interlayer ply does not present any failure, as well as the inner one.

In the Figure 6.7 some step-by-step contour plots of the von Mises stress and plastic strain are shown. Again in this case it can see that in the beginning of the impact only the center zone plate is involved in the phenomenon with a maximum value of the von Mises stress around $2.8 \cdot 10^8 Pa$. In addition after 1.5 millisecond when there is an evident failure of the plate that propagates to the bottom right corner, only the intact zone of the plate still has a load-carrying capacity left.

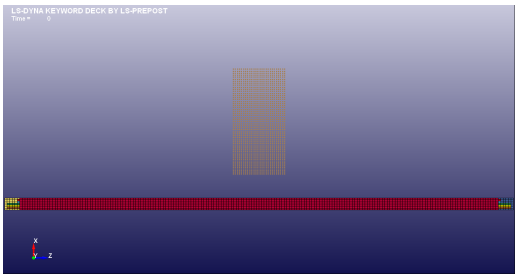

(a) t=0.0000 sec - Lateral View

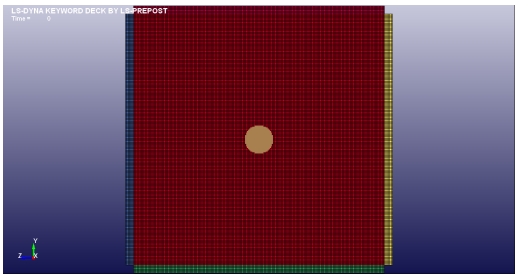

(b) t=0.0000 sec - Front View

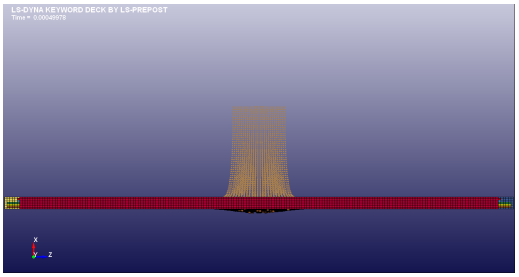

(c) t=0.0005 sec - Lateral View

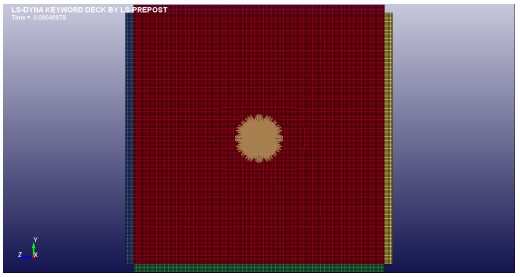

(d) t=0.0005 sec - Front View

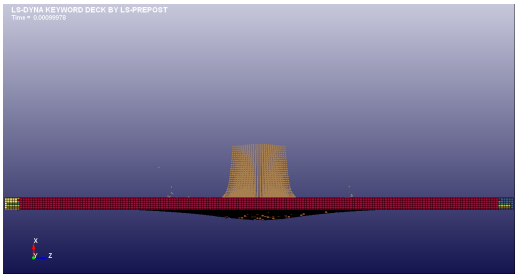

(e) t=0.0010 sec - Lateral View

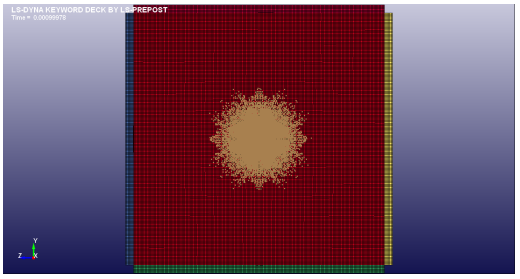

(f) t=0.0010 sec - Front View

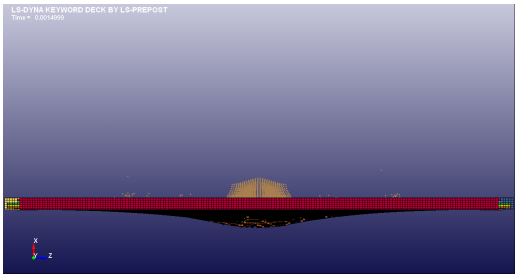

(g) t=0.0015 sec - Lateral View

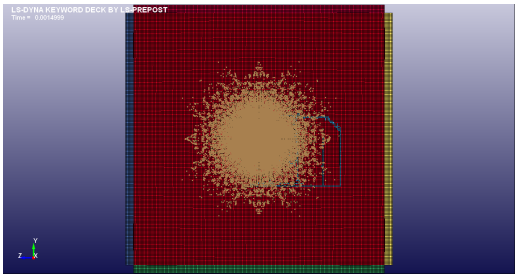

(h) t=0.0015 sec - Front View

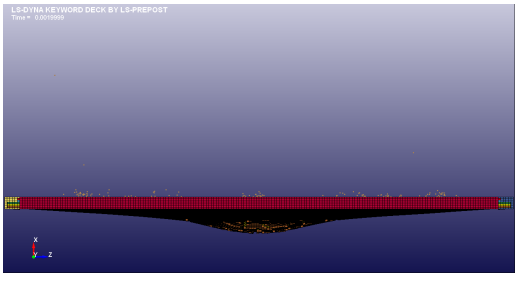

(i) t=0.0020 sec - Lateral View

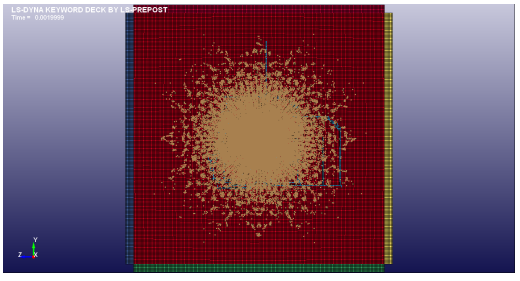

(j) t=0.0020 sec - Front View

Figure 6.3: Sequence of plate deformation between 0-0.0020 sec

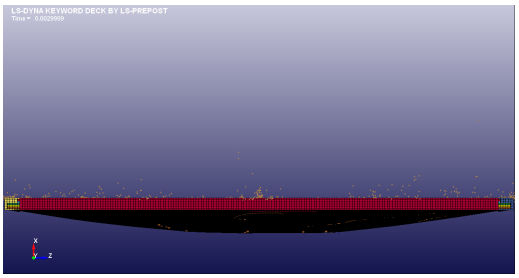

(a) t=0.0030 sec - Lateral View

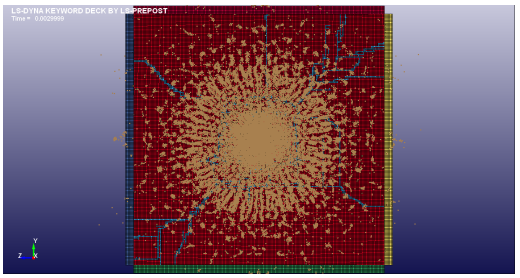

(b) t=0.0030 sec - Front View

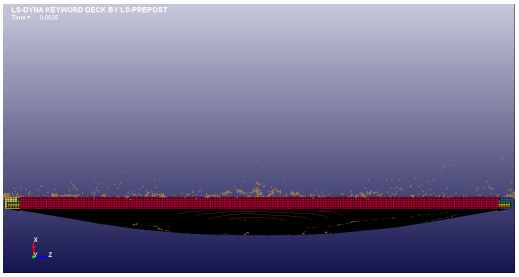

(c) t=0.0035 sec - Lateral View

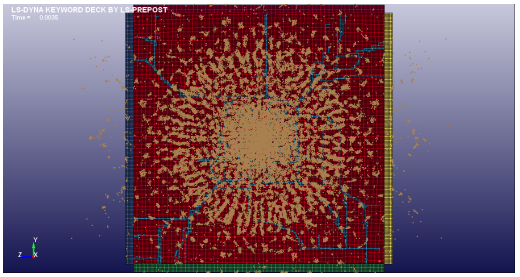

(d) t=0.0035 sec - Front View

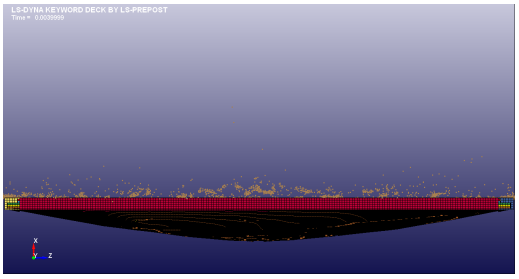

(e) t=0.0040 sec - Lateral View

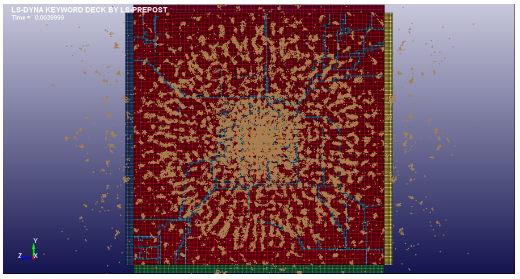

(f) t=0.0040 sec - Front View

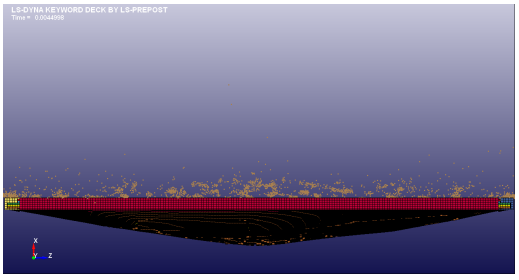

(g) t=0.0045 sec - Lateral View

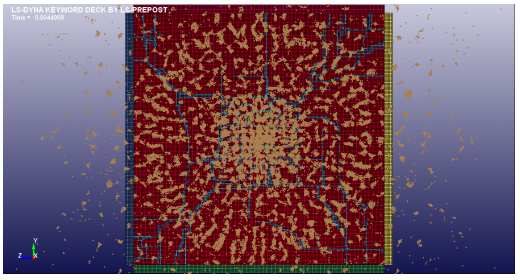

(h) t=0.0045 sec - Front View

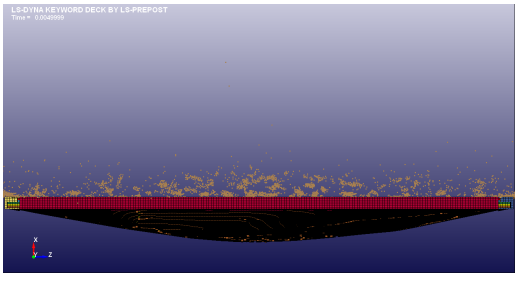

(i) t=0.0050 sec - Lateral View

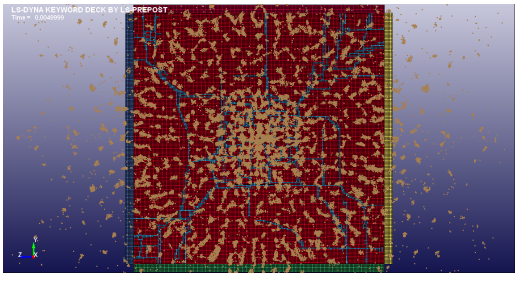

(j) t=0.0050 sec - Front View

Figure 6.4: Sequence of plate deformation berween 0.0030-0.0050sec

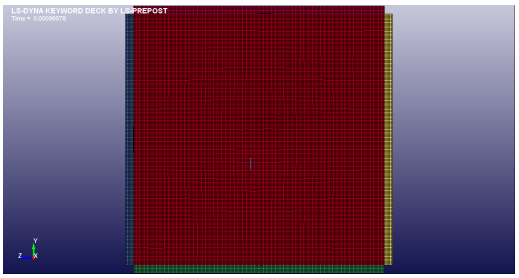

(a) t=0.0010 sec - Outer Glass

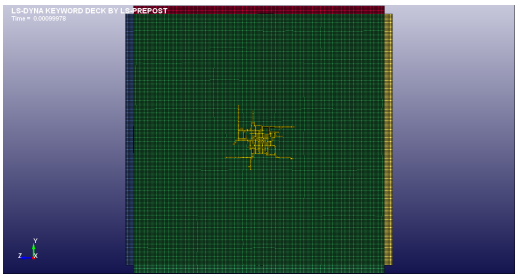

(b) t=0.0010 sec - Middle Glass

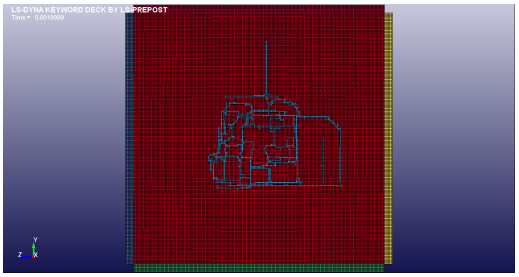

(c) t=0.0020 sec - Outer Glass

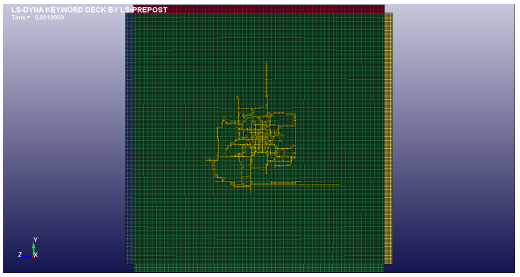

(d) t=0.0020 sec - Middle Glass

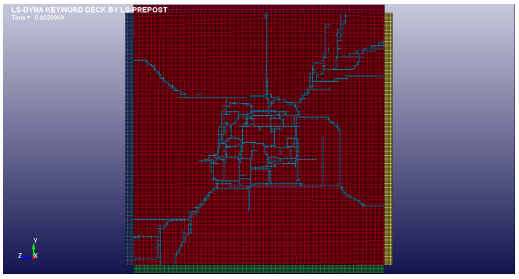

(e) t=0.0030 sec - Outer Glass

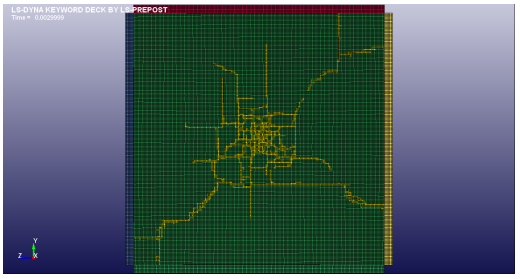

(f) t=0.0030 sec - Middle Glass

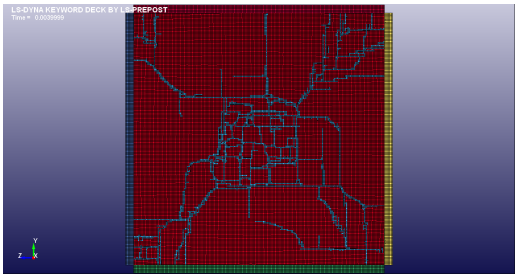

(g) t=0.0040 sec - Outer Glass

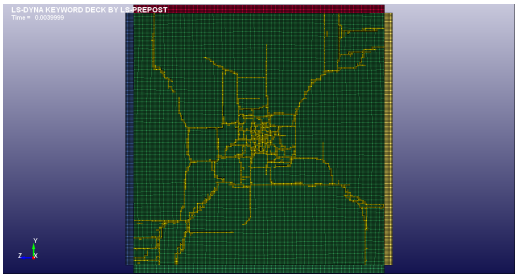

(h) t=0.0040 sec - Middle Glass

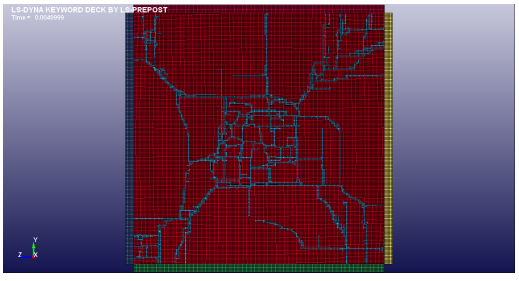

(i) t=0.0050 sec - Outer Glass

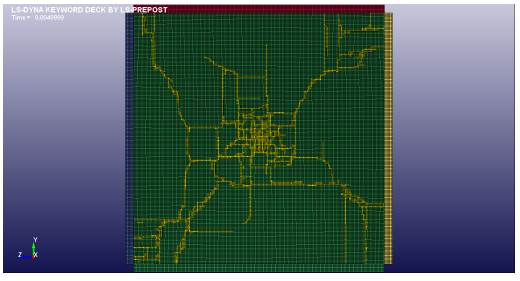

(j) t=0.0050 sec - Middle Glass

Figure 6.5: Failure propagation of the Outer and Middle Glass

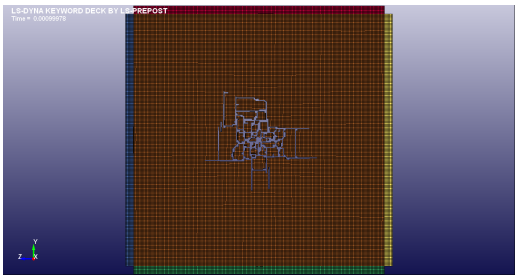

(a) t=0.0010 sec - Inner Glass

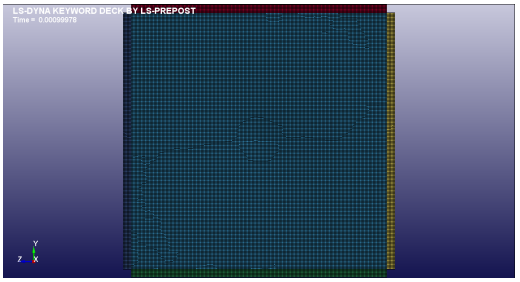

(b) t=0.0010 sec - Outer PVB

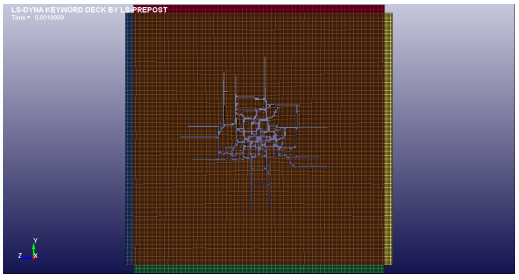

(c) t=0.0020 sec - Inner Glass

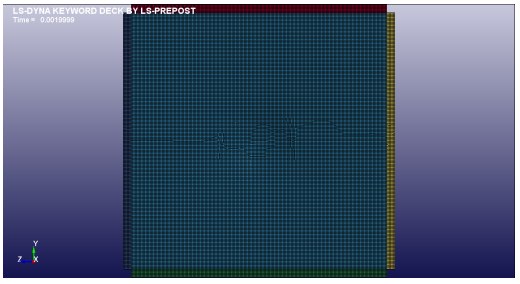

(d) t=0.0020 sec - Outer PVB

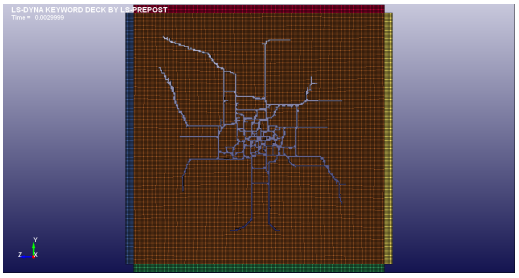

(e) t=0.0030 sec - Inner Glass

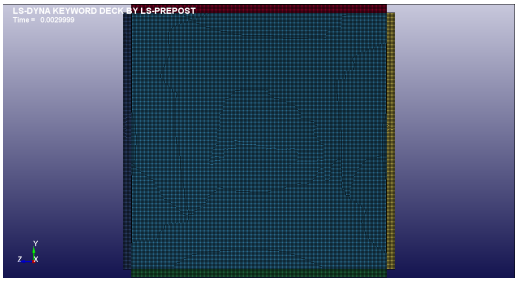

(f) t=0.0030 sec - Outer PVB

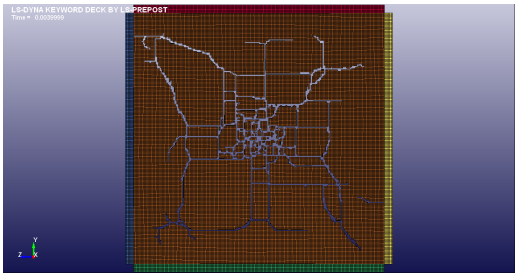

(g) t=0.0040 sec - Inner Glass

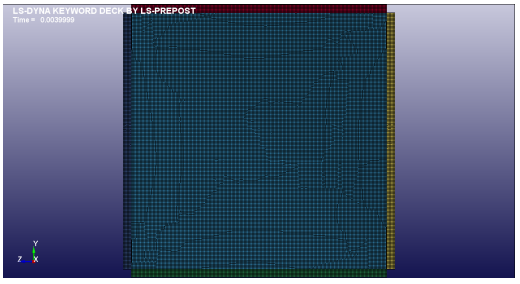

(h) t=0.0040 sec - Outer PVB

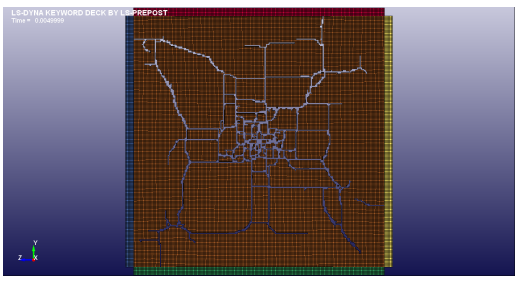

(i) t=0.0050 sec - Inner Glass

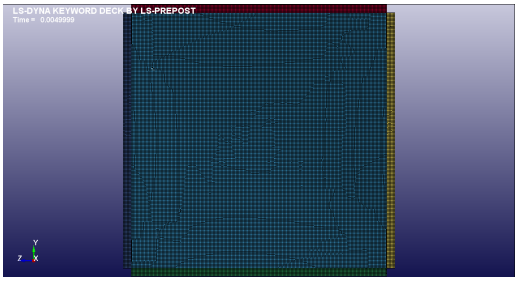

(j) t=0.0050 sec - Outer PVB

Figure 6.6: Failure propagation of the Inner Glass and Outer PVB

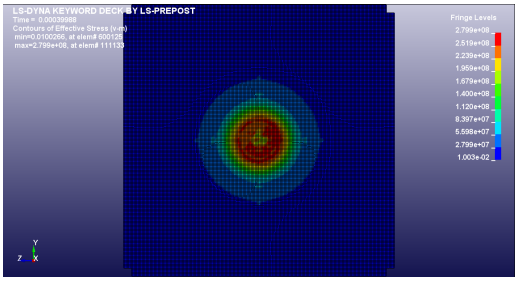

(a) t=0.0004 sec - Von Mises Stress

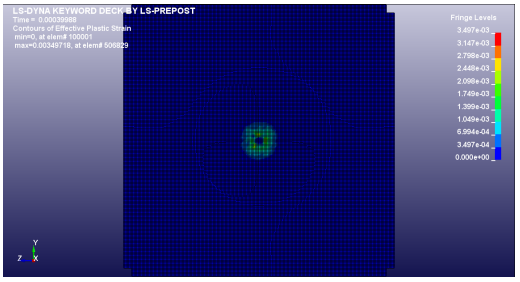

(b) t=0.0004 sec - Plastic Strain

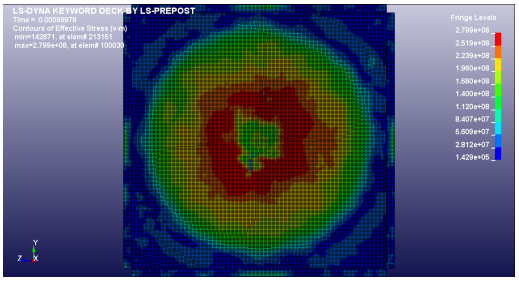

(c) t=0.0010 sec - Von Mises Stress

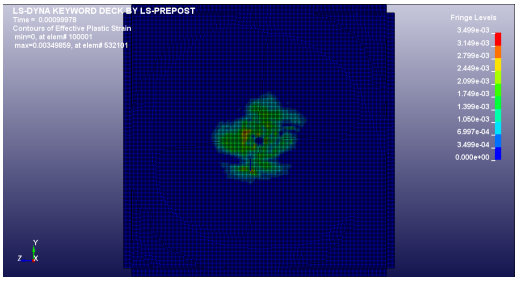

(d) t=0.0010 sec - Plastic Strain

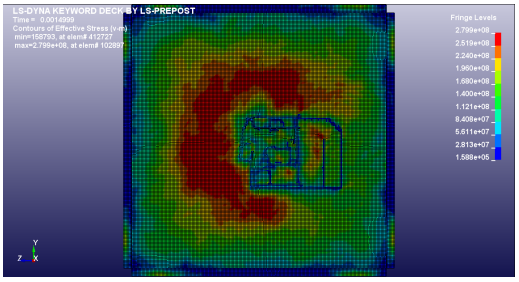

(e) t=0.0015 sec - Von Mises Stress

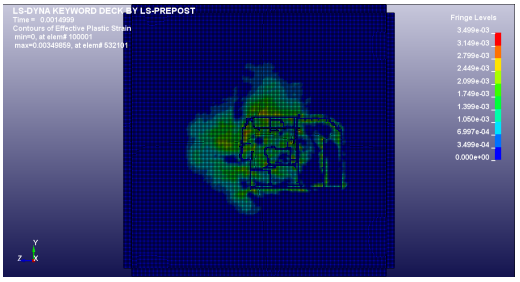

(f) t=0.0015 sec - Plastic Strain

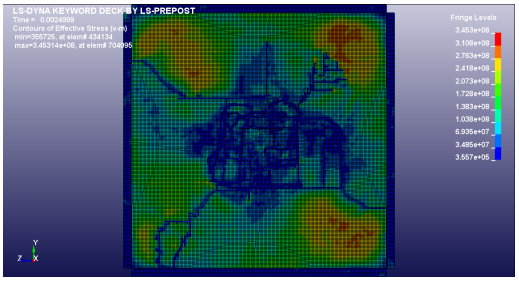

(g) t=0.0025 sec - Von Mises Stress

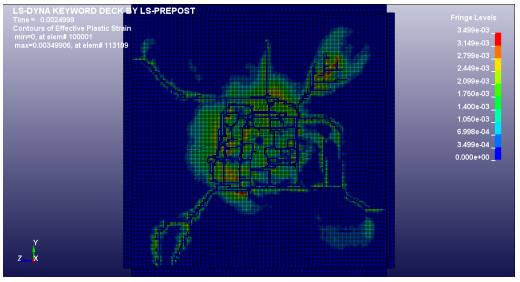

(h) t=0.0025 sec - Plastic Strain

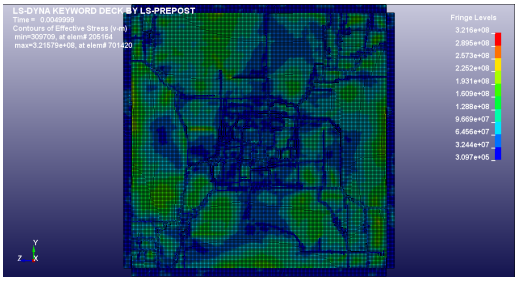

(i) t=0.0050 sec - Von Mises Stress

(j) t=0.0050 sec - Plastic Strain

Figure 6.7: von Mises Stress e Plastic Strain

In the Figure 6.8 the resultant displacement for the central element (the element of the impact) of the plate is reported. At the end of the simulation it presents a maximum value of $\simeq 6.7mm$.

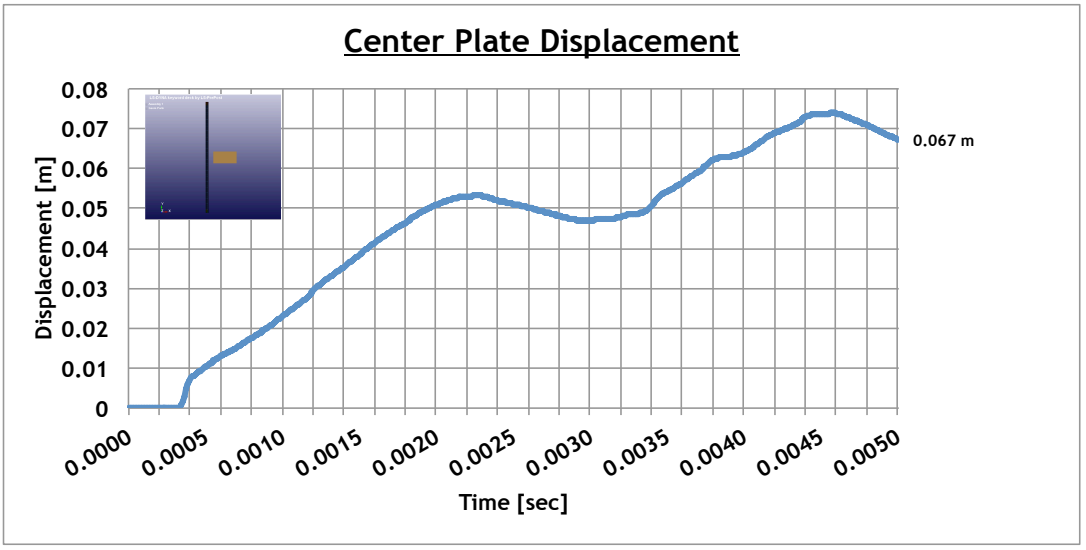

Figure 6.8: Central element displacement

The reaction forces are calculated normally to the section plane along the x-axis (the impact direction) for each model at the top of the plate. The Figure 6.9 depicts the time-history of the interfacial resultant contact force between the bird and the external face of the target plate, and it presents a maximum value of $\simeq 1.41 \cdot 10^6 N$.

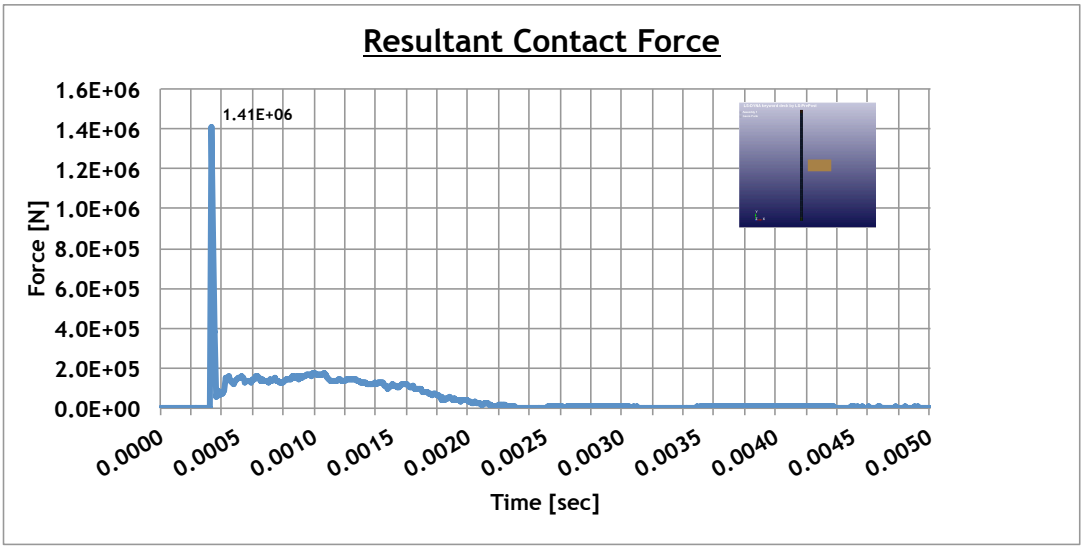

Figure 6.9: Resultant contact force

In order to perform a check on the analysis it can be useful to carry out a balance of the energy data. The following Equation 6.1 should hold at all times during an analysis:

$$E_{kin} + E_{int} + E_{hg} + E_{si} + E_{rw} + E_{damp} = E_{kin0} + E_{int0} + W_{ext} \tag{6.1}$$

where

E_{kin0} : Initial Kinetic Energy

E_{int0} : Initial Internal Energy

W_{ext} : External Work

E_{kin} : Kinetic Energy

E_{int} : Internal Energy

E_{hg} : Hourglass Energy

E_{si} : Sliding Interface Energy

E_{rw} : Rigid Wall Energy

E_{damp} : Damping Energy

In this birdstrike analysis there is not rigid wall and damping energy, the sliding energy is negligible and the initial energy is only represented by kinetic energy of the bird, given by

$$E_{kin0} = \frac{1}{2}mv^2 = 21622.5Joule \tag{6.2}$$

In order to define the hourglass energy, it is necessary focusing on the difficult to control the zero energy modes associated to the deformation of the one-point integration elements. Undesirable hourglass modes (Figure 6.10) tend to have periods that are typically much shorter than the periods of the structural response, and they are often observed to be oscillatory. However, hourglass modes that have periods that are comparable to the structural response periods may be a stable kinematic component of the global deformation modes and must be admissible. One way of resisting undesirable hourglassing is with a viscous damping or small elastic stiffness capable of stopping the formation of the anomalous modes but having a negligible affect on the stable global modes.

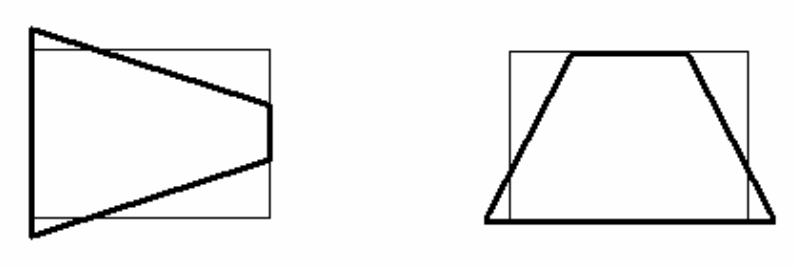

Figure 6.10: Hourglass modes of under-integrated solid elements

Since the hourglass deformation modes are orthogonal to the strain calculations, work done by the hourglass resistance is neglected in the energy equation. This may lead to a slight loss of energy; however hourglass control is always recommended for the under integrated solid elements.

LS-DYNA has various algorithms for inhibiting hourglass modes. The default algorithm (type 1) is generally not the most effective algorithm. In this work it was used the hourglass option ♯6, based on elastic constants and an assumed strain field, it produces accurate coarse mesh bending results for elastic material (like glass) when is set to 1.0. In absence of contact friction, like in our case, an amount of hourglass energy equal to 10% of peak internal energy might be considered acceptable for the simulation.

The time-history of the internal energy for each layers of the laminated glass is reported in the Figure 6.11. The outer glass, on which the bird impacts directly, is the ply that absorbs the bigger amount of the bird impact energy, but contrarily to what you might think, after that the two PVB layers turn out to be very efficient about the energy absorbing, because of their plastic behavior.

In the following figures 6.12, 6.13 and 6.14 are shown the time-histories of the internal energy associated, respectively, to the whole glass laminate, to the surround structure and to the bird. As it can see that the total internal energy of the whole glass laminate is just the sum of the energy associated to each layer, the internal energy correspondent with deformation of the surround structure is negligible, while the most consistent amount of internal energy is just related to the "deformation" of the bird, or to be more exact associated with its squashing onto the panel.

The time-history of the hourglass energy in function of time is reported in the Figure 6.15, it is equal to 10% of peak of the total internal energy and therefore it may be considered acceptable for the analysis.

The check on the total energy, shown in the Figure 6.16, ensures the accuracy of the results obtained by the birdstrike numerical analysis performed.

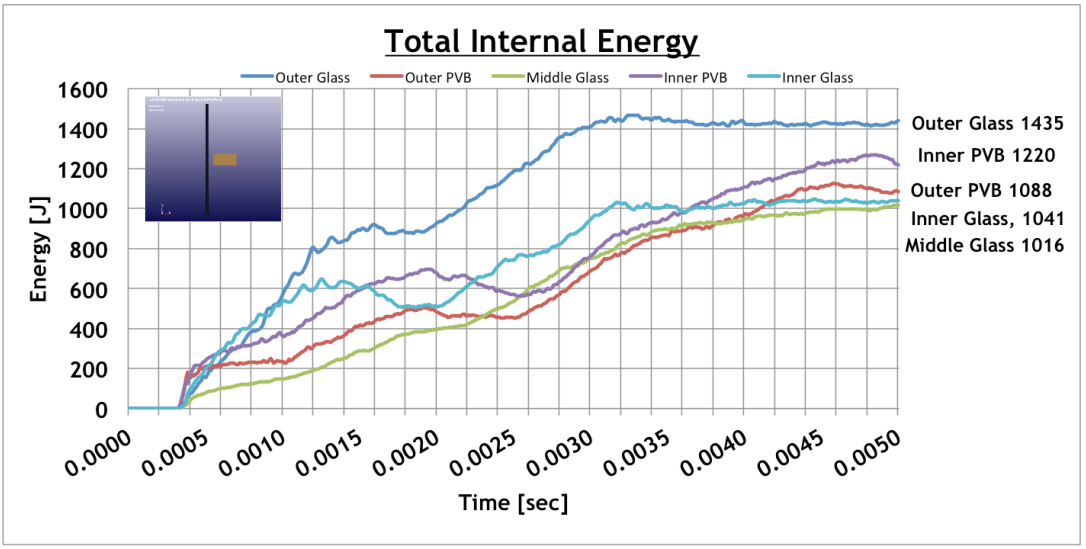

Figure 6.11: Total internal energy for each layer

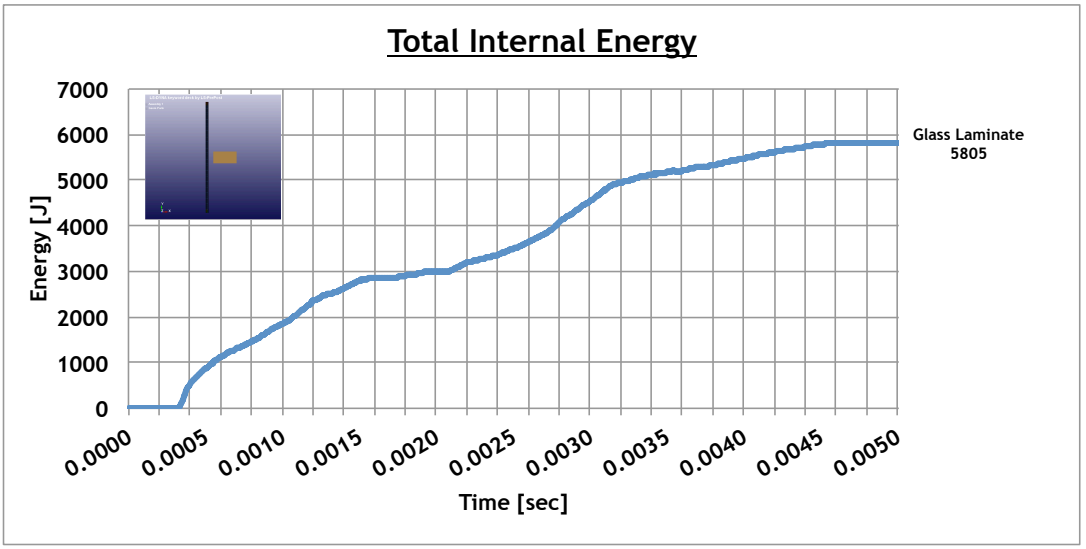

Figure 6.12: Total internal energy for glass laminate

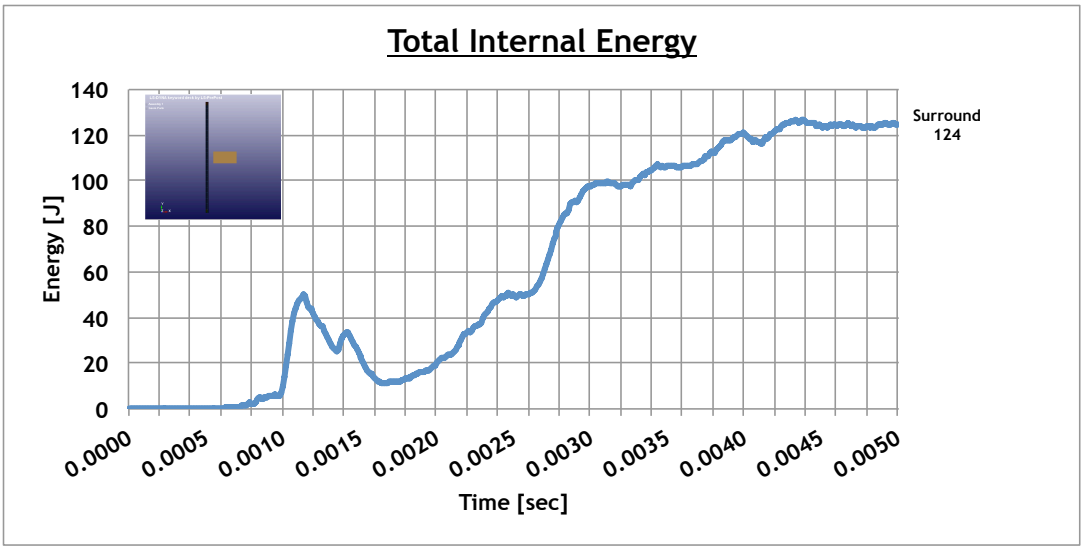

Figure 6.13: Total internal energy for surround

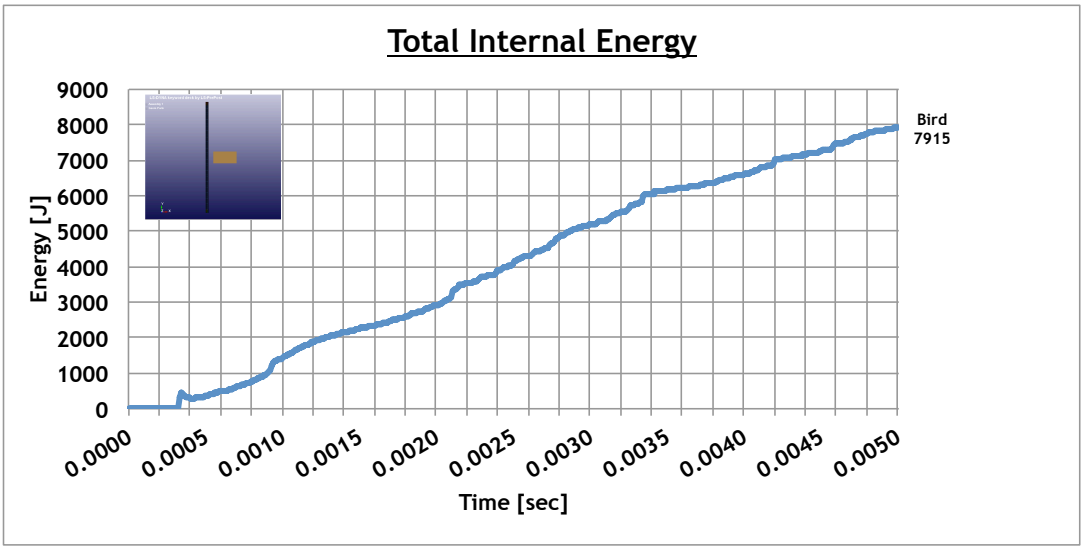

Figure 6.14: Total internal energy for bird

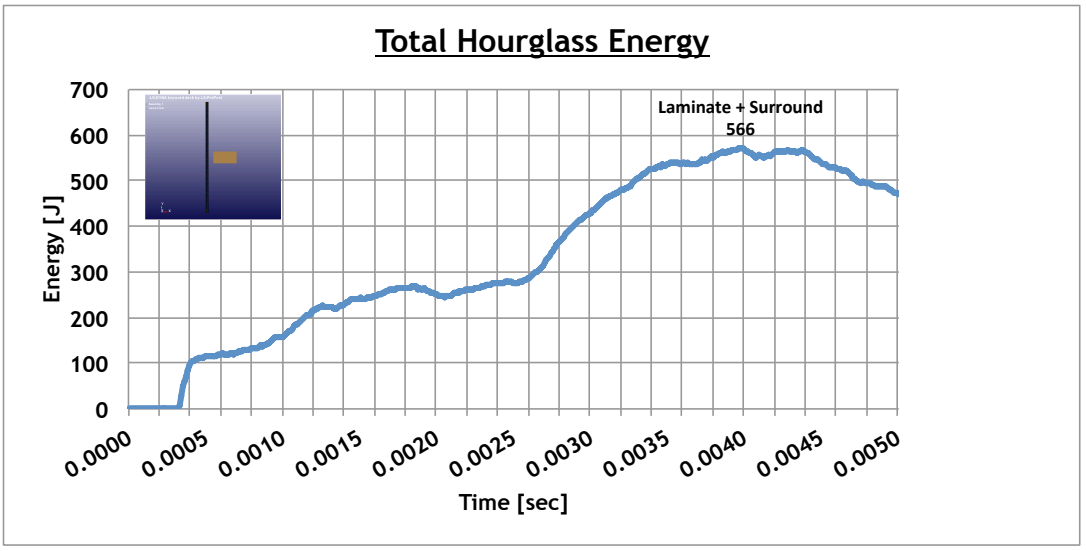

Figure 6.15: Total hourglass energy

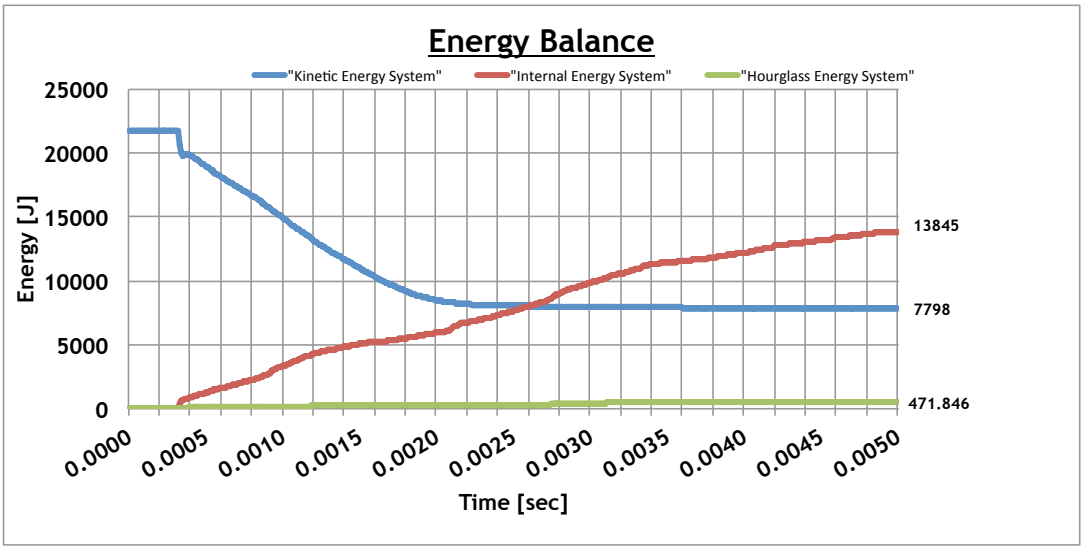

Figure 6.16: Energy balance

6.2 Parametric Study of the Impact Response

Before studying the case of the birdstrike against a full-scale windshield structure, a parametric analysis was carried out to investigate the influence of various geometric parameters on the impact response of the windshield, and in particular respect to the capability to absorb the impact energy in a safe way without any failure.
For the parametric study it was studied the influence of these three parameters: 1) *Windshield Curvature*, 2) *Impact Angle* and 3) *Glass-PVB Thickness Ratio*.

The first parameter investigated was the curvature of the windshield. In addition to the case of a square *flat* plate, analysed in previous section, the birdstrike analysis was also performed onto two further types of windshield with a radius of curvature of $1.273m$ and $0.636m$, as shown in the Figure 6.17.

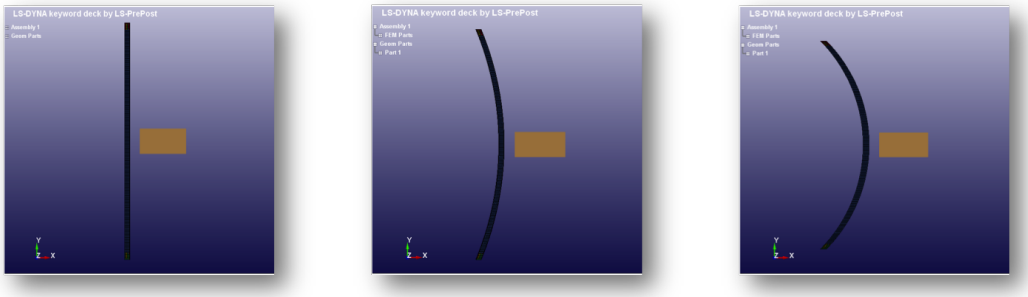

(a) $r = \infty$ (b) $r = 1.273$ (c) $r = 0.636$

Figure 6.17: Curvature changes

The second parameter analysed was the impact angle of the bird respect to the horizontal x-axis. The simulation was performed for three impact angles: α =90°, α =60°, and α =30°, as it was reported in the Figure 6.18.

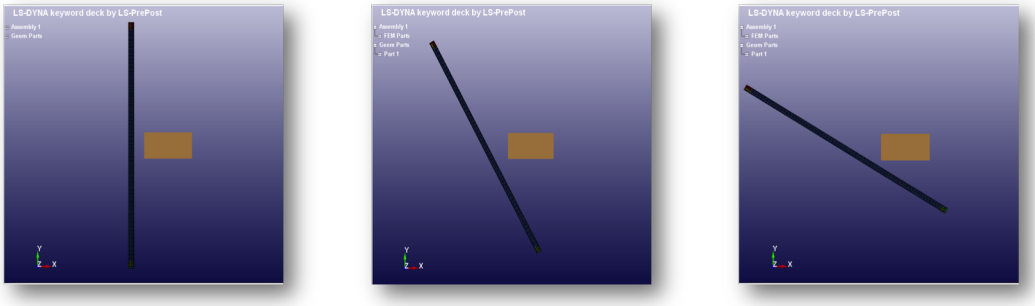

(a) α =90° (b) α =60° (c) α =30°

Figure 6.18: Impact angle changes

Combining this two parameters it was obtained the matrix of 9 analysis presented in Figure 6.19, i.e. for each curvature they were performed three simulations correspondent to the three impact angles.

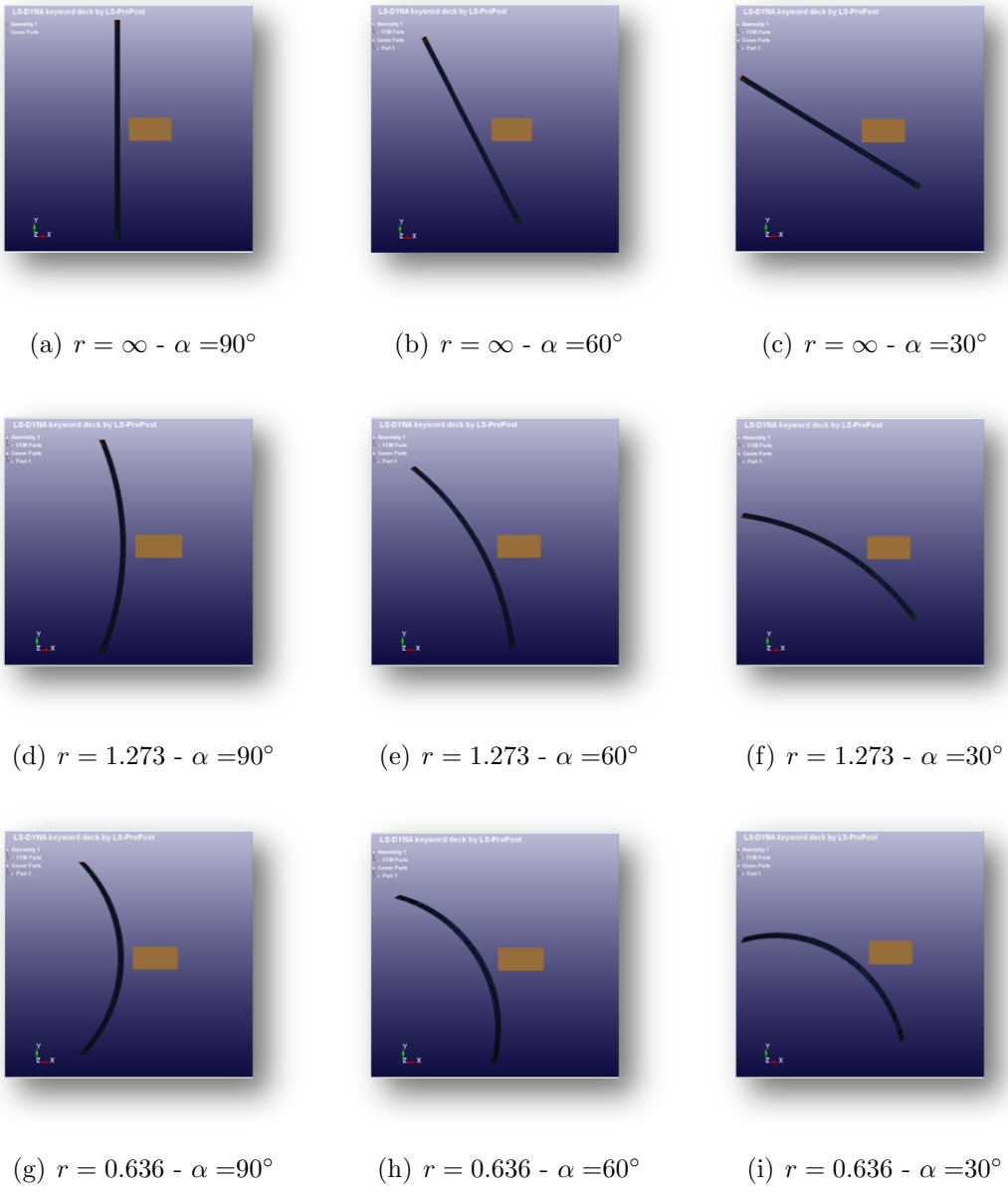

(a) $r = \infty$ - α =90° (b) $r = \infty$ - α =60° (c) $r = \infty$ - α =30°

(d) $r = 1.273$ - α =90° (e) $r = 1.273$ - α =60° (f) $r = 1.273$ - α =30°

(g) $r = 0.636$ - α =90° (h) $r = 0.636$ - α =60° (i) $r = 0.636$ - α =30°

Figure 6.19: Cases studied as changes of curvature and impact angle

The third parameter analysed was the thickness ratio between the glass and PVB layers, with a constant total thickness equal to $20mm$. In detail they were studied three type of lay-up configurations for which: a) glass and PVB layers have the same thickness b) the thickness of the glass is twice as much as the PVB one, c) the thickness of the glass is 3 times the PVB one, as shown in the Figure 6.20.

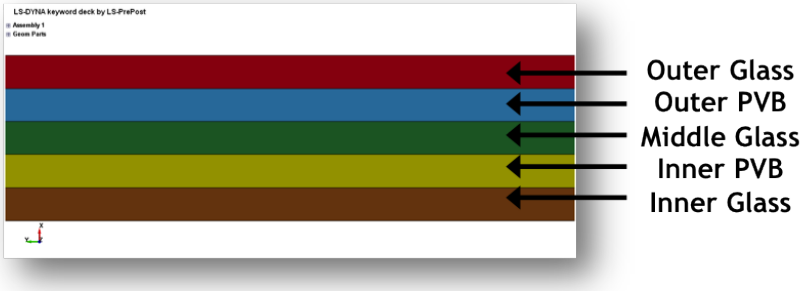

(a) $t_{glass} = t_{PVB}$

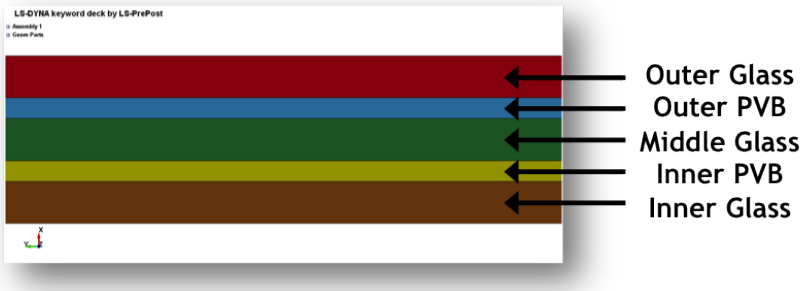

(b) $t_{glass} = 2 \times t_{PVB}$

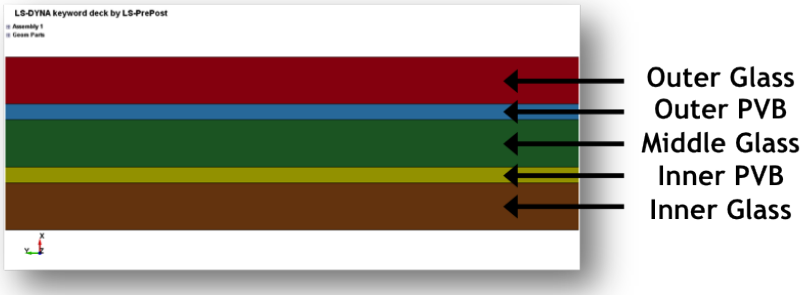

(c) $t_{glass} = 3 \times t_{PVB}$

Figure 6.20: Thichness lay-up configurations

Each of these 3 thickness lay-up configurations was applied to the 9 previous cases obtained from the combination of curvature and impact angle, and finally it was defined a number of 27 different impact scenarios in order to identify the best case scenario and to get a deep insight into the behaviour of the windshield in term of energy absorbing and failure. The complete simulation matrix is shown in the Table 6.1

Text n°	Curvature [m]	Impact Angle [°]	Thickness Ratio	File Name	Failure
1	$r = \infty$	α =90°	$t_{glass} = t_{PVB}$	Test-curv0-90d-t100%	Failure
2	$r = \infty$	α =90°	$t_{glass} = 2 \times t_{PVB}$	Test-curv0-90d-t50%	Failure
3	$r = \infty$	α =90°	$t_{glass} = 3 \times t_{PVB}$	Test-curv0-90d-t33%	Failure
4	$r = \infty$	α =60°	$t_{glass} = t_{PVB}$	Test-curv0-60d-t100%	Failure
5	$r = \infty$	α =60°	$t_{glass} = 2 \times t_{PVB}$	Test-curv0-60d-t50%	Failure
6	$r = \infty$	α =60°	$t_{glass} = 3 \times t_{PVB}$	Test-curv0-60d-t33%	Failure
7	$r = \infty$	α =30°	$t_{glass} = t_{PVB}$	Test-curv0-30d-t100%	No Failure
8	$r = \infty$	α =30°	$t_{glass} = 2 \times t_{PVB}$	Test-curv0-30d-t50%	No Failure
9	$r = \infty$	α =30°	$t_{glass} = 3 \times t_{PVB}$	Test-curv0-30d-t33%	No Failure
10	$r = 1.273$	α =90°	$t_{glass} = t_{PVB}$	Test-curv0-90d-t100%	Failure
11	$r = 1.273$	α =90°	$t_{glass} = 2 \times t_{PVB}$	Test-curv0-90d-t50%	Failure
12	$r = 1.273$	α =90°	$t_{glass} = 3 \times t_{PVB}$	Test-curv0-90d-t33%	Failure
13	$r = 1.273$	α =60°	$t_{glass} = t_{PVB}$	Test-curv0-60d-t100%	Failure
14	$r = 1.273$	α =60°	$t_{glass} = 2 \times t_{PVB}$	Test-curv0-60d-t50%	Failure
15	$r = 1.273$	α =60°	$t_{glass} = 3 \times t_{PVB}$	Test-curv0-60d-t33%	Failure
16	$r = 1.273$	α =30°	$t_{glass} = t_{PVB}$	Test-curv0-30d-t100%	No Failure
17	$r = 1.273$	α =30°	$t_{glass} = 2 \times t_{PVB}$	Test-curv0-30d-t50%	No Failure
18	$r = 1.273$	α =30°	$t_{glass} = 3 \times t_{PVB}$	Test-curv0-30d-t33%	No Failure
19	$r = 0.636$	α =90°	$t_{glass} = t_{PVB}$	Test-curv0-90d-t100%	Failure
20	$r = 0.636$	α =90°	$t_{glass} = 2 \times t_{PVB}$	Test-curv0-90d-t50%	Failure
21	$r = 0.636$	α =90°	$t_{glass} = 3 \times t_{PVB}$	Test-curv0-90d-t33%	Failure
22	$r = 0.636$	α =60°	$t_{glass} = t_{PVB}$	Test-curv0-60d-t100%	Failure
23	$r = 0.636$	α =60°	$t_{glass} = 2 \times t_{PVB}$	Test-curv0-60d-t50%	Failure
24	$r = 0.636$	α =60°	$t_{glass} = 3 \times t_{PVB}$	Test-curv0-60d-t33%	Failure
25	$r = 0.636$	α =30°	$t_{glass} = t_{PVB}$	Test-curv0-30d-t100%	No Failure
26	$r = 0.636$	α =30°	$t_{glass} = 2 \times t_{PVB}$	Test-curv0-30d-t50%	No Failure
27	$r = 0.636$	α =30°	$t_{glass} = 3 \times t_{PVB}$	Test-curv0-30d-t33%	No Failure

Table 6.1: Numerical simulations matrix

6.2.1 Effect of the Curvature

In this section is described the variation of the impact energy absorbed from windshield as the curvature changes. In detail the Figure 6.21 shows the maximum values of the energy transferred from bird to windshield during the impact as curvature changes for an impact angle of 90° and for each thickness lay-up configuration. It can see that the amount of the energy of impact remains almost constant going from a flat plate (blue bar) through a curvature radius of $r = 1.273$ (red bar), while it decreases by 10% going from a curvature radius of $r = 1.273$ (red bar) through a curvature radius of $r = 0.636$ (green bar).

It can also see similar trends of the energy as curvature changes in the case of impact with an impact angle of 60° (Figure 6.22) and 30° (Figure 6.23), with the difference that only for the impact angle of 30° there is no failure of any glass layer.

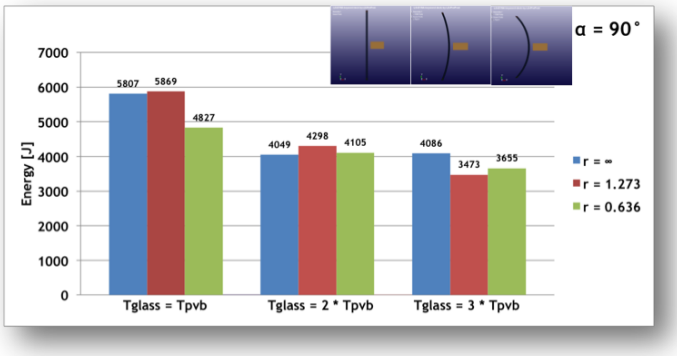

Figure 6.21: Maximum energy as the curvature changes for α =90°

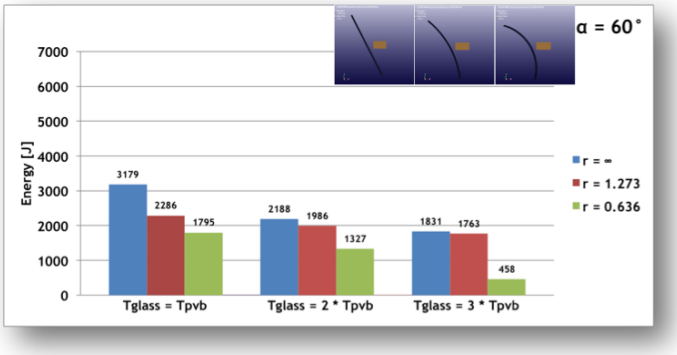

Figure 6.22: Maximum energy as the curvature changes for α =60°

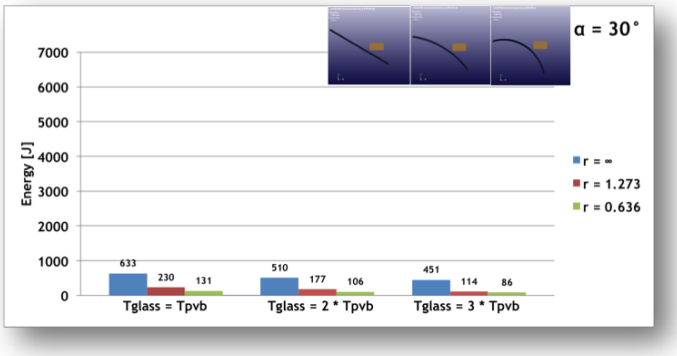

Figure 6.23: Maximum energy as the curvature changes for α =30°

6.2.2 Effect of the Impact Angle

In this section is presented the variation of the energy as the impact angle changes. The Figure 6.24 shows the maximum values of the energy for a flat plate and for each thickness lay-up configuration. It can see that the amount of the energy of impact decreases by ∼40-50% going from an impact angle of 90° (blue bar) through 60° (red bar), and again decreases even by ∼70-80% going from an impact angle of 60° (red bar) through 30° (green bar).

The Figures 6.25 and 6.26 report similar trends of the energy as curvature changes in the case of impact against a windshield with a curvature $r = 1.273$ and $r = 0.636$, the only difference is a light decrease of the absolute values with increase of the curvature. Again in this case only the impacts with an angle of 30° do not present any failure in the glass layers.

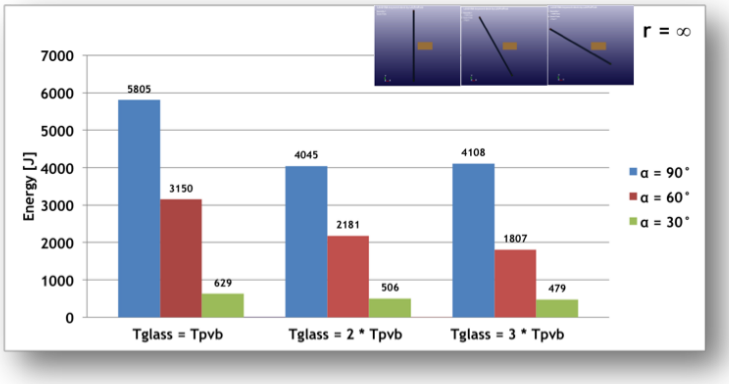

Figure 6.24: Maximum energy as the impact angle changes for $r = \infty$

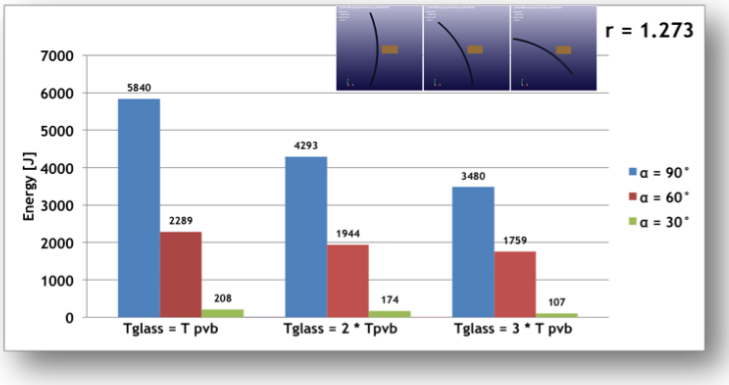

Figure 6.25: Maximum energy as the impact angle changes for $r = 1.273$

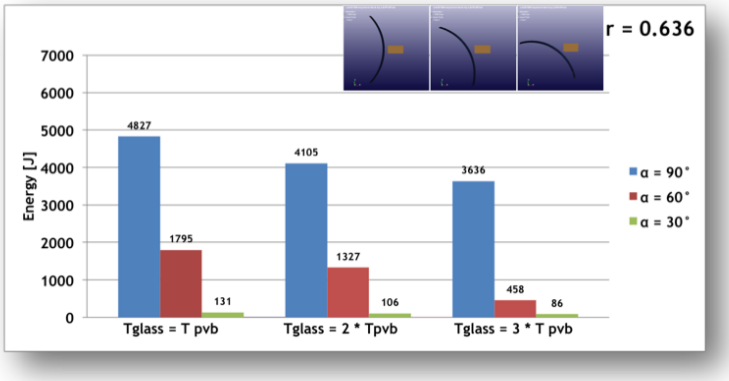

Figure 6.26: Maximum energy as the impact angle changes for $r = 0.636$

6.2.3 Effect of the Thickness Lay-up Configuration

In this section is presented the variation of the energy as the glass-PVB thickness ratio changes. The Figure 6.27 shows the maximum values of the energy for a flat plate and for each impact angle. It can see that the amount of the energy of impact decreases by ∼20-30% going from ratio of 1 to 1 (blue bar) through to a ratio of 1 to 2, while it remain constant going from ratio of 1 to 2 (red bar) through to a ratio of 1 to 3 (green bar).

The Figures 6.28 and 6.29 report similar trends of the energy as curvature changes in the case of impact against a windshield with a curvature $r = 1.273$ and $r = 0.636$. Again in this case only the impacts with an angle of 30° do not present any failure in the glass layers.

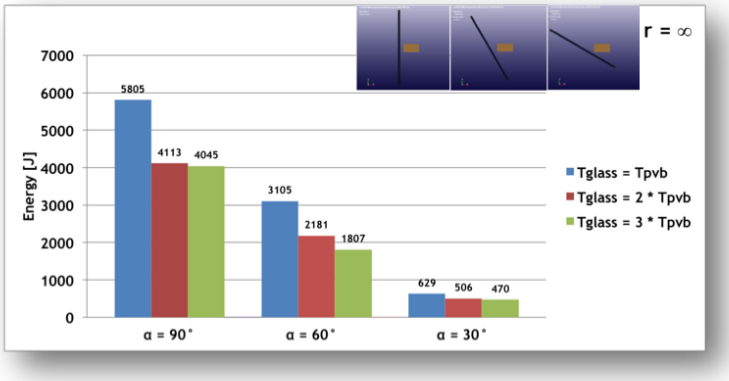

Figure 6.27: Maximum energy as the curvature changes for α =90°

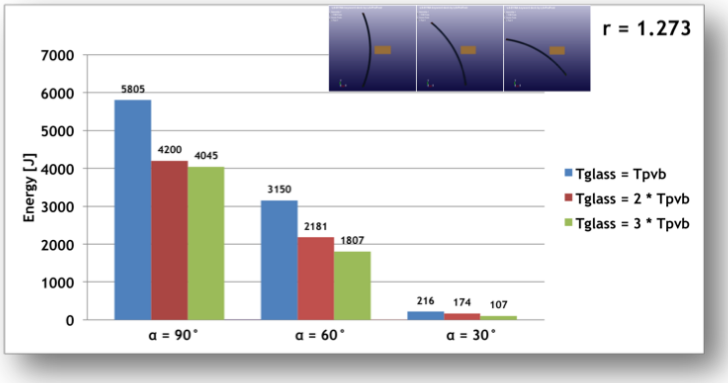

Figure 6.28: Maximum energy as the curvature changes for α =60°

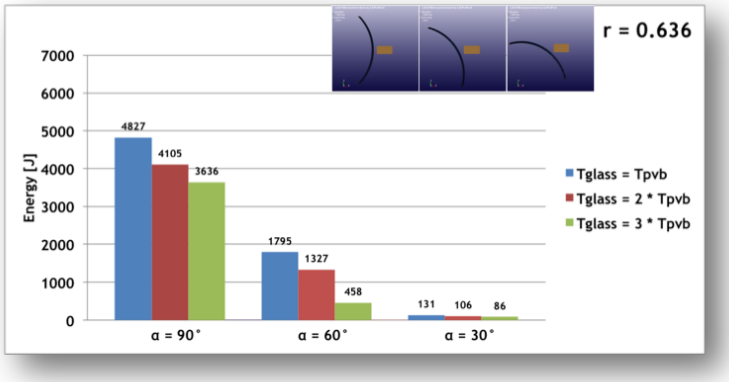

Figure 6.29: Maximum energy as the curvature changes for α =30°

To summarize the results showed it can say that the energy transferred to the windshield during the impact is strongly dependent of the impact angle. It must taking into account that in according with the CS 25, it is necessary, not only, to design a structure capable to absorb the energy of impact involved during the birdstrike, but also to ensure that it occurs without any catastrophic failure of the glass laminate. And, as described in Table 6.1 it happens only when the bird hits the windshield with an angle of 30°.

It is clear that the choice of this angle can not to be only function of birdstrike requirements, because further factors, like for example optical problems, come into play in the design of a windshield structure.

6.3 Birdstrike vs the Full-scale Windshield Model

As well as for the simplified square plate model, the numerical results of the birdstrike analysis against the full-scale windshield structure are reported in this section.

Before presenting the results, it is necessary to provide a deeper description about configuration of the real windshield structure, comparing it with the cases studied in previous parametric analysis carried out on the simplified model.

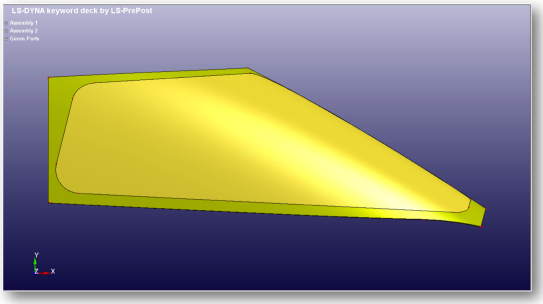

(a)

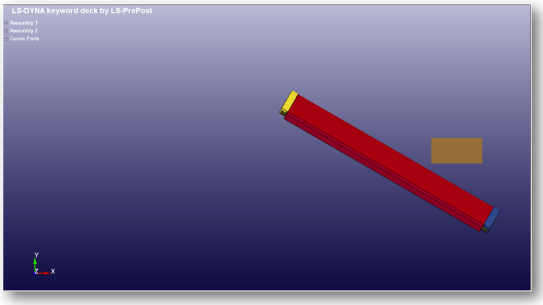

(b)

Figure 6.30: Real and Simplified windshield models

In the Figure 6.30 is presented two lateral views of the full-scale windshield model and of the simplified one with a radius of curvature equal to 1.273 and an impact angle α =30°.

The overlapping of the two models reported in the Figures 6.31a and 6.31b shows that the simplified model simulates rather well the real model, without taking into account the difference of surface.

Furthermore, recalling that for the full-scale model the averaged thickness of the glass ply is twice as much as the interlayer one (5.1), it may say that between the 27 simulations performed in the parametric analysis there is one that comes close to the real case and results to be the most realistic simulation.

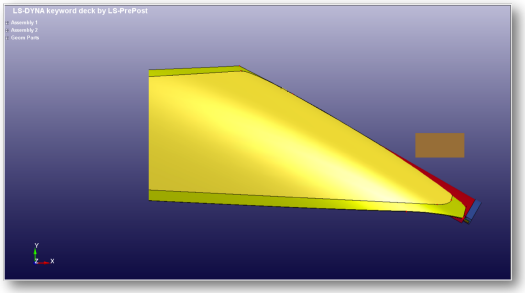

(a) Lateral View

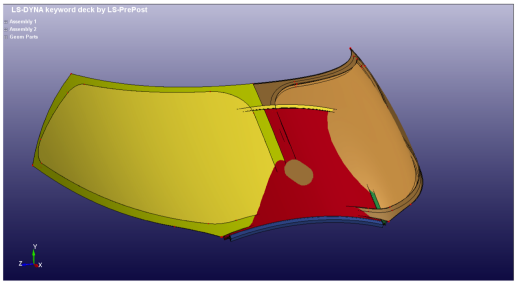

(b) Iso View

Figure 6.31: Comparison between Real and Simplified windshield models

The Figure 6.32 shows a sequence plots of the birdstrike against the real windshield model, from the moment of the impact until the bird is completely squashed into the panel. It is clearly visible the deformation of the bird during the impact and its squashing into the windshield.

Furthermore in the Figure 6.33 is reported the step-by-step contour plots of the von Mises stress of the windshield impacted by the bird. As it was expected, the impacted zone of the windshield reaches the maximum stress during the first 1.5 milliseconds, but it does not arrive to values for which the glass fails. In fact in the Figure 6.33(j), that depicts the last plot of the simulation, there is no failure of any glass layer.

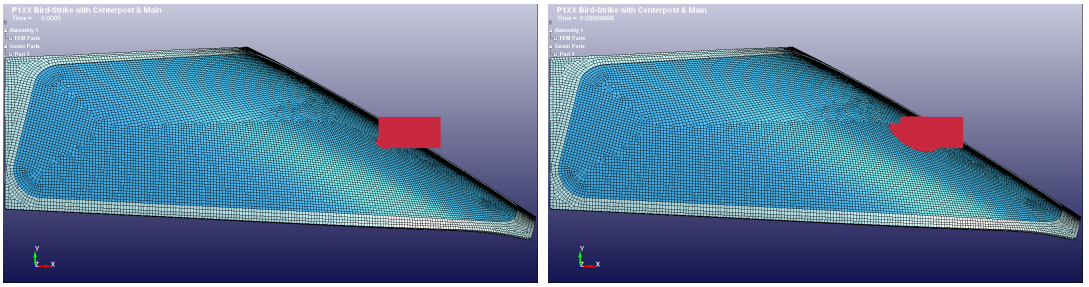

(a) t=0.0005 s (b) t=0.0010 s

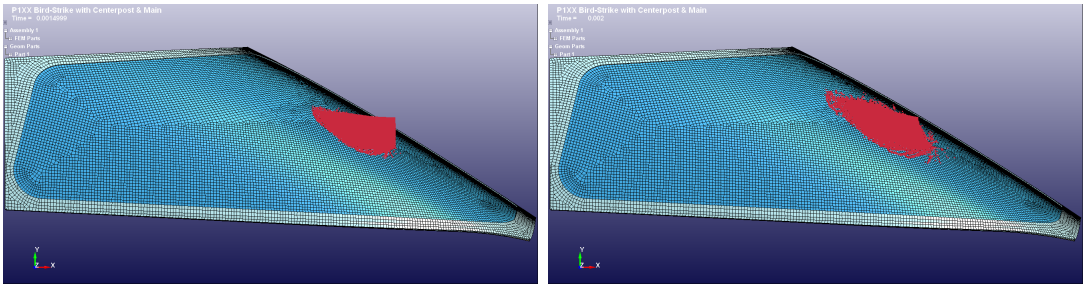

(c) t=0.0015 s (d) t=0.0020 s

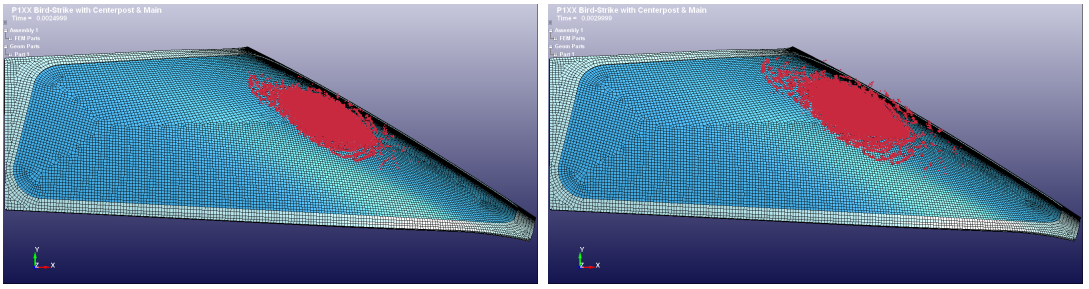

(e) t=0.0025 s (f) t=0.0030 s

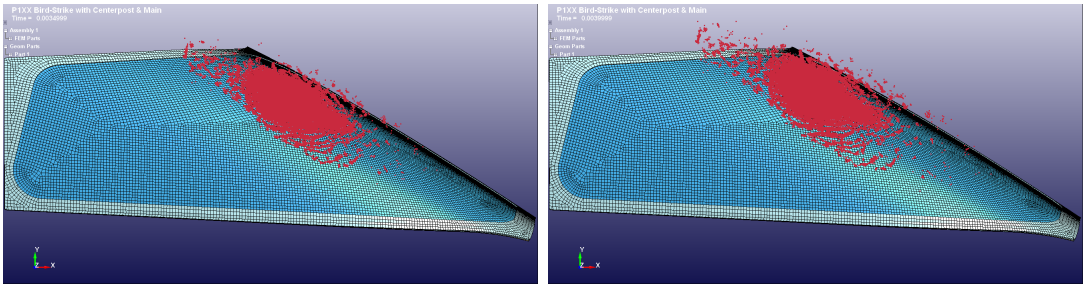

(g) t=0.0035 s (h) t=0.0040 s

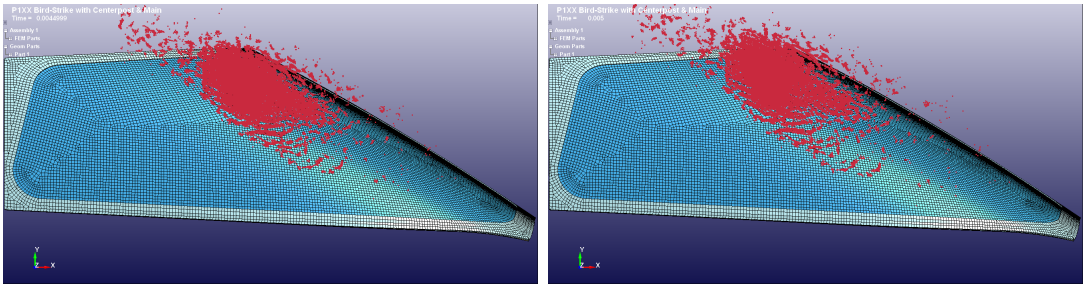

(i) t=0.0045 s (j) t=0.0050 s

Figure 6.32: Sequence of the birdstrike vs Full-scale windshield

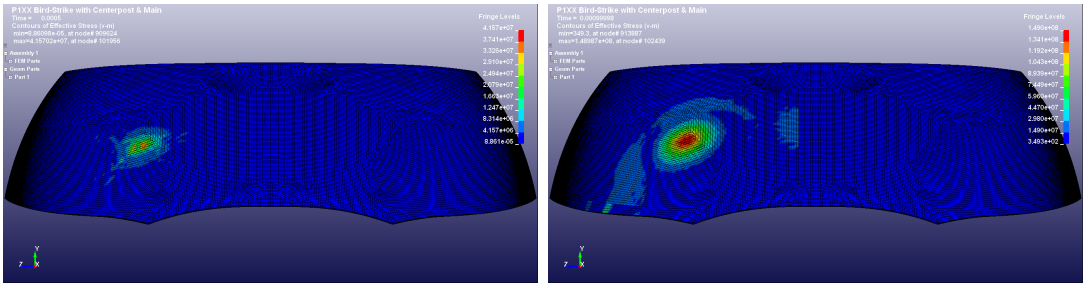

(a) t=0.0005 s (b) t=0.0010 s

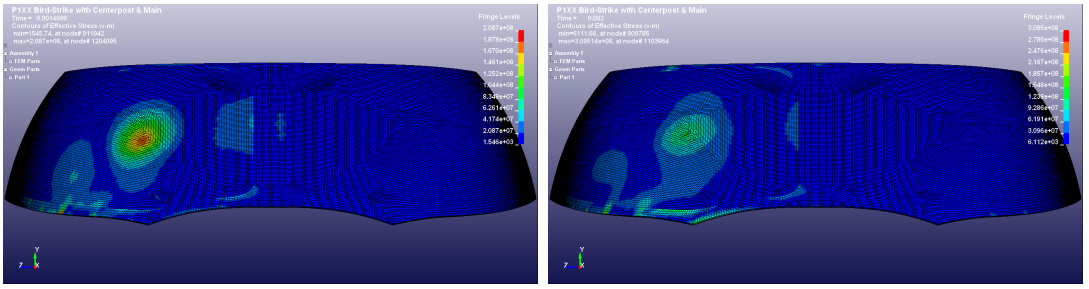

(c) t=0.0015 s (d) t=0.0020 s

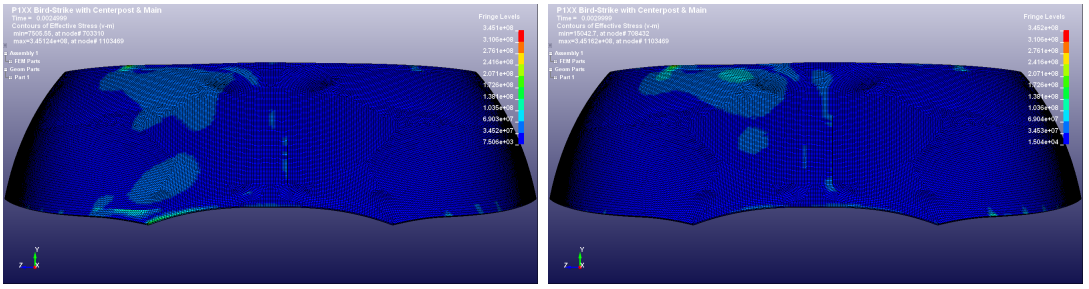

(e) t=0.0025 s (f) t=0.0030 s

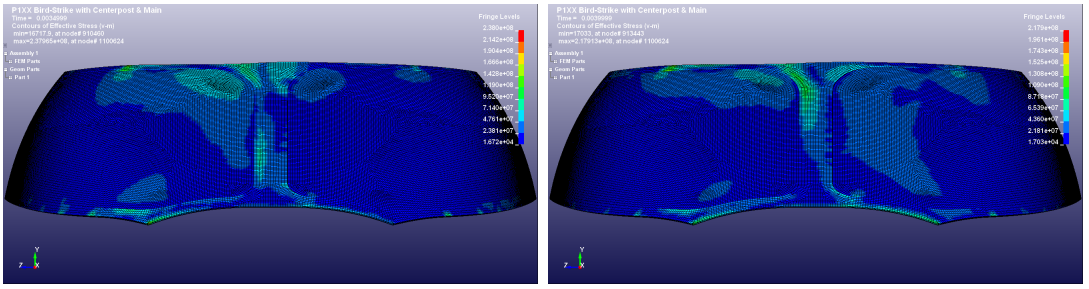

(g) t=0.0035 s (h) t=0.0040 s

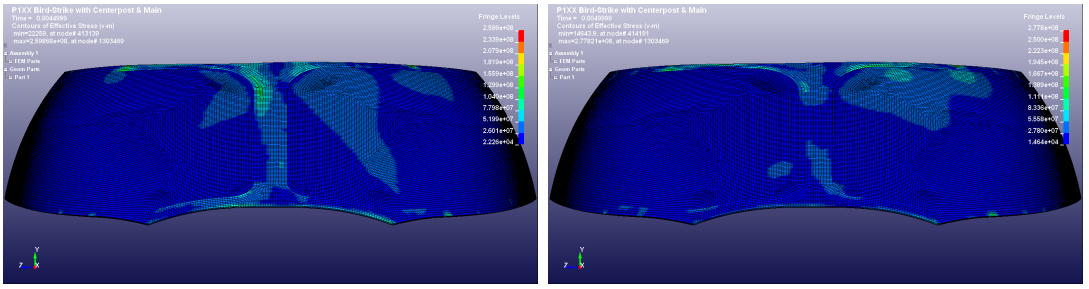

(i) t=0.0045 s (j) t=0.0050 s

Figure 6.33: Sequence of the plate deformation

In the Figure 6.34 the resultant displacement for the impacted zone of the right windshield panel is reported. It presents a maximum value of 3.7mm after 17 milliseconds, behind which the panel tends to return to the initial configuration, reaching a final value of 2.6mm at the end of the simulation.

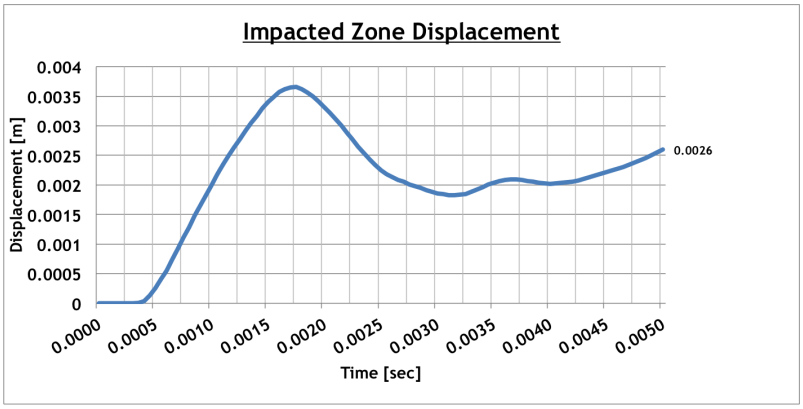

Figure 6.34: Displacement of the impacted zone of the right panel

The Figure 6.35 depicts the time-history of the interfacial resultant contact force between the bird and the external face of the left windshield panel, and it presents a maximum value of 81163 N. The trend of the time-history is different from that obtained in case of birdstrike with an impact angle of 90°, shown in the Figure 6.9, because of the sliding of the bird windshield caused by the impact angle of 30°.

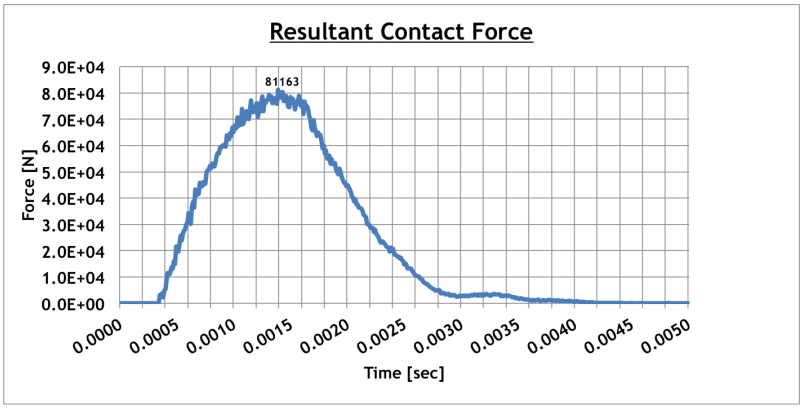

Figure 6.35: Resultant contact force

In the Figures 6.36 and 6.37 are shown the time-histories of the internal energy for each layers of the right and left panel of the windshield, taking into account that in this simulation only the right panel is subjected to the impact. First of all it can see that the amount of the energy transferred is very little, and this permits to avoid any failure of the layers. Furthermore it results very interesting to note that the peaks of the time-histories related to internal energy absorbed by the layers of

the left panel, not subjected to the impact directly, have an offset in time, because the panel "feels" the birdstrike lately, and as consequence presents a later impact response.

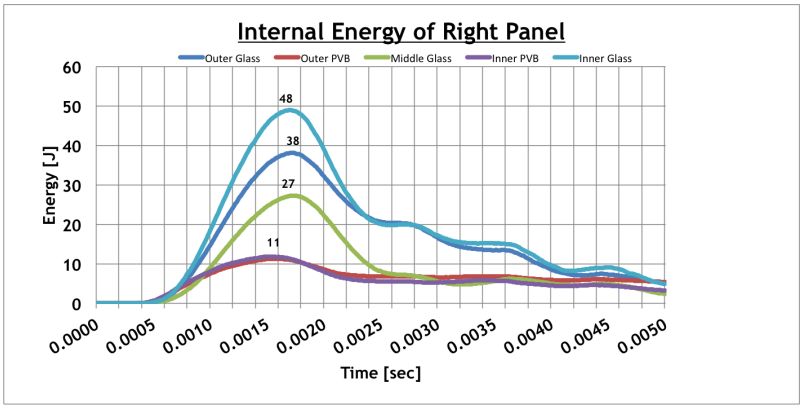

Figure 6.36: Internal energy for each layer of right panel

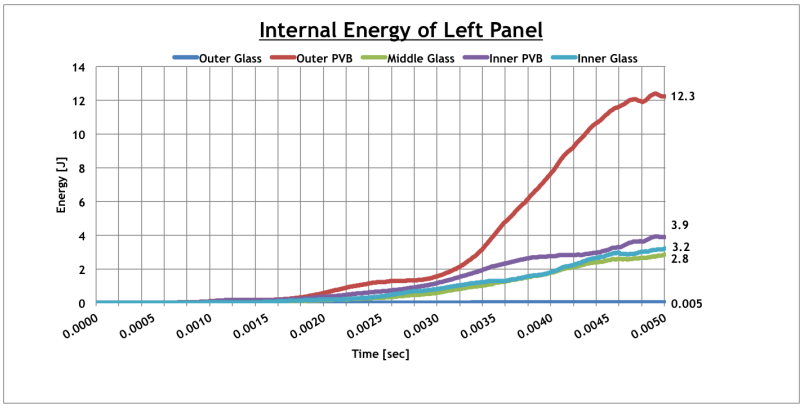

Figure 6.37: Internal energy for each layer of left panel

In addition to the numerical analysis just described, it was performed a considerable number simulation choosing different zone of the windshield impacted by the bird. Between these It is interesting to analyse the case shown in the Figure 6.38, for which the bird hits the center beam of the surround, that divides the two panels of the windshield. It could seems very critical, because, at least in theory, it might cause a failure of both panels at the same time, with a propagation of the crack in both directions and a consequent loss of visibility for both panels.

But the numerical simulation provided very good results, because at the end of the analysis there are no failures and the stresses reached from the structure were even less then the stresses obtained in the previous case (Figure 6.39).

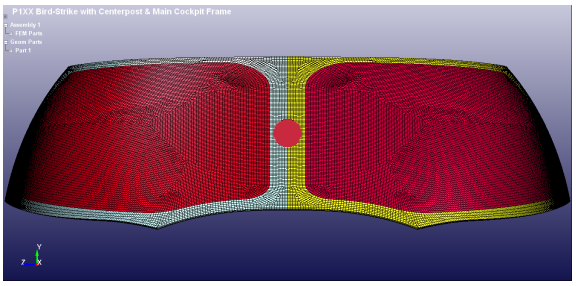

Figure 6.38: Birdstrike against the center beam of the surround structure

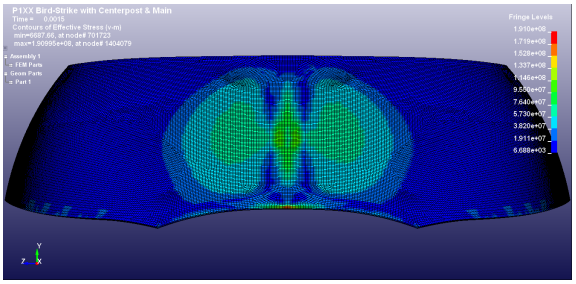

Figure 6.39: von Mises stress plot for birdstrike vs the center beam

The last time-history, shown in the Figure 6.40, represents a key aspect of this birdstrike against the full scale windshield, in fact it shows that the kinetic energy of the bird is still equal to 19600$Joule$ at the end of the simulation. This implies that only the 9% of the impact energy of the bird is transferred to the windshield, and most part of this is dissipated in other forms of energy, such as heat, elastic, sliding energy and so on. This is mainly consequence of the impact angle of the bird, and of the double curvature of the windshield, that result design parameters favourable to avoid any problem caused by a birdstrike in terms of penetration of the bird, and complete fragmentation of the glass.

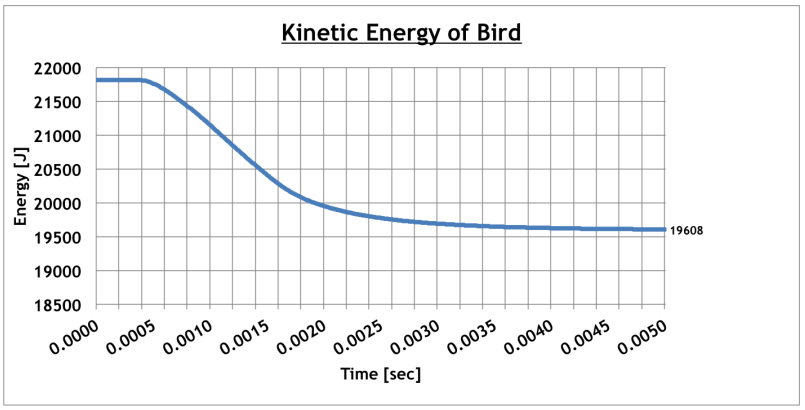

Figure 6.40: Kinetic energy of the bird

Chapter 7

Conclusions

The goal of this research work was the development a scientific and methodological approach to the study of the birdstrike problem for the design, verification, and optimization of a bird-proof windshield of a business jet airplane. It was studied an innovative concept of aircraft windshield, composed by just two windshield panels, unlike most part of the commercial airplane windshield configurations made up of four or more panels.

Before getting to the heart of the analysis, it was given an overview regarding the theoretical aspect of the birdstrike phenomenon, the basics of the non-linear analysis and the most used finite element modeling approaches: a) pure Lagrangian, b) Arbitrary Lagrangian Eulerian (ALE), and c) Smoothed Particle Hydrodynamics (SPH). The advantages and disadvantages of these various formulations were briefly discussed in this work and it was defined, also thanks to a deep bibliographic research, that the SPH approach is the most suitable and feasible methodology to simulate the dynamics of an high speed impact phenomenon, like the birdstrike against an aircraft component.

Both bird SPH and target FE model were prepared by the LS-PrePost preprocessor software, while every numerical simulation was performed by using LSTC/LS-Dyna explicit solver.

A preliminary validation of the birdstrike methodology was achieved through a simulation on a simplified, but representative, windshield structure. It was studied a simplified flat square windshield model impacted by a 1.8 kg bird model at 155m/sec with an impact angle of 90°. Numerical results for this pane showed that it would not withstand the bird impact under the conditions stated in the CS 25 Standard.

Secondly a parametric analysis was executed on the previous square model to evaluate the effects on its structural response of: 1) the target geometry, 2) the impact angle, and 3) the plate curvature. The aim of this analysis was to evaluate the

capability of windshield to absorb the impact energy, involving during a birdstrike event, in a safe and efficient way without any damage.

The results of the parametric analysis reveal that: 1) the energy transferred to the windshield during impact is strongly dependent of the impact angle, 2) in order to design a structure capable to absorb *safely* the energy of impact involved during the birdstrike, it is preferable to have a windshield structure with an impact angle smaller than 30°.

It is also clear that the choice of this angle can not to be only function of birdstrike requirements, because further factors, like for example optical problems, come into play in the design of a windshield structure.

The second part of the work was focused on the development of a numerical simulation of birdstrike on a full-scale aircraft windshield-surround model. The numerical analysis on this finite element model showed that the windshield is capable to withstand to the impact force transferred by the bird during the impact, thanks to its smaller impact angle respect to the x-axis (path of the bird) and also for its double curvature, that permits the bird to slides on the windshield and continue its path keeping the most part of the kinetic energy.

The main achievement of this research was the collection of results and experiences, obtained by both simplified realistic and full-scale FE model analysis, to define a design "*rule of thumb*" assessment with regard to the Birdstrike problem. It has permitted to trace the guidelines to perform a certification test simulation and provide a birdstrike test article proposal (Figure 7.1), necessary for a design of an airplane windshield structure able to withstand to a birdstrike event in according with the conditions stated in the CS 25 standard requirements.

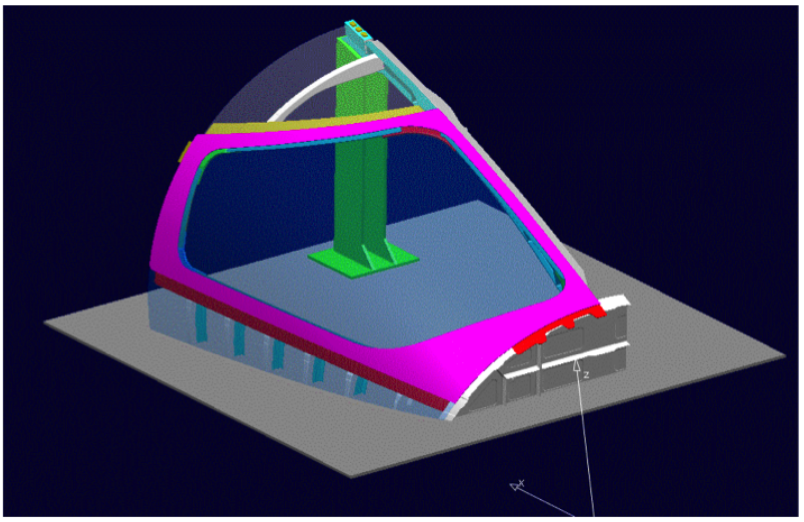

Figure 7.1: Birdstrike test article proposal

References

Airoldi, A. & Cacchione, B. (2006). Modelling of impact forces and pressures in lagrangian bird strike analyses. *International Journal of Impact Engineering*, **32**, 1651 – 1677. 5

Allock, A.W.R. & Collin, D.M. (1969). *The Development of a Dummy Bird for use in Bird Strike*. H.M. Stationery Off. (London). 5

Anghileri, M., Castelletti, L.M.L. & Mazza, V. (2004). Birdstrike: approaches to the analysis of impacts with penetration. In *International Conference on Impact Loading of Lightweight Structures*. 7

Ansys (2006). *Ansys User's Manual*. Ansys Inc., Canonsburg, USA. 6

Barber, J.P. & Peterson, R.L. (1976). Bird impact forces in aircraft windshield design. Tech. rep., Research Institute - University of Dayton - Ohio. 4

Barber, J.P., Taylor, H.R. & Wilbeck, J.S. (1975). Characterization of bird impacts on a rigid plate: Part i. Tech. rep., Research Institute - University of Dayton - Ohio. 4

Barber, J.P., Taylor, H.R. & Wilbeck, J.S. (1977). Bird impact forces and pressures on rigid and compliant targets. Tech. rep., Research Institute - University of Dayton - Ohio. 4

Benson, D.J. (1992). Computational methods in lagrangian and eulerian hydrocodes. *Computer Methods in Applied Mechanics and Engineering*, **99**, 235 – 394. 5

Birnbaum, N.K., Francis, N.J. & Gerber, B.I. (1997). Coupled techniques for the simulation of fluid-structure and impact problems. Tech. rep., Century Dynamics, Inc. - San Ramon, CA. 6

Cassenti, B.N. (1979). Hugoniot pressure loading in soft body impacts. Tech. rep., United Technologies Research Center - East Hartford. 4

Cleary, E.C., Dolbeer, R.A. & Wright, S.E. (2003). Wilflife strike to civil aircraft in the united states 1990-2002. Tech. rep., Federal Aviation Administration, Office of Airport Safety and Standards, Washington, DC. 1

CS25.631, E. (2003). Bird strike damage. Tech. rep., EASA Cer- tification Specifications for Large Aeroplane. iii

Donea, J., Huerta, A., Ponthot, J. & Rodriguez-Ferran, A. (2004). *Arbitrary Lagrangian-Eulerian methods - Encyclopedia of Computational Mechanics*, vol. 1. John Wiley and Sons, Ltd. 6

Georgiadis, S., Gunnion, A.J., Thomson, R.S. & Cartwright, B.K. (2008). Bird-strike simulation for certification of the boeing 787 composite moveable trailing edge. *Composite Structures*, **86**, 258 – 268, fourteenth International Conference on Composite Structures - ICCS/14. 6

Guan, Y., Zhao, Z., Chen, W. & Gao, D. (2008). Foreign object damage to fan rotor blades of aeroengine part ii: Numerical simulation of bird impact. *Chinese Journal of Aeronautics*, **21**, 328 – 334. 5

Guida, M. (2008). *Design and Testing Methods of Aeronautical Components Resistant to a Bird-strike*. Ph.D. thesis, Department of Aerospace Engineering - University of Naples. 7

Guida, M., Marulo, F., Meo, M., Grimaldi, A. & Olivares, G. (2011). Sph - lagrangian study of bird impact on leading edge wing. *Composite Structures*, **93**, 1060 – 1071, fourteenth International Conference on Composite Structures - ICCS/14. 6

Hallquist, J.O. (2005). *LS-PrePost Manual, Version 1.0*. Livermore Software Technology Corporation, 7374 Las Positas Road, Livermore CA 94551, USA. 39

Hallquist, J.O. (2006). *LS-Dyna Theory Manual*. Livermore Software Technology Corporation, 7374 Las Positas Road, Livermore CA 94551, USA. 3, 6, 38

Hanssen, A., Girard, Y., Olovsson, L., Berstad, T. & Langseth, M. (2006). A numerical model for bird strike of aluminium foam-based sandwich panels. *International Journal of Impact Engineering*, **32**, 1127 – 1144. 7

Hermann, L.R. & Peterson, F.E. (1968). A numerical procedure for viscoelastic stress analysis. In *Seventh Meeting of ICRPG Mechanical Behavior Working Group,*, 177, Orlando FL. 34

Hut, P., Hernquist, L., Lake, G., Makino, J., McMillan, S. & Sterling, T. (1997). Smooth particle hydrodynamics: Models, applications, and enabling technologies. Tech. rep., Institute for Advance Study at Princeton. 6

Lacome, J.L. (2000). Smooth particle hydrodynamics (sph): a new feature in ls-dyna. In *6th International LS-Dyna Users Conference*. 6

Langrand, B., Bayart, A.S., Chauveau, Y. & Deletombe, E. (2001). Assessment of multi-physics fe methods for bird strike modelling-application to a metallic riveted airframe. *International Journal of Crashworthiness*, **7**, 415–428. 6

Linder, C. (2003). *An Arbitrary Lagrangian-Eulerian Finite Element Formulation for Dynamics and Finite Strain Plasticity Models*. Master's thesis, Department of Structural Mechanics - University of Stuttgart. 6

Liu, J., Li, Y. & Xu, F. (2008). The numerical simulation of a bird-impact on an aircraft windshield by using the spc method. *Advanced Materials Research*, **33-37**, 851–856. 7

McCarthy, M.A., Xiao, J.R., McCarthy, C.T., Kamoulakos, A., Ramos, J., Gallard, J.P. & Melito, V. (2004). Modelling of bird strike on an aircraft wing leading edge made from fibre metal laminates – part 2: Modelling of impact with sph bird model. *Applied Composite Materials*, **11**, 317–340, 10.1023/B:ACMA.0000037134.93410.c0. 6

Monaghan, J.J. (1992). Smoothed particle hydrodynamics. *Annual Review of Astronomy and Astrophysics*, **30**, 543–574. 25

Niering, E. (1990). Simulation of bird strikes on turbine engines. *Journal of Engineering for Gas Turbines and Power*, **112**, 573–578. 5

PAM-CRASH (2008). *Pam-Crash Solver Notes Manual*. Engineering Systems International, 94578 Rungis Cedex, France. 5

Radioss (2008). *Radioss Theory Manual*. Altair Engineering Inc., Troy MI, USA. 6

Salehi, H., Ziaei-Rad, S. & Vaziri-Zanjani, M.A. (2010). Bird impact effects on different types of aircraft bubble windows using numerical and experimental methods. *International Journal of Crashworthiness*, **15**, 93–106. 7

Shultz, C. & Peters, J. (2002). Bird strike simulation using ansys ls/dyna. Tech. rep., Phoenix Analysis And Design Technologies, Inc. 6

Souli, M., Wang, J., Do, I. & Hao, C. (2004). Ale and fluid-structure interaction in ls-dyna. In *8th International LS-Dyna Users Conference*. 6

Stroker, C. (1997). *Development of the Arbitrary Lagrangian-Eulerian method in nonlinear solid mechanics*. Ph.D. thesis, HC Stoker Enschedel. 5

Thorpe, J. (2003). Fatalities and destroyed civil aircraft due to birdstrikes 1912–2002. Tech. rep., International Bird Strike Committee. 4

Timmel, M., Kolling, S., Osterrieder, P. & Bois, P.D. (2007). A finite element model for impact simulation with laminated glass. *International Journal of Impact Engineering*, **34**, 1465 – 1478. 32

Ubels, L., Johnson, A., Gallard, J. & Sunaric, M. (2003). Design and testing of a composite bird strike resistant leading edge. Tech. rep., National Aerospace Laboratory NLR, Amsterdam, The Netherlands. 6

Wilbeck, J.S. (1977). *Impact behavior of low strength projectiles*. Ph.D. thesis, Texas A and M University. 4

Wilbeck, J.S. & Rand, J.L. (1981). The development od a substitute bird model. *ASME Journal of Engineering for Gas Turbine and Power*, **103**, 725–730. 5, 11, 13

Yang, J., Cai, X. & Wu, C. (2003). Experimental and fem study of windshield subjected to high speed bird impact. *Acta Mechanica Sinica*, **19**, 543–550, 10.1007/BF02484547. 7